REPORT NO.
UCB/EERC-82/24
NOVEMBER 1982

EARTHQUAKE ENGINEERING RESEARCH CENTER

A MATHEMATICAL MODEL FOR THE RESPONSE OF MASONRY WALLS TO DYNAMIC EXCITATIONS

by

HULUK SUCUOGLU
YALCIN MENGI
HUGH D. McNIVEN

Report to the National Science Foundation

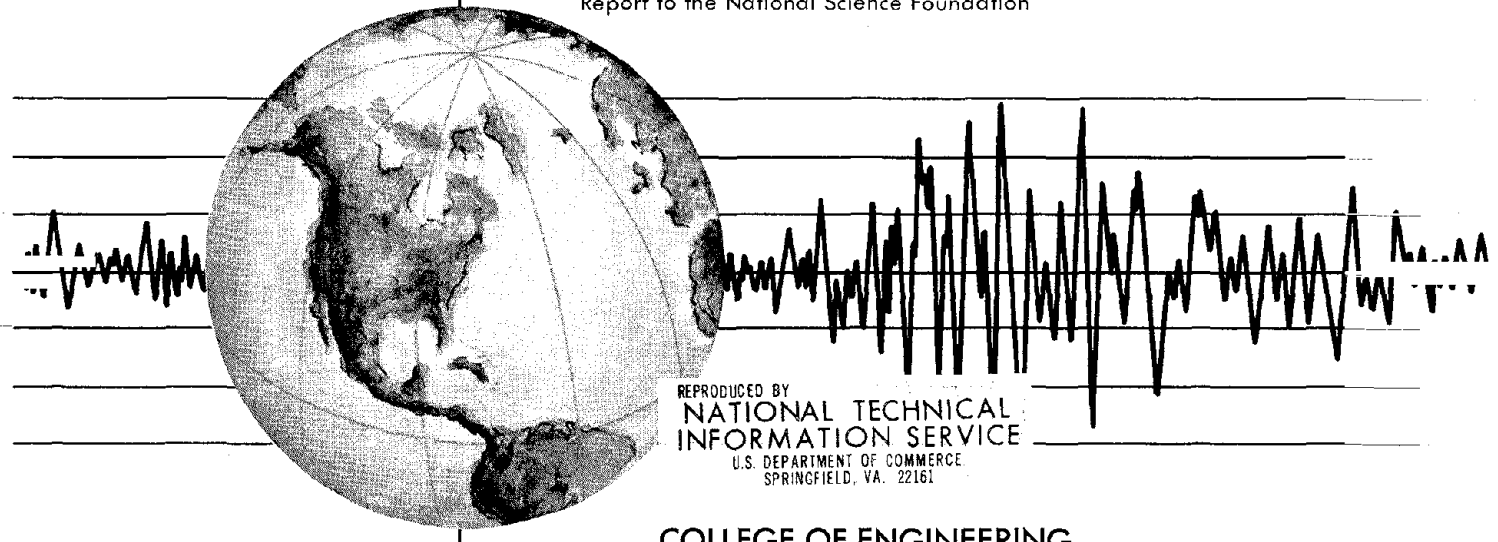

COLLEGE OF ENGINEERING

UNIVERSITY OF CALIFORNIA · Berkeley, California

For sale by the National Technical Information Service, U.S. Department of Commerce, Springfield, Virginia 22161.

See back of report for up to date listing of EERC reports.

DISCLAIMER

50272-101

REPORT DOCUMENTATION PAGE	1. REPORT NO. NSF/CEE-82069	2.	3. Recipient's Accession No. PB83 169011
4. Title and Subtitle: A Mathematical Model for the Response of Masonry Walls to Dynamic Excitations			5. Report Date: November 1982 6.
7. Author(s): H. Sucuoglu, Y. Mengi, H. D. McNiven			8. Performing Organization Rept. No. UCB/EERC-82/24
9. Performing Organization Name and Address: Earthquake Engineering Research Center, University of California, Berkeley, 47th Street & Hoffman Blvd, Richmond, Ca. 94804			10. Project/Task/Work Unit No. 11. Contract(C) or Grant(G) No. (C) (G) 0-21851
12. Sponsoring Organization Name and Address: National Science Foundation, 1800 G Street, N.W., Washington, D.C. 20550			13. Type of Report & Period Covered 14.

15. Supplementary Notes

16. Abstract (Limit: 200 words)

The study involves three stages: experimental observations, choice of the form for a mathematical model, and optimization analysis.

The masonry wall specimens were subjected to simulated earthquake ground motions, and horizontal and vertical periodic excitations. Evaluation of the experimental data indicates that the first two modal frequencies are close to each other. This is attributed, on physical grounds, to strong interaction between the brick and mortar phases of the wall. Hence, a two phase mathematical model (mixture model) is chosen to describe the wall behavior because of its capability of differentiating between the two phases of the wall and of taking into account the interaction between them. The equations of the mixture model are put into a discrete form to simplify the analysis.

The parameters appearing in the model are determined, through optimization, by matching theoretical and experimental responses in frequency space.

17. Document Analysis a. Descriptors

b. Identifiers/Open-Ended Terms

c. COSATI Field/Group

18. Availability Statement: Release Unlimited	19. Security Class (This Report)	21. No. of Pages: 133
	20. Security Class (This Page)	22. Price

(ANSI-Z39.18) See Instructions on Reverse

OPTIONAL FORM 272 (4-77) (Formerly NTIS-35) Department of Commerce

A MATHEMATICAL MODEL FOR THE RESPONSE OF MASONRY WALLS TO DYNAMIC EXCITATIONS

by

Haluk Sucuoğlu

and

Yalçin Mengi

Department of Engineering Sciences
Middle East Technical University
Ankara, Turkey

and

Hugh D. McNiven

Department of Civil Engineering
University of California
Berkeley, California

Report to the National Science Foundation

Report No. UCB/EERC-82/24
Earthquake Engineering Research Center
College of Engineering
University of California
Berkeley, California

November 1982

ABSTRACT

In this study a mathematical model is proposed to predict the linear dynamic behavior of masonry walls. The study involves three stages: experimental observations, choice of the form for a mathematical model, and optimization analysis.

The experimental work was carried out using a shaking table, where the masonry wall specimens were subjected to simulated earthquake ground motions, and horizontal and vertical periodic excitations. Time histories of accelerations were recorded at the lower and upper ends of the specimens.

Evaluation of the experimental data indicates that the first two modal frequencies are close to each other. This is attributed, on physical grounds, to strong interaction between the brick and mortar phases of the wall. Accordingly, a two phase mathematical model, namely a mixture model, is chosen to describe the wall behavior because of its capability of differentiating between the two phases of the wall and of taking into account the interaction between them. The equations of the mixture model are put into a discrete form to simplify the analysis.

The parameters appearing in the model are determined, through optimization, by matching theoretical and experimental responses. Optimization analysis is performed in frequency space. The response quantities to be matched are chosen to be the complex frequency response functions (experimental and theoretical) relating the Fourier transforms of the top and base accelerations of the wall. Computations in the optimization analysis are carried out by introducing an object (error) function and minimizing it using a Gauss-Newton method.

The results show that the mixture model is capable of predicting correctly the dynamic response of masonry walls up to a frequency which is well above

the second modal frequency. It is also found that the mixture model remains valid in the presence of micro cracks which may exist between mortar and brick constituents.

ACKNOWLEDGEMENTS

The research reported here was supported by Grant No. O-21851 from the National Science Foundation to the University of California at Berkeley, and NATO Project No. 1446 with the Middle East Technical University in Ankara, Turkey and the University of California at Berkeley. The support is gratefully acknowledged.

TABLE OF CONTENTS

LIST OF TABLES

LIST OF FIGURES

1. INTRODUCTION

This report describes the first phase of a study the object of which is to develop a mathematical model for predicting the response of masonry walls to dynamic excitation. To our knowledge, such a model has not previously been developed, although a considerable number of experimental studies [1-6], aimed at modifying and improving the existing codes for masonry structures, have been undertaken. Mayes et al. [1-3] were concerned essentially with the strength, failure modes and cyclic shear behavior of masonry piers. Hidalgo et al. [4] studied the cyclic behavior of masonry piers subjected to load reversals. Gülkan et al. [5,6] tested single-story masonry houses on a shaking table and investigated their experimental behavior by subjecting them to earthquake excitations.

This phase of the analysis is concerned with the dynamic behavior of masonry walls in the linear range. The second phase of the work, which will be done in the future, will use the results established here and the insight gained to extend the analysis to the nonlinear range.

The study is presented in three main stages: first, the experimental dynamic behavior of the masonry wall specimens is examined, then a mathematical model is chosen; finally, the parameters appearing in the model are determined through optimization. The selection of the form of the mathematical model is the most crucial stage in the analysis. An appropriate model can be chosen only after careful interpretation of the experimental data. With a poor model the analysis may fail to produce the optimum values of the model parameters even if the most powerful optimization algorithm is used.

The experiments were performed at the Earthquake Engineering Research Center of the University of California, Berkeley, U.S.A.. In these experiments

masonry wall specimens were subjected to base motions on the shaking table. Two types of base motion were applied in the experiments; one periodic (parallel to the wall, in both the horizontal and vertical directions), the other derived from ground motion records of the El Centro 1940 earthquake. The amplitudes of the base motions were kept small since the linear behavior of the walls was our primary concern. During the tests, accelerations at the top and bottom of the wall were recorded using accelerometers.

The most distinct feature of the experimentally observed behavior of the masonry wall specimens is that their first and second modal frequencies are close to each other. They are approximately equal to 19 and 24 Hz for horizontal motions of the wall specimens. It is suspected, on physical grounds, that the closeness of these modal frequencies is due to strong interaction between the mortar and brick phases of the wall. Consequently, the model should be capable of predicting these close frequencies but also able to differentiate between the two phases of the wall. In view of this reasoning, the mixture model is chosen for the analysis. (The theoretical framework of the mixture model has already been established in references [8-11].) The mixture model replaces the heterogeneous wall material by a two phase homogeneous material and takes into account the interaction between the two phases. The results obtained using this model indicate that the above speculation is well-founded. In fact, it is found that the mixture model has the ability to describe correctly, not only the closely spaced modal frequencies, but also other experimentally observed characteristics of the wall behavior. Moreover, the model is valid for both horizontal and vertical motions and has the flexibility of incorporating the debonding characteristics of the wall.

In this study, the equations of the mixture model, which are partial differential equations, are simplified and put in a discrete form by following

a procedure outlined in reference [12]. The resulting equations relate the top displacements to the base displacements of the wall. The use of a discrete mixture model is preferred because it simplifies the analysis. For the discrete model the determination of the theoretical response requires the solution of ordinary differential equations only, rather than the partial differential equations of a continuum model. In deriving the discrete model from the continuum model, care is taken to preserve the capabilities of the model discussed in the previous paragraph. The discrete model contains mass, elastic stiffness and damping coefficients, which are to be determined through optimization.

The mixture model has the property that it reduces to a simple model, called the effective modulus model, as a special case. The effective modulus model is a one phase homogeneous model describing the wall behavior only up to the first modal frequency. This simple model is also considered in the analysis.

The model parameters are obtained through optimization by matching the theoretical and experimental complex response functions (which are designated by H_u^t and H_u^e, respectively) in frequency space. The response function used in the study relates the top acceleration (output) to the base acceleration (input) and is defined by the ratio (Fourier transform of output) / (Fourier transform of input). The use of frequency space (rather than time space) and matching H_u^e and H_u^t are preferred in the optimization analysis for several reasons. First, the analysis indicates that matching the response functions in frequency space is very crucial and can be used as a criterion for the accuracy of the model. This criterion determines the frequency range over which the model is valid. Then with this knowledge, we can determine in advance whether or not the model adequately predicts

the response of the wall in time space to a given input by studying the Fourier spectrum of that input. Secondly, working in frequency space simplifies the optimization analysis because in frequency space the equations are simpler and there are less data points than in time space. In fact, to determine the theoretical response of the wall in time space we have to solve differential equations, but only simple algebraic equations in frequency space.

The response function (theoretical and experimental) is found using the definition given above. The Fast Fourier Transform (FFT) algorithm is used to evaluate H_u^e. A full discussion of Fourier analysis and of the FFT can be found in references [13-21].

In the optimization, an object (error) function is introduced to measure the accuracy of the match between H_u^e and H_u^t. It is defined as the integral of $|H_u^t - H_u^e|^2$ over the frequency interval considered in the analysis and is a function of the model parameters. Optimum values of the model parameters are computed by using the Gauss-Newton method to minimize the object function. For this and other optimization methods, see references [22-27].

The results for both horizontal and vertical motions of the wall are presented and discussed in Chapters 6 and 7. It is found that the mixture model describes the wall behavior correctly up to a frequency which is well above the second modal frequency. It is also observed that the mixture model, with optimum values of the parameters computed through optimization in frequency space, predicts accurately the response of the wall in time space as expected in view of the argument given previously.

Finally we should point out that, although the two wall specimens tested have the same dimensions and are made of the same type of mortar and brick, they have quite different response functions (see Figs. 13,14). This

difference is due to their having different distributions of micro cracks which may exist between mortar and brick layers. Figures 13 and 14 show that the mixture model gives a good match for the response of both walls. This is anticipated because, as mentioned previously, the mixture model has the capability of taking into account the debonding characteristics of the wall.

Presentation of the study is arranged as follows. The experimental work is outlined in Chapter 2. The theoretical models are presented in Chapter 3, the theoretical and experimental frequency response functions are evaluated in Chapter 4. The optimization analysis is given in Chapter 5. In Chapter 6 the numerical results are presented and discussed and an assessment of the proposed models is made in Chapter 7.

2. EXPERIMENTS

The experiments were performed on a brick masonry wall specimen at the laboratories of Earthquake Engineering Research Center of the University of California during July and August 1979.

2.1 The Test Specimen

The test specimen was composed of two parallel walls connected to a steel base frame which, in turn, was attached to the shaking table. The upper ends of the two walls were connected to each other by means of a second steel frame. During experiments weights (concrete blocks) were put on the top frame (see Figs. 1 to 4). The total weight was 45,210 N (10,160 lbs). The dimensions of the walls are shown in Fig. 5. The mortar thicknesses and the dimensions of the brick used in constructing the walls are also indicated in Fig. 5.

In both of the walls no reinforcing was used and the mortar was of type S. The compressive strength (per gross unit area) of the bricks was 3304 N/cm^2 (4790 psi).

2.2 Instrumentation

The following instruments were used for each wall:

(i) Two accelerometers (at the middle of the lower and upper edges of the wall) measuring inplane horizontal base and top accelerations. (Figs. 3 and 6)

(ii) Two accelerometers (at the middle of the lower and upper edges of the wall) measuring vertical base and top accelerations. (Figs. 3 and 6)

(iii) Two potentiometers (directed along the two vertical edges of the wall) measuring vertical displacements.

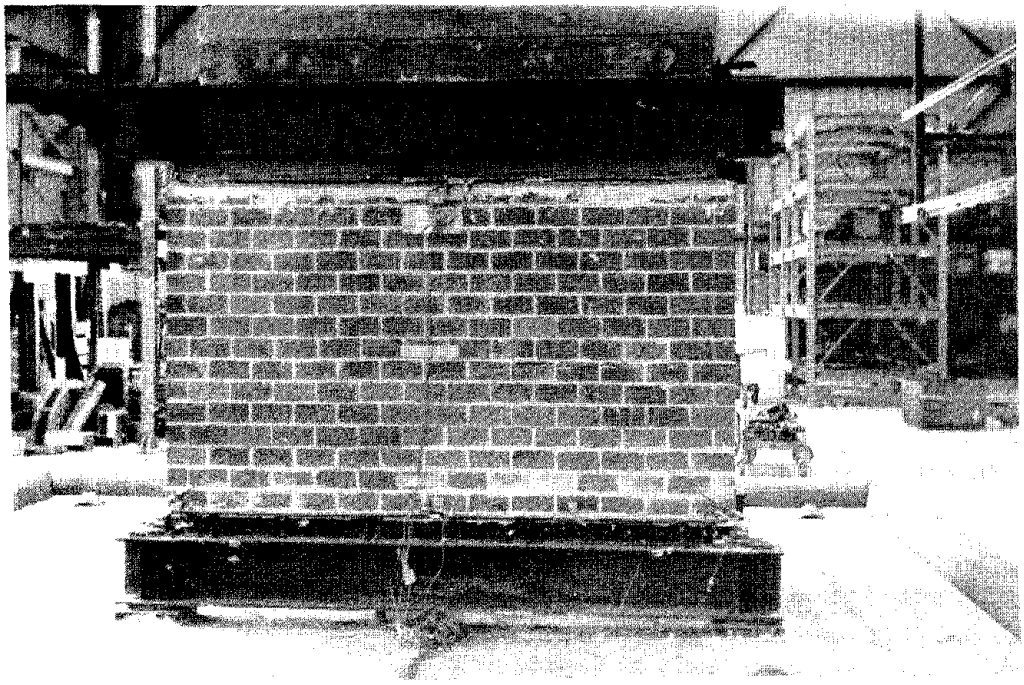

Figure 1. Front view photograph of the wall specimen on the shaking table

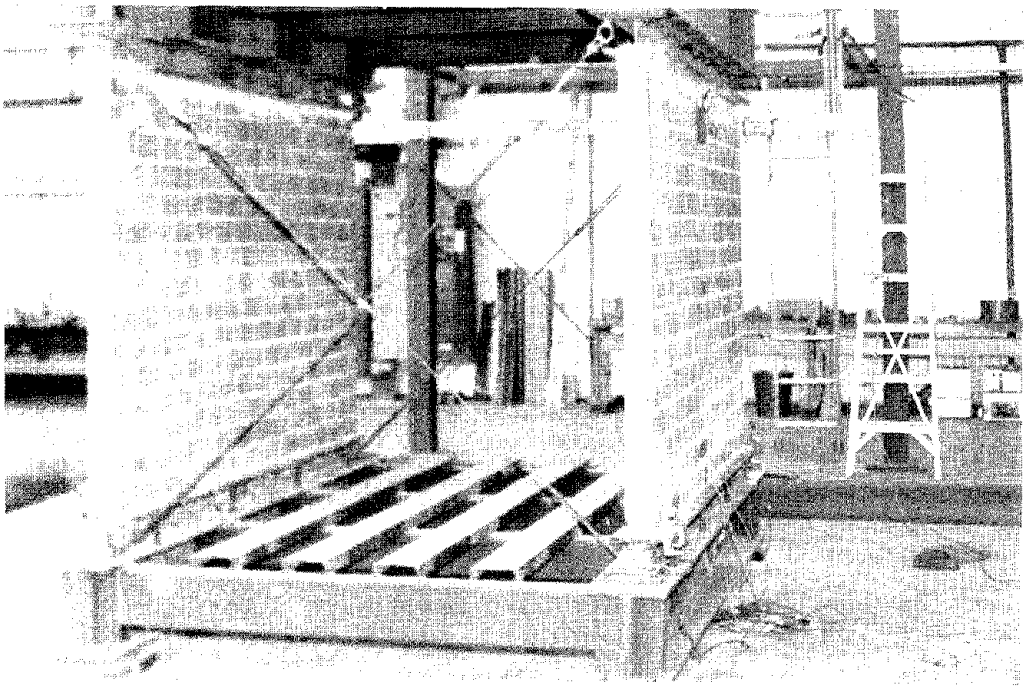

Figure 2. Side view photograph of the wall specimen on the shaking table

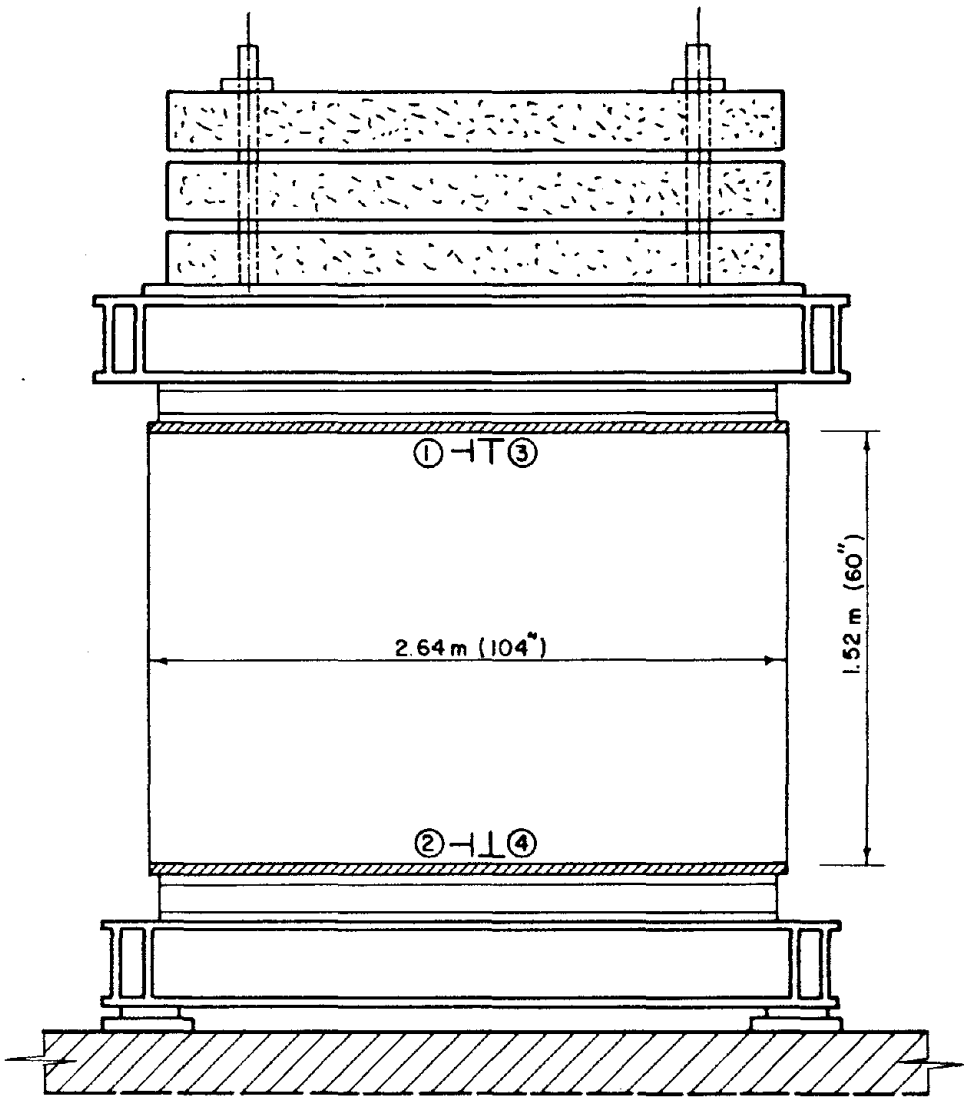

Figure 3. Front view of the wall specimen on the shaking table

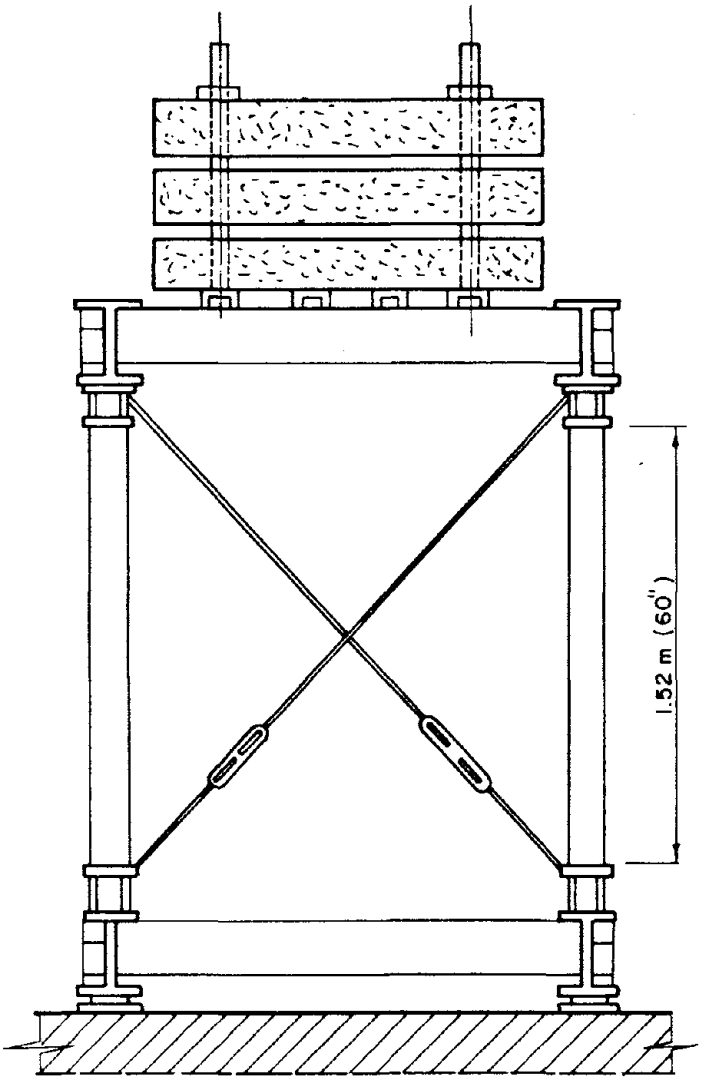

Figure 4. Side view of the wall specimen on the shaking table

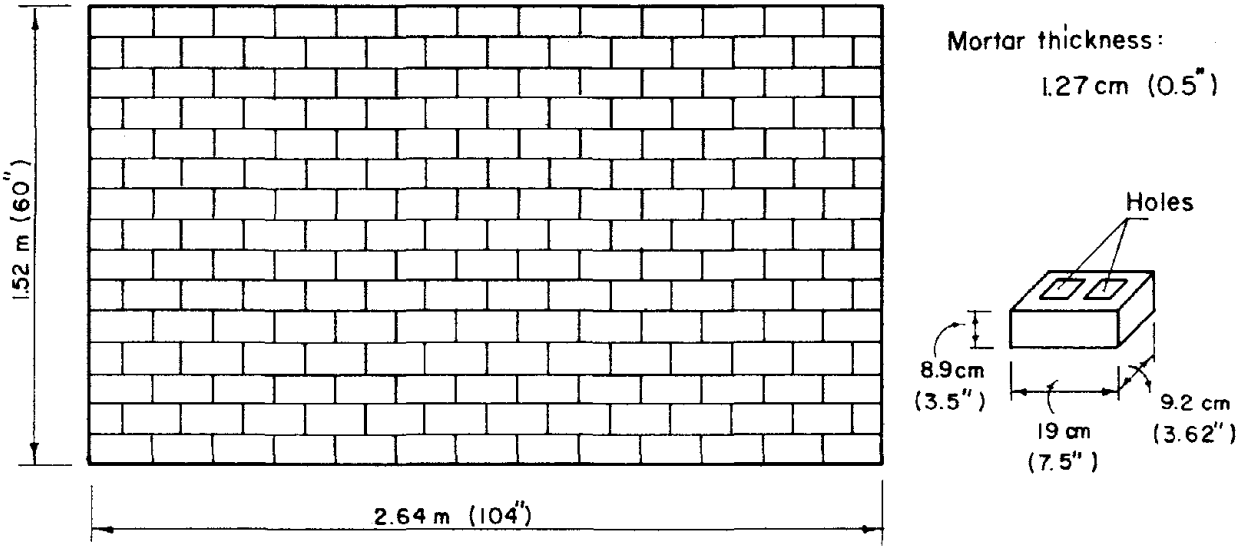

Figure 5. Geometric properties of the wall specimen, brick and mortar

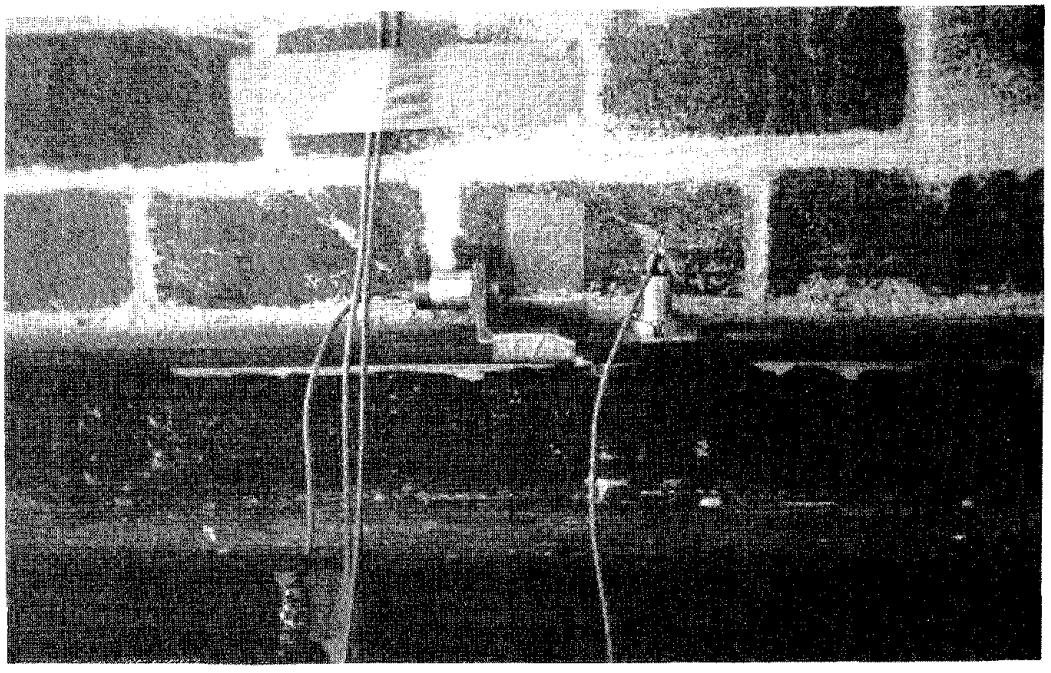

Figure 6. Photograph of the accelerometers measuring vertical and horizontal base accelerations

(iv) Two DCDT's (directed along the two diagonals of the rectangular flat surface of the wall) measuring the displacements in the directions of the diagonals.

(v) One potentiometer measuring the absolute inplane horizontal displacement of the upper edge of the wall from a fixed point.

2.3 Types of Input

The test specimen was subjected to the following three types of inplane base motion generated by the shaking table: horizontal periodic, vertical periodic and modified El Centro 1940. All types of input motion were recorded at equally spaced intervals along the time axis with a time increment of 0.00988 second.

2.3.1 Horizontal Periodic Input

The direction of motion was horizontal and in the plane of the wall. The periodic motion was approximately harmonic and possessed a fundamental driving frequency which was kept constant during the experiment. This frequency varied from 3 Hz to 30 Hz for different tests, with an increment between tests of 3 Hz or 1 Hz, depending on the occurrence of the resonance phenomena. The amplitude was about 0.05 g (g is gravitational acceleration).

2.3.2 Vertical Periodic Input

The direction of motion was vertical and the driving frequency varied from 3 Hz to 30 Hz for different tests, as in Section 2.3.1. The amplitude was about 0.05 g.

2.3.3 Modified El Centro 1940 Input

This input is obtained from the El Centro 1940 record by modifying it as follows: The shape of the time variation of the El Centro record is kept the same. The time scale is squeezed by dividing the times in the original

record by a scale factor. In mathematical terms, if f(t) and g(t) are the original and modified records respectively, where t = time, then g(t) would be related to f(t) by the relation g(t) = f(st), where s is the time scale factor. This equation indicates that the value of the original record at a certain time, say at $t = \hat{t}$, would be shifted to the time $\hat{t}/s$ in the modified record. The scale factors are shown to be 2.45, 3.46 and 7.7. The reason for changing the time scale was to make the contributions coming to the output from high frequency components of the input significant. Thus the mathematical model can be established in a larger frequency range and consequently the high frequency behavior of the wall will be taken into consideration.

Since our objective was to determine the model parameters of the wall in the linear range, the amplitudes of the inputs were kept small in the tests. Maximum amplitudes of various modified El Centro inputs having different scale factors are shown in Table 1 (in Table 1, üg designates the table acceleration). After all of the tests were completed, the wall was subjected to the El Centro input with the scale factor 7.7 and its amplitude was increased until the wall cracked.

Table 1

Maximum amplitudes of modified El Centro inputs

Time Scale Factor	1.0 (Normal Scale)							2.45			
Run No.	1	2	3	4	5	6	7	8	9	10	11
Max |üg| /g	0.043	0.097	0.155	0.198	0.361	0.403	0.525	0.074	0.233	0.314	0.457

Time Scale Factor	3.46			7.70							
Run No.	12	13	14	15	16	17	18	19	20	21	22
Max |üg| /g	0.155	0.338	0.569	0.236	0.359	0.488	0.597	0.750	0.874	1.046	1.203

Typical records are shown in Figs. 7 and 8 for a horizontal periodic table acceleration with a driving frequency of 18.58 Hz and for the modified El Centro input with the time scale factor 3.46, respectively ($\ddot{u}^+$ is the horizontal top acceleration).

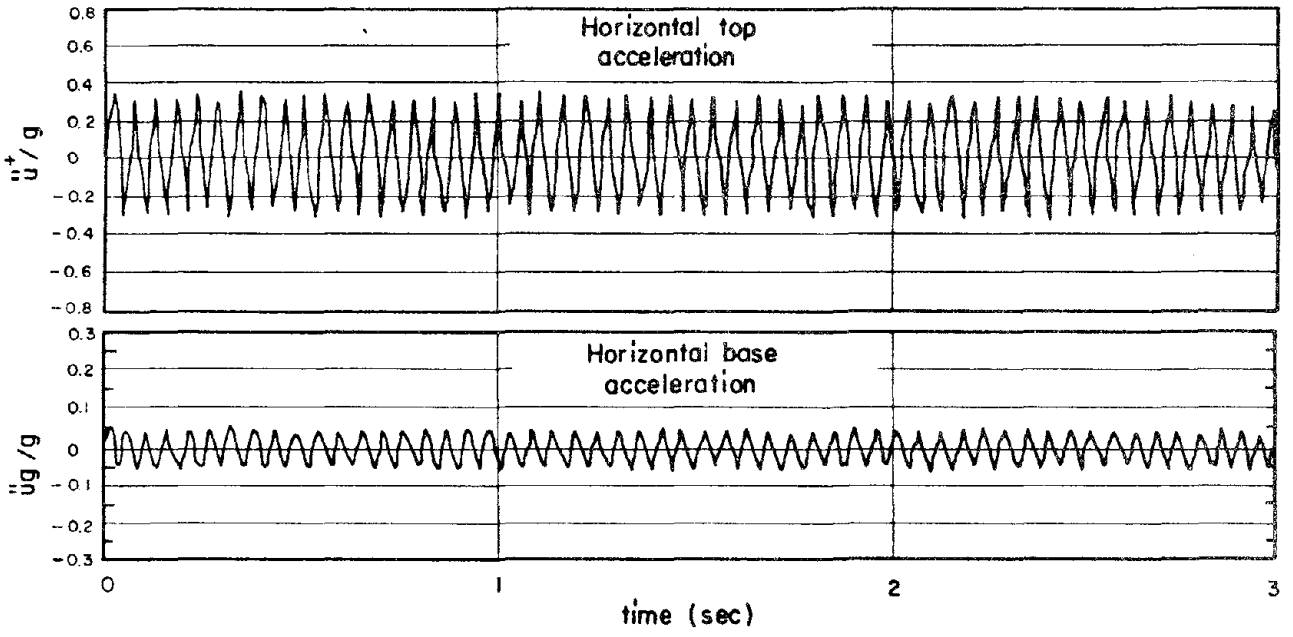

Figure 7. A sample record of an input-output acceleration pair in a periodic run (driving frequency = 18.58 Hz)

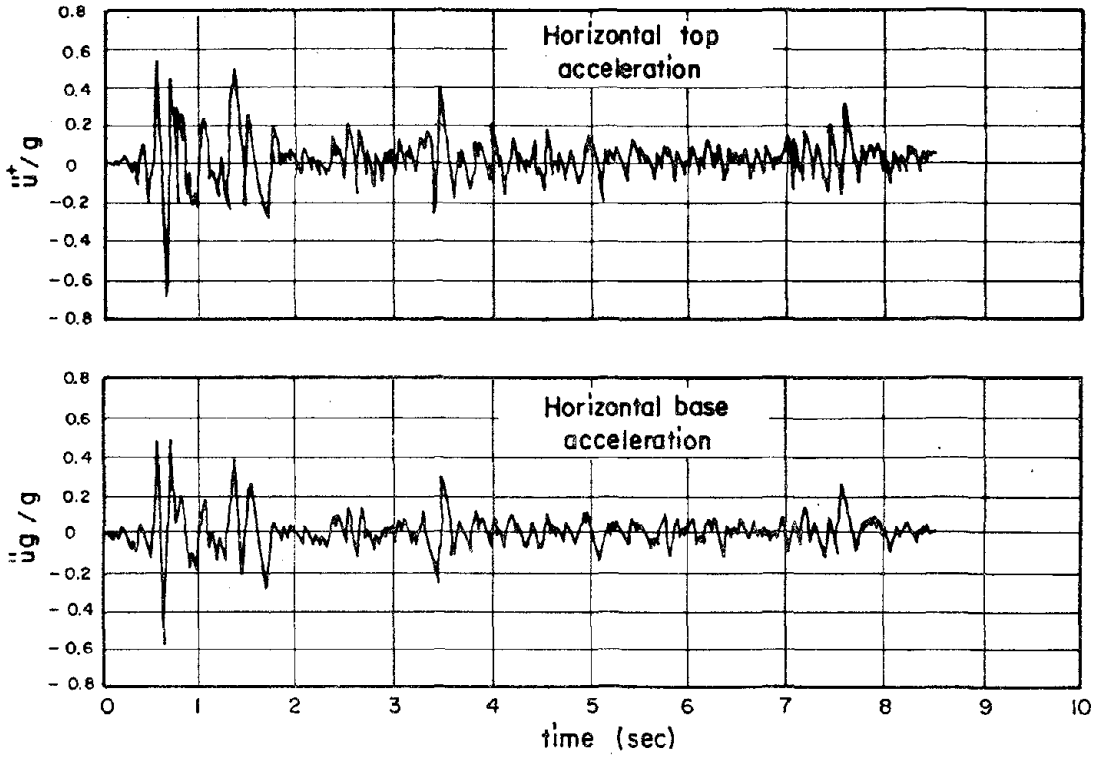

Figure 8. A sample record of an input-output acceleration pair in an El Centro run (time scale factor = 3.46)

3. THEORETICAL MODEL

To predict the dynamic behavior of the masonry wall two different mathematical models are chosen, namely the models based on mixture and effective modulus theories. Since the effective modulus model is a special case of the mixture model, the model based on mixture theory is discussed first.

3.1 General Theory

The mixture model replaces the heterogeneous material of the wall by a homogeneous one exhibiting orthotropic symmetry. It treats the wall as a composite made of brick and mortar constituents and takes into account the interaction between them. The equations of the model are composed of constitutive equations, linear momentum equations and strain - displacement relations. The wall under study is referred to a Cartesian coordinate system (x_1, x_2, x_3) where the origin is coincident with the centroid of the wall. The $(x_1 - x_2)$ plane coincides with the midplane of the wall and the x_1 axis is parallel to the horizontal layering (see Fig. 9). Then, using the results established in references [8-11], the governing equations for the inplane motions of the wall are as follows:

Linear momentum equations:

$$\begin{aligned} \partial_j \sigma^1_{ji} + F^1_i + Q_{ij}(u^2_j - u^1_j) &= m^1_{ij}\ddot{u}^1_j - q_{ij}\ddot{u}^2_j \\ \partial_j \sigma^2_{ji} + F^2_i + Q_{ij}(u^1_j - u^2_j) &= -q_{ij}\ddot{u}^1_j + m^2_{ij}\ddot{u}^2_j \end{aligned} \tag{3.1}$$

Constitutive equations:

$$\begin{bmatrix} \sigma^1_{11} \\ \sigma^1_{22} \\ \sigma^1_{12} \end{bmatrix} = \begin{bmatrix} s^{11}_{11} & s^{11}_{12} & 0 \\ s^{11}_{12} & s^{11}_{22} & 0 \\ 0 & 0 & s^{11}_{44} \end{bmatrix} \begin{bmatrix} e^1_{11} \\ e^1_{22} \\ 2e^1_{12} \end{bmatrix} + \begin{bmatrix} s^{12}_{11} & s^{12}_{12} & 0 \\ s^{12}_{21} & s^{12}_{22} & 0 \\ 0 & 0 & s^{12}_{44} \end{bmatrix} \begin{bmatrix} e^2_{11} \\ e^2_{22} \\ 2e^2_{12} \end{bmatrix}$$

$$\begin{bmatrix} \sigma^2_{11} \\ \sigma^2_{22} \\ \sigma^2_{12} \end{bmatrix} = \begin{bmatrix} s^{12}_{11} & s^{12}_{21} & 0 \\ s^{12}_{12} & s^{12}_{22} & 0 \\ 0 & 0 & s^{12}_{44} \end{bmatrix} \begin{bmatrix} e^1_{11} \\ e^1_{22} \\ 2e^1_{12} \end{bmatrix} + \begin{bmatrix} s^{22}_{11} & s^{22}_{12} & 0 \\ s^{22}_{12} & s^{22}_{22} & 0 \\ 0 & 0 & s^{22}_{44} \end{bmatrix} \begin{bmatrix} e^2_{11} \\ e^2_{22} \\ 2e^2_{12} \end{bmatrix} \qquad (3.2)$$

Strain-displacement relations:

$$e^\alpha_{ij} = \frac{1}{2}\left(\partial_i u^\alpha_j + \partial_j u^\alpha_i\right), \qquad (\alpha=1,2) \qquad (3.3)$$

where

σ^α_{ij} : partial stress components for the α phase measured per unit area of the wall material

F^α_i : partial body force components for the α phase measured per unit volume of the wall material

u^α_i : displacement components averaged over the α phase

e^α_{ij} : strain components for the α phase.

In writing Eqs. (3.1, 3.3) the indicial notation is used. The subscripts i,j take the values 1 and 2 only, and a repeated index implies summation over the range of that index. The dot denotes partial differentiation with respect to time and ∂_j stands for $\partial/\partial x_j$.

In Eqs. (3.1 - 3.3) the superscripts 1 and 2 differentiate the two phases of the wall. In the following analysis the superscript 1 designates the mortar phase while the superscript 2 designates the brick phase.

It is noted that the constitutive equations, Eqs. (3.2), exhibit orthotropic symmetry, and the constitutive equations of the mortar and brick phases are coupled. This implies that the partial stress of one phase would be affected not only by the deformation of that phase, but also by the deformation of the other. In order to accommodate the dissipated energy, which may be due to various causes (e.g., to friction produced by slipping between the brick and mortar phases), it is assumed that the constitutive equations are viscoelastic and viscoelastic moduli $s_{mn}^{\alpha\beta}$ appearing in these equations are differential operators in time. The Kelvin (Voight) model has been chosen for the viscoelastic constitutive equations. Accordingly the viscoelastic moduli $s_{mn}^{\alpha\beta}$ have the form $s_{mn}^{\alpha\beta} = k_{mn}^{\alpha\beta} + c_{mn}^{\alpha\beta}D$, where $D = d/dt$. The constants $k_{mn}^{\alpha\beta}$ and $c_{mn}^{\alpha\beta}$ represent elastic and viscous (damping) coefficients, respectively.

The terms Q_{ij}, m_{ij}^{α} (α=1,2) and q_{ij} in Eqs. (3.1) have the forms

$$(Q_{ij}) = \begin{bmatrix} Q_1 & 0 \\ 0 & Q_2 \end{bmatrix} \; ; \; \underline{m}^{\alpha} = (m_{ij}^{\alpha}) = \begin{bmatrix} (\rho_{\alpha} + q_1) & 0 \\ 0 & (\rho_{\alpha} + q_2) \end{bmatrix} ; \tag{3.4}$$

$$\underline{q} = (q_{ij}) = \begin{bmatrix} q_1 & 0 \\ 0 & q_2 \end{bmatrix}$$

which, as noted before, exhibit orthotropic symmetry. In Eqs. (3.4) ρ_{α} denotes the partial mass, defined as the mass of the α phase per unit volume of the wall. q_1 and q_2 are constants with the dimension of mass per unit volume. Q_1 and Q_2 are some viscoelastic time dependent operators which, in view of the Kelvin model chosen in the analysis, take the form $Q_{\alpha}=k_{\alpha}+c_{\alpha}D$. It is observed from Eqs. (3.1) that (Q_{ij}) and (q_{ij}) represent the linear momentum interaction between the phases. A detailed discussion and interpretation of the terms Q_{ij}, m_{ij}^{α} and q_{ij} can be found in [8].

A comment regarding some conditions to be satisfied by the constants $k_{mn}^{\alpha\beta}$, $c_{mn}^{\alpha\beta}$, q_α, q_α, k_α and c_α is now in order. Since the kinetic energy, strain energy and the energy loss due to dissipation are always positive the matrices

$$\begin{bmatrix} \underline{m}^1 & -\underline{q} \\ -\underline{q} & \underline{m}^2 \end{bmatrix} ; \begin{bmatrix} \underline{k}^{11} & \underline{k}^{12} \\ \underline{k}^{12T} & \underline{k}^{22} \end{bmatrix} ; \begin{bmatrix} \underline{c}^{11} & c^{12} \\ \underline{c}^{12T} & \underline{c}^{22} \end{bmatrix} ; \begin{bmatrix} k_1 & 0 \\ 0 & k_2 \end{bmatrix} ; \begin{bmatrix} c_1 & 0 \\ 0 & c_2 \end{bmatrix} \tag{3.5}$$

should be positive definite, where $\underline{m}^\alpha = (m_{ij}^\alpha)$, $\underline{q} = (q_{ij})$, $\underline{k}^{\alpha\beta} = (k_{mn}^{\alpha\beta})$, $\underline{c}^{\alpha\beta} = (c_{mn}^{\alpha\beta})$ and $(\cdot)^T$ designates the transpose of $(\cdot)$. It should be noted that the first is a 4 x 4 matrix, the second and third are 6 x 6 matrices and the last two are 2 x 2 matrices.

Since this study is concerned with analysis involving the motion of the wall in its own plane, the equations of the mixture theory in the preceding paragraphs are given for the two dimensional case. However, if the out-of-plane motion of the wall is to be considered as well as the in-plane, the three dimensional equations of mixture theory should be considered. These equations will have exactly the same form as Eqs. (3.1 - 3.3) and again the terms q_{ij}, Q_{ij}, m_{ij}^α will exhibit orthotropic symmetry. But in the three dimensional case the indices i, j in Eqs. (3.1, 3.3) take values from 1 to 3; the matrices associated with Q_{ij}, q_{ij}, m_{ij}^α would be three dimensional and the matrices formed by the material moduli $s_{mn}^{\alpha\beta}$ in Eqs. (3.2) would be six dimensional.

3.2 Formulation of Special Problem Associated with Experiments

Using the loading and geometric conditions of the wall specimen we now establish equations governing the theoretical response of the wall. Because the width b of the wall is large compared to its height H (see Figs. 3 and 5) and the input in the experiments (base acceleration) is uniform

over the lower end of the wall, boundary effects coming from vertical edges of the wall will be disregarded. With this assumption, the dependent variables are functions of x_2 and t only. Then the governing equations, Eqs. (3.1 - 3.3), for the inplane horizontal and vertical motions of the wall reduce to the following forms;

linear momentum equations:

$$\begin{aligned} \partial_x \sigma_1 + Q(u_2 - u_1) &= (\rho_1 + q)\ddot{u}_1 - q\ddot{u}_2 \\ \partial_x \sigma_2 + Q(u_1 - u_2) &= -q\ddot{u}_1 + (\rho_2 + q)\ddot{u}_2 \end{aligned} \tag{3.6}$$

constitutive equations:

$$\begin{bmatrix} \sigma_1 \\ \sigma_2 \end{bmatrix} = \begin{bmatrix} s_{11} & s_{12} \\ s_{12} & s_{22} \end{bmatrix} \begin{bmatrix} \partial_x u_1 \\ \partial_x u_2 \end{bmatrix} \tag{3.7}$$

where

$$(\sigma_\alpha, u_\alpha, Q, q, s_{\alpha\beta}) = \begin{cases} (\sigma_{12}^\alpha, u_1^\alpha, Q_1, q_1, s_{44}^{\alpha\beta}) \text{ for horizontal motion} \\ \\ (\sigma_{22}^\alpha, u_2^\alpha, Q_2, q_2, s_{22}^{\alpha\beta}) \text{ for vertical motion} \end{cases} \tag{3.8}$$

and x stands for x_2. In Eq. (3.8), the indices α and β distinguish the phases and take values 1 or 2 for mortar or brick constituents, respectively. In writing Eqs. (3.6, 3.7) it is assumed that, for the vertical motion, σ_α, u_α represent the deviations of stress and displacement from their static values. These static values are associated with the equilibrium state of the wall which exists initially under the influence of the weight of the wall and the top weight.

Before writing the boundary conditions along the upper and lower ends of the wall, volume ratios will be introduced. The volume ratio n_α is defined as the volume of the α phase per unit volume of the wall and satisfies the equation $n_1 + n_2 = 1$. The partial mass ρ_α and actual mass density

ρ_α^R of the α phase are related through n_α by $\rho_\alpha = \rho_\alpha^R n_\alpha$ (α=1,2).

In writing the boundary conditions at the upper end x=H/2, it is assumed that the inertia force due to top weight is resisted by the partial phase stresses σ_1 and σ_2 associated with the factors n_1 and n_2, respectively. This leads to

$$n_1 \frac{\bar{m}}{h'} (n_1\ddot{u}_1^+ + n_2\ddot{u}_2^+) + \sigma_1^+ = 0 \qquad (3.9)$$

$$n_2 \frac{\bar{m}}{h'} (n_1\ddot{u}_1^+ + n_2\ddot{u}_2^+) + \sigma_2^+ = 0$$

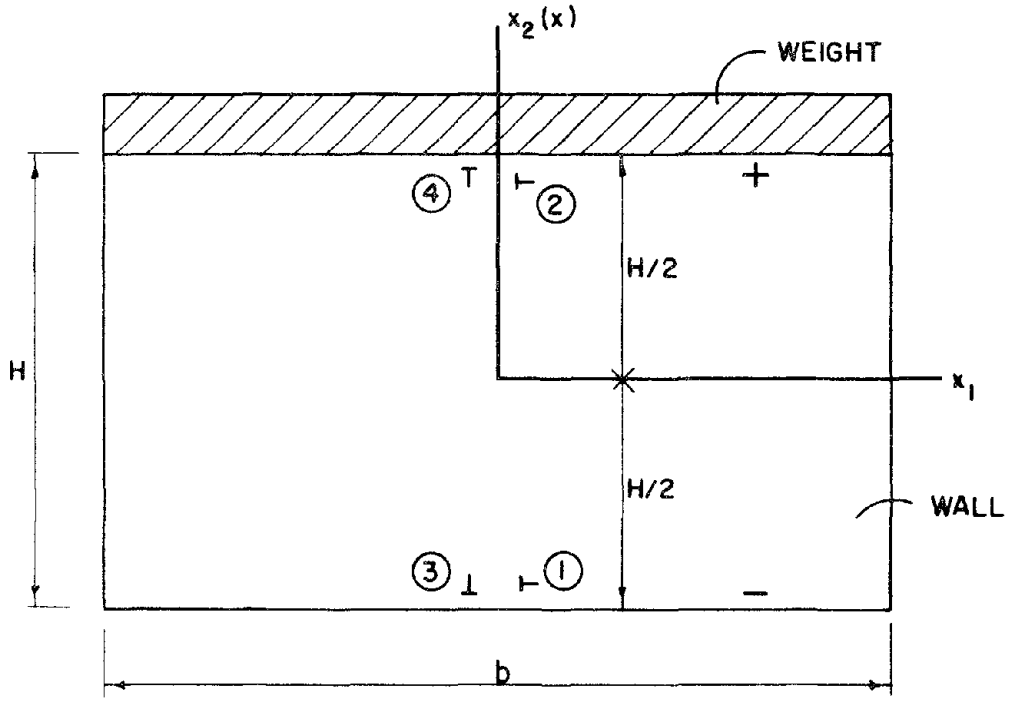

Figure 9. Geometric description of the wall and the locations of accelerometers

where $\bar{m}$ is the mass of the top weight per unit length of the wall and h' is the thickness of the wall. In Eqs. (3.9), the notation $(\cdot)^{\mp} = (\cdot)|_{x=\mp H/2}$ is used (see Fig. 9). In writing Eqs. (3.9) it is assumed that the acceleration of the top weight can be expressed in terms of phase accelerations at the top by $(n_1\ddot{u}_1^+ + n_2\ddot{u}_2^+)$. This assumption is consistent with smoothing operations used in the development of the mixture theory.

The boundary conditions at the lower end of the wall (x = -H/2) can be expressed in terms of base acceleration (measured using accelerometers 1 and 3). In agreement with the idealization implied by the mixture theory (see [8-11]), the phase accelerations are both assumed to be equal to the base acceleration at the lower end. Thus,

$$\ddot{u}_1^- = \ddot{u}_2^- = \ddot{u}_g(t). \tag{3.10}$$

In Eq. (3.10) $\ddot{u}_g$ represents the horizontal or vertical base acceleration depending upon whether the horizontal or vertical motion of the wall is being considered.

In this analysis it is more convenient to work with the dependent variables σ, τ, u, ψ defined by

$$\begin{aligned} &\sigma = \sigma_1 + \sigma_2 \quad ; \quad \tau = \sigma_1 - \sigma_2 \\ &u = (u_1 + u_2)\ /\ 2; \quad \psi = (u_1 - u_2)\ /2 \end{aligned} \tag{3.11}$$

rather than the variables σ_α, u_α. Note that σ defined in Eqs. (3.11) is the total stress measured per unit area of the wall and u is the average of the phase displacements. In terms of these new variables, the governing equations, Eqs. (3.6, 3.7), and the boundary conditions, Eqs. (3.9, 3.10), are as follows;

linear momentum equations:

$$\begin{aligned} &\partial_x\sigma = \rho\ddot{u} + s\ddot{\psi} \\ &\partial_x\tau - Q'\psi = s\ddot{u} + n\ddot{\psi} \end{aligned} \tag{3.12}$$

constitutive equations:

$$\begin{bmatrix} \sigma \\ \tau \end{bmatrix} = \begin{bmatrix} S_{11} & S_{12} \\ S_{12} & S_{22} \end{bmatrix} \begin{bmatrix} \partial_x u \\ \partial_x \psi \end{bmatrix} \tag{3.13}$$

boundary conditions:

$$\begin{aligned} &\frac{\bar{m}}{h'}(e_{11}\ddot{u}^{+} + e_{12}\ddot{\psi}^{+}) + \sigma^{+} = 0 \\ &\frac{\bar{m}}{h'}(e_{12}\ddot{u}^{+} + e_{22}\ddot{\psi}^{+}) + \tau^{+} = 0 \\ &\ddot{u}^{-} = \ddot{u}_g(t); \qquad \ddot{\psi}^{-} = 0 \end{aligned} \tag{3.14}$$

where

$$\begin{aligned} &\rho = \rho_1 + \rho_2 \; ; \qquad s = \rho_1 - \rho_2 \; ; \qquad n = \rho + 4q \\ &S_{11} = s_{11} + s_{22} + 2s_{12} \\ &S_{12} = s_{11} - s_{22} \\ &S_{22} = s_{11} + s_{22} - 2s_{12} \\ &Q' = 4Q \\ &e_{11} = 1 \; ; \qquad e_{12} = (n_1 - n_2) \; ; \qquad e_{22} = (n_1 - n_2)^2 \end{aligned} \tag{3.15}$$

The total mass density ρ defined in Eqs. (3.15) designates the mass of the wall material per unit volume.

Since the matrices (3.5) are positive definite, the matrices

$$\begin{bmatrix} \rho & s \\ s & n \end{bmatrix} \; ; \begin{bmatrix} k_{11} & k_{12} \\ k_{12} & k_{22} \end{bmatrix} \; ; \begin{bmatrix} c_{11} & c_{12} \\ c_{12} & c_{22} \end{bmatrix}$$

are also positive definite, and k and c are positive, where ($k_{\alpha\beta}$, k) and $c_{\alpha\beta}$, c) are, respectively, elastic and viscous coefficients of the operators ($S_{\alpha\beta}$, Q'); i.e., $S_{\alpha\beta} = k_{\alpha\beta} + c_{\alpha\beta}D$ and $Q' = k + cD$.

The solution of Eqs. (3.12, 3.13) subject to the boundary conditions, Eqs. (3.14), and zero initial conditions (the motion is assumed to start from rest position) determines the theoretical response.

3.3 The Discrete Model

The governing equations, Eqs. (3.12, 3.13), constitute a system of partial differential equations and determination of the theoretical response involves integration of these complicated equations. Therefore it is desirable to reduce them to a simpler form that is more suitable for optimization analysis. This reduction is made using a modified version of Galerkin's method proposed in [12] in connection with developing a higher order dynamic approximate theory for plates. As will be seen shortly, the resulting equations describe a discrete model.

Derivation of the equations of the discrete model starts by referring to Fig. 9. Let h be half of the weight of the wall, i.e., h = H/2, and $\bar{x}$ be a nondimensional distance measured in the vertical direction, defined by $\bar{x} = x/h$. To develop a discrete model we first choose a set of distribution functions $\{\phi_i(\bar{x}),\ i = 0,1,\ldots\}$, which form a complete set in the sense that a given function $f(\bar{x})$ in the interval $-1 \leq \bar{x} \leq 1$ can be represented by the series

$$\sum_{i=0}^{\infty} \alpha_i \phi_i(\bar{x}), \quad \text{i.e.,} \quad \lim_{N\to\infty} \sum_{i=0}^{N} \alpha_i \phi_i(\bar{x}) = f(\bar{x}),$$

where α_i are some constants. For developing an m th order model, the elements $\{\phi_0, \phi_1, \ldots\ldots, \phi_m, \phi_{m+1}, \phi_{m+2}\}$ of the set should be retained, since the two additional functions ϕ_{m+1}, ϕ_{m+2} are necessary to satisfy the end boundary conditions of the wall exactly. To keep the discrete model as simple as possible and for reasons which will be discussed later, the value of m is taken to be zero in the analysis, i.e., only the elements ϕ_0, ϕ_1

and ϕ_2 of the set are retained. The resulting equations will then constitute a zeroth order model. Legendre polynomials, which are orthogonal, are chosen as distribution functions to simplify the analysis; i.e., $\phi_i = P_i$ (i = 0,1,2 and P_i is the i th order Legendre polynominal) or, explicitly,

$$\phi_0 = 1 \; ; \quad \phi_1 = \bar{x} \; ; \quad \phi_2 = (-1 + 3\bar{x}^2) / 2 \; . \tag{3.16}$$

It should be noted that ϕ_i thus chosen satisfy

$$\int_{-1}^{+1} \phi_i \phi_j d\bar{x} = \frac{2}{2\underline{i} + 1} \; \delta_{\underline{ij}}$$

$$\phi_0(\mp 1) = \phi_2(\mp 1) = 1 \; ; \quad \phi_1(\mp 1) = \mp 1 \tag{3.17}$$

$$\phi_0'(\mp 1) = 0 \; ; \quad \phi_1'(\mp 1) = 1 \; ; \; \phi_2'(\mp 1) = \mp 3$$

where δ_{ij} is the Kronecker delta, $(\cdot)' = d(\cdot) / d\bar{x}$ and a line appearing under a repeated index implies that the summation rule does not hold for that index.

Before starting the analysis, we will introduce an averaging operator, generalized displacements, and the end quantities involving the values of stresses and displacements at the lower and upper end of the wall, which are defined as follows.

Averaging operator:

$$L = \frac{1}{2h} \int_{-h}^{+h} (\cdot)\phi_0 dx, \tag{3.18}$$

generalized displacements:

$$(u_0, \psi_0) = L(u \; , \psi) \tag{3.19}$$

end quantities:

$$S^{\mp} = u^{+} \mp u^{-} \; ; \qquad \psi^{\mp} = \psi^{+} \mp \psi^{-}$$
$$R^{\mp} = \sigma^{+} \mp \sigma^{-} \; ; \qquad T^{\mp} = \tau^{+} \mp \tau^{-} \; . \tag{3.20}$$

To establish the equations of the zeroth order theory, first the weighted average of the linear momentum equations is taken over the height of the wall using ϕ_0 as the weighting function, i.e., the operator L is applied to Eqs. (3.12). This gives

$$\frac{R^{-}}{H} = \rho\ddot{u}_0 + s\ddot{\psi}_0$$
$$\frac{T^{-}}{H} - Q'\psi_0 = s\ddot{u}_0 + n\ddot{\psi}_0 \; . \tag{3.21}$$

To complete the equations of the approximate theory, the constitutive relations for the end quantities are added to Eqs. (3.21). With the object of establishing these equations, u and ψ are expanded in terms of ϕ_0, ϕ_1 and ϕ_2 as

$$u = a_0\phi_0 + a_1\phi_1 + a_2\phi_2$$
$$\psi = b_0\phi_0 + b_1\phi_1 + b_2\phi_2 \tag{3.22}$$

where a_i and b_i are some functions of time. Then in order to relate a_i and b_i to the dependent variables appearing in the approximate theory the operator L is applied to both of the equations in (3.22). Because the ϕ_i are orthogonal this gives

$$(a_0, b_0) = (u_0, \psi_0) \; . \tag{3.23}$$

To find the other (a_i, b_i), the values of u and ψ from Eqs. (3.22) at $x = \mp h$ are substituted into the expressions for $S^{\mp}$ and $\psi^{\mp}$ defined by Eqs. (3.20). This yields

$$a_1 = \frac{S^-}{2} \quad ; \quad b_1 = \frac{\psi^-}{2}$$
$$a_2 = \frac{S^+}{2} - u_o \quad ; \quad b_2 = \frac{\psi^+}{2} - \psi_o \ . \tag{3.24}$$

The final step in obtaining the constitutive relations of the end quantities involves first the substitution of Eqs. (3.22) into Eqs. (3.13), from which we obtain

$$\sigma = \frac{2S_{11}}{H}(a_1\phi_1' + a_2\phi_2') + \frac{2S_{12}}{H}(b_1\phi_1' + b_2\phi_2')$$
$$\tau = \frac{2S_{12}}{H}(a_1\phi_1' + a_2\phi_2') + \frac{2S_{22}}{H}(b_1\phi_1' + b_2\phi_2') \ . \tag{3.25}$$

Finally, if these expressions for σ and τ at $x = \mp h$ are substituted into the relations $R^{\mp} = \sigma^+ \mp \sigma^-$ and $T^{\mp} = \tau^+ \mp \tau^-$ the constitutive equations for the end quantities are

$$R^+ = \frac{2}{H}(S_{11}S^- + S_{12}\psi^-)$$
$$R^- = \frac{6}{H}[S_{11}(S^+ - 2u_o) + S_{12}(\psi^+ - 2\psi_o)]$$
$$T^+ = \frac{2}{H}(S_{12}S^- + S_{22}\psi^-) \tag{3.26}$$
$$T^- = \frac{6}{H}[S_{12}(S^+ - 2u_o) + S_{22}(\psi^+ - 2\psi_o)] \ .$$

In obtaining Eqs. (3.26), the defining expressions of ϕ_i $(i = 0,1,2)$ in Eqs. (3.16) are used.

The boundary conditions of the problem, Eqs. (3.14), can be expressed in terms of end quantities of the approximate theory. In view of Eqs. (3.20), they take the form

$$\frac{\bar{m}}{h'}[e_{11}(\ddot{S}^+ + \ddot{S}^-) + e_{12}(\ddot{\psi}^+ + \ddot{\psi}^-)] + R^+ + R^- = 0$$
$$\frac{\bar{m}}{h'}[e_{12}(\ddot{S}^+ + \ddot{S}^-) + e_{22}(\ddot{\psi}^+ + \ddot{\psi}^+)] + T^+ + T^- = 0$$
$$\ddot{S}^+ - \ddot{S}^- = 2\ddot{u}_g \tag{3.27}$$
$$\ddot{\psi}^+ - \ddot{\psi}^- = 0 \ .$$

The equations of the approximate theory are now complete. They are Eqs. (3.21, 3.26 and 3.27), which constitute ten equations governing the ten unknowns (u_o, ψ_o, $S^{\mp}$, $\psi^{\mp}$, $R^{\mp}$, $T^{\mp}$).

The reduced model equations can be simplified further by employing a procedure explained below. The procedure begins by taking the Fourier transforms of the model equations, Eqs. (3.21, 3.27 and 3.27), from which we obtain the following matrix equations:

linear momentum equations:

$$\frac{1}{\bar{H}} \begin{bmatrix} R^{-F} \\ T^{-F} \end{bmatrix} = - \begin{bmatrix} \rho\omega^2 & s\omega^2 \\ s\omega^2 & n\omega^2 - \bar{Q}' \end{bmatrix} \begin{bmatrix} u_o^F \\ \psi_o^F \end{bmatrix} \tag{3.28}$$

constitutive equations for end quantities:

$$\begin{bmatrix} R^{+F} \\ T^{+F} \end{bmatrix} = \frac{2}{\bar{H}} \begin{bmatrix} \bar{S}_{11} & \bar{S}_{12} \\ \bar{S}_{12} & \bar{S}_{22} \end{bmatrix} \begin{bmatrix} S^{-F} \\ \psi^{-F} \end{bmatrix} \tag{3.29}$$

$$\begin{bmatrix} R^{-F} \\ T^{-F} \end{bmatrix} = \frac{6}{\bar{H}} \begin{bmatrix} \bar{S}_{11} & \bar{S}_{12} \\ \bar{S}_{12} & \bar{S}_{22} \end{bmatrix} \begin{bmatrix} S^{+F} \\ \psi^{+F} \end{bmatrix} - \frac{12}{\bar{H}} \begin{bmatrix} \bar{S}_{11} & \bar{S}_{12} \\ \bar{S}_{12} & \bar{S}_{22} \end{bmatrix} \begin{bmatrix} u_o^F \\ \psi_o^F \end{bmatrix} \tag{3.30}$$

boundary conditions:

$$-\omega^2 \frac{\bar{m}}{h^T} \begin{bmatrix} e_{11} & e_{12} \\ e_{12} & e_{22} \end{bmatrix} \begin{bmatrix} S^{+F} + S^{-F} \\ \psi^{+F} + \psi^{-F} \end{bmatrix} + \begin{bmatrix} R^{+F} \\ T^{+F} \end{bmatrix} + \begin{bmatrix} R^{-F} \\ T^{-F} \end{bmatrix} = \underline{0} \tag{3.31}$$

$$\begin{aligned} S^{+F} - S^{-F} &= 2u_g^F \\ \psi^{+F} - \psi^{-F} &= 0, \end{aligned} \tag{3.32}$$

where $\bar{Q}' = k + i\omega c$; $\bar{S}_{\alpha\beta} = k_{\alpha\beta} + i\omega c_{\alpha\beta}$, $(\alpha,\beta = 1,2)$; ω is angular frequency; $i^2 = -1$ and $(\cdot)^F$ designates the Fourier transform of $(\cdot)$. Equations (3.28 to 3.32) correspond to the wall being initially at rest.

When $\underline{f}^{-F} = [R^{-F}\ T^{-F}]^T$ from Eq. (3.28) is substituted into Eq. (3.30),

$$-H\ \underline{A}\ \underline{W}_o^F = \frac{6}{H}\ \bar{\underline{S}}\ \underline{W}^{+F} - \frac{12}{H}\ \bar{\underline{S}}\ \underline{W}_o^F \quad . \tag{3.33}$$

Here

$$\underline{A} = \begin{bmatrix} \rho\omega^2 & s\omega^2 \\ s\omega^2 & n\omega^2 - \bar{Q}' \end{bmatrix}; \quad \bar{\underline{S}} = \begin{bmatrix} \bar{S}_{11} & \bar{S}_{12} \\ \bar{S}_{12} & \bar{S}_{22} \end{bmatrix} \quad ; \tag{3.34}$$

$$\underline{W}_o^F = [\ u_o^F \quad \psi_o^F\ ]^T \quad ; \quad \underline{W}^{+F} = [\ S^{+F} \quad \psi^{+F}\ ]^T \ .$$

After some manipulation, Eq. (3.33) can be written as

$$(\underline{I} - \frac{H^2}{12}\ \bar{\underline{S}}^{-1}\ \underline{A})\ \underline{W}_o^F = \frac{1}{2}\ \underline{W}^{+F} \tag{3.35}$$

where $\underline{I}$ is the identity matrix, and $(\cdot)^{-1}$ is the inverse of $(\cdot)$. It will be shown in Appendix A that the norm of $(H^2/12)\bar{\underline{S}}^{-1}\ \underline{A}$ is small compared to unity for the frequency range considered in this study and for the optimum values of the model parameters which will be found later. Accordingly, the inverse of the coefficient matrix of $\underline{W}_o$ in Eq. (3.35) is approximately equal to $(\underline{I} + (H^2/12)\bar{\underline{S}}^{-1}\ \underline{A})$. Thus, the approximate solution of $\underline{W}_o$ in terms of $\underline{W}^+$ would be

$$\underline{W}_o^F = \frac{1}{2}\ (\underline{I} + \frac{H^2}{12}\ \bar{\underline{S}}^{-1}\ \underline{A})\ \underline{W}^{+F} \ . \tag{3.36}$$

Substitution of the equation above into Eq. (3.30) yields after some manipulation

$$\underline{f}^{-F} = -\frac{H}{2}\ \underline{A}\ \underline{W}^{+F} \ . \tag{3.37}$$

Finally, substituting the expressions of $\underline{f}^{-F}$ and $[R^{+F}\ \ T^{+F}]^T$ given in Eqs. (3.37, 3.29) into Eq. (3.31), gives

$$-\omega^2\ \frac{\bar{m}}{h'}\ \underline{E}\ (\underline{W}^{+F} + \underline{W}^{-F}) + \frac{2}{H}\ \bar{\underline{S}}\ \underline{W}^{-F} - \frac{H}{2}\ \underline{A}\ \underline{W}^{+F} = 0 \tag{3.38}$$

where

$$\underline{E} = \begin{bmatrix} e_{11} & e_{12} \\ e_{12} & e_{22} \end{bmatrix}; \quad \underline{W}^{-F} = [\ S^{-F} \quad \psi^{-F}\ ]^T \ . \tag{3.39}$$

Let y and r be the relative values of u and ψ at the upper end of the wall with respect to their values at the lower end, i.e.,

$$y = u^+ - u^- \quad ; \quad r = \psi^+ - \psi^- \ . \tag{3.40}$$

Then with the boundary conditions at the lower end, Eqs. (3.40) take the form

$$y = u^+ - u_g \ ; \quad r = \psi^+ \ . \tag{3.41}$$

Then, from Eqs. (3.20),

$$\begin{aligned} S^+ &= y + 2u_g \ ; \quad S^- = y \\ \psi^+ &= \psi^- = r \end{aligned} \tag{3.42}$$

Eqs. (3.42) and the expressions defining $\underline{W}^{\mp}$ yield

$$\begin{aligned} \underline{W}^{+F} &= \underline{a}^F + 2u_g^F \, \underline{b} \\ \underline{W}^{-F} &= \underline{a}^F \end{aligned} \tag{3.43}$$

where

$$\underline{a} = [\, y \quad r \,]^T \ ; \quad \underline{b} = [\, 1 \quad 0 \,]^T \ . \tag{3.44}$$

Substituting Eqs. (3.43) into (3.38) and multiplying the resulting equation by bh' gives

$$-\omega^2(M\underline{E} + \frac{bh'H}{4}\underline{A}')\underline{a}^F + (\frac{bh'}{H}\bar{\underline{S}} + \frac{bh'H}{4}\bar{Q}'\underline{B})\underline{a}^F = \omega^2 u_g^F(M\underline{E} + \frac{bh'H}{2}\underline{A}')\underline{b} \tag{3.45}$$

where $M = \bar{m}b$ is the total mass of the top weight for one wall and

$$\underline{A}' = \begin{bmatrix} \rho & s \\ s & n \end{bmatrix} \ ; \ \underline{B} = \begin{bmatrix} 0 & 0 \\ 0 & 1 \end{bmatrix} \ . \tag{3.46}$$

In obtaining Eq. (3.45), the fact that $\underline{B}\,\underline{b} = \underline{0}$ is used.

Taking into account the relations $\bar{Q}' = k + i\omega c$, $\bar{S}_{\alpha\beta} = k_{\alpha\beta} + i\omega c_{\alpha\beta}$ Eq. (3.45) can be written finally in expanded form as

$$\left(-\omega^2 \begin{bmatrix} M_{11} & M_{12} \\ M_{12} & M_{22} \end{bmatrix} + i\omega \begin{bmatrix} C_{11} & C_{12} \\ C_{12} & C_{22} \end{bmatrix} + \begin{bmatrix} K_{11} & K_{12} \\ K_{12} & K_{22} \end{bmatrix}\right) \begin{bmatrix} y^F \\ r^F \end{bmatrix} = \omega^2 \begin{bmatrix} M'_{11} \\ M'_{12} \end{bmatrix} u_g^F \tag{3.47}$$

where

$$M_{11} = e_{11}M + \frac{f_{11}}{4} \; ; \qquad M_{12} = e_{12}M + \frac{f_{12}}{4}$$

$$M_{22} = e_{22}M + \frac{f_{22}}{4}$$

$$M'_{11} = e_{11}M + \frac{f_{11}}{2} \; ; \qquad M'_{12} = e_{12}M + \frac{f_{12}}{2}$$

$$f_{11} = \rho bh'H \text{ (mass of the wall)} \tag{3.48}$$

$$f_{12} = sbh'H \qquad ; \qquad f_{22} = nbh'H$$

$$C_{11} = \frac{bh'c_{11}}{H} \qquad ; \qquad C_{12} = \frac{bh'c_{12}}{H} \; ; \qquad C_{22} = \frac{bh'c_{22}}{H} + \frac{bh'Hc}{4}$$

$$K_{11} = \frac{bh'k_{11}}{H} \qquad ; \qquad K_{12} = \frac{bh'k_{12}}{H} \; ; \qquad K_{22} = \frac{bh'k_{22}}{H} + \frac{bh'Hk}{4} \; .$$

Inversion of Eq. (3.47) would give the equations of the discrete model in the time domain. They are, in matrix form

$$\begin{bmatrix} M_{11} & M_{12} \\ M_{12} & M_{22} \end{bmatrix} \begin{bmatrix} \ddot{y} \\ \ddot{r} \end{bmatrix} + \begin{bmatrix} C_{11} & C_{12} \\ C_{12} & C_{22} \end{bmatrix} \begin{bmatrix} \dot{y} \\ \dot{r} \end{bmatrix} + \begin{bmatrix} K_{11} & K_{12} \\ K_{12} & K_{22} \end{bmatrix} \begin{bmatrix} y \\ r \end{bmatrix} = - \begin{bmatrix} M'_{11} \\ M'_{12} \end{bmatrix} \ddot{u}_g \tag{3.49}$$

This is a system of two coupled ordinary differential equations in time and has a form encountered widely in structural dynamics. The equations of the discrete model, Eqs. (3.49), are simpler to handle than the equations of the continuous system, Eqs. (3.12 to 3.14), which are composed of partial differential equations in the time-space domain.

3.4 Force and Displacement Distributions

The object of this section is to relate the displacement and force distributions within the wall to the variables y and r of the discrete model.

3.4.1 Displacement Distribution

To determine the displacement distribution, we first take the Fourier transform of Eqs. (3.22). This gives

$$\begin{aligned} u^F &= a_o^F \phi_o + a_1^F \phi_1 + a_2^F \phi_2 \\ \psi^F &= b_o^F \phi_o + b_1^F \phi_1 + b_2^F \phi_2 \quad . \end{aligned} \tag{3.50}$$

In view of the Eqs. (3.23, 3.24), Eqs. (3.50) can be written as

$$\underline{W}^F = \underline{W}_o^F(\phi_o - \phi_2) + \frac{1}{2}\underline{W}^{-F}\phi_1 + \frac{1}{2}\underline{W}^{+F}\phi_2 \tag{3.51}$$

where $\underline{W}^F = [u^F \quad \psi^F]^T$. When Eq. (3.36) is substituted into this equation, and the distribution functions given by Eqs. (3.16) are taken into account, Eq. (3.51) becomes

$$\underline{W}^F = \frac{1}{2}\left[\underline{I} + \frac{H^2}{8}(1 - \bar{x}^2)\,\underline{\bar{S}}^{-1}\underline{A}\right]\underline{W}^{+F} + \frac{1}{2}\bar{x}\,\underline{W}^{-F}. \tag{3.52}$$

In this equation, it is to be noted that the factor $(1 - \bar{x}^2)$ is less than one. Hence in accordance with the assumption used in deriving Eq. (3.36), the second term in the parentheses will be neglected. Substituting Eqs. (3.43) into Eq. (3.52) gives

$$\underline{W}^F \simeq \frac{1}{2}(1 + \bar{x})\underline{a}^F + \underline{b}u_g^F \tag{3.53}$$

which, after inversion, can be written in expanded form as

$$\begin{bmatrix} u - u_g \\ \psi \end{bmatrix} \simeq \frac{\bar{x} + 1}{2}\begin{bmatrix} y \\ r \end{bmatrix} \quad . \tag{3.54}$$

Eq. (3.54) indicates that the average displacement (the average of the phase displacements) relative to the base $(u - u_g)$ and the difference of the phase displacements ψ have approximately linear distributions over the height of the wall.

3.4.2 Force Distribution

The determination of the force distribution starts with multiplying Eqs. (3.25) by bh' and taking the Fourier transform of the resulting equations. This yields

$$\underline{F}^F = \frac{2bh'}{H} (\bar{\underline{S}}\, \underline{d}_1^F\, \phi_1' + \bar{\underline{S}}\, \underline{d}_2^F\, \phi_2') \tag{3.55}$$

where

$$\underline{d}_\alpha^F = [\, a_\alpha^F \quad b_\alpha^F \,]^T \,, \quad (\alpha = 1,2)$$

$$\underline{F}^F = [\, V^F \quad \Delta^F \,]^T \tag{3.56}$$

$$V = bh'\sigma \qquad ; \quad \Delta = bh'\tau \,.$$

Now σ was the total stress measured per unit area of the wall material, so V defined in Eqs. (3.56) describes the usual force acting on the whole horizontal cross section of the wall. On the other hand, from the definition $\tau = \sigma_1 - \sigma_2$, it follows that Δ is a force quantity associated with the difference of phase stresses (partial stresses), which appears in the analysis because the mixture model distinguishes the two phases of the wall. Further, it should be noted that V describes the shear force for the horizontal motion of the wall and the deviation of the normal force from its static value for the vertical motion of the wall.

When the expressions for $\underline{d}_\alpha^F$, ϕ_α' ($\alpha = 1,2$) are carried into Eqs. (3.55) from Eqs. (3.16, 3.24), respectively, and Eq. (3.36) is used, Eq. (3.55) reduces to

$$\underline{F}^F = \frac{bh'}{H} \bar{\underline{S}}\, \underline{W}^{-F} - \frac{bh'H}{4}\, \bar{x}\, \underline{A}\, \underline{W}^{+F} \,. \tag{3.57}$$

Substituting Eqs. (3.43) into the equation above gives

$$\underline{F}^F = (\frac{bh'}{H} \bar{\underline{S}} - \bar{x}\, \frac{bh'H}{4}\, \underline{A})\, \underline{a}^F - \bar{x}\, \frac{bh'H}{2}\, \underline{A}\, \underline{b}\, u_g^F \,. \tag{3.58}$$

Using the definitions of $\bar{\underline{S}}$, $\underline{A}$, $\underline{a}^F$ and $\underline{b}$, the first component V^F of $\underline{F}^F$ is given by

$$V^F = (K_{11} + i\omega C_{11} - \omega^2 \bar{x} \frac{f_{11}}{4}) y^F + (K_{12} + i\omega C_{12} - \omega^2 \bar{x} \frac{f_{12}}{4}) r^F - \omega^2 \bar{x} \frac{f_{11}}{2} u_g^F \tag{3.59}$$

from $\bar{S}_{\alpha\beta} = k_{\alpha\beta} + i\omega c_{\alpha\beta}$ and the definitions given in Eqs. (3.48). In the time domain, Eq. (3.59) takes the form

$$V = (K_{11} y + C_{11} \dot{y} + \bar{x} \frac{f_{11}}{4} \ddot{y}) + (K_{12} r + C_{12} \dot{r} + \bar{x} \frac{f_{12}}{4} \ddot{r}) + \bar{x} \frac{f_{11}}{2} \ddot{u}_g \ . \tag{3.60}$$

From Eq. (3.58), it is clear that the forces V and Δ vary linearly over the height of the wall.

3.5 Effective Modulus Model

Up to this point we have been considering the mixture model. A second model, the effective modulus model, can be obtained from the mixture model as a special case.

To reduce the length of the analysis, the equations of the effective modulus theory are presented only for the special one dimensional problems formulated in Section 3.2 for the loading and geometrical conditions of the wall specimen tested experimentally. The effective modulus model replaces the wall material by one-phase homogeneous material and does not differentiate mortar and brick phases. To derive the equations of the effective modulus theory let $u_1 = u_2$ and then, from Eq. (3.11), $u = u_1 = u_2$ and $\psi = 0$. Then Eqs. (3.12 - 3.14) show that the dependent variables of the effective modulus theory, u and σ are governed by the first members of these equations. They are

$$\begin{aligned} &\partial_x \sigma = \rho \ddot{u} \\ &\sigma = S_{11} \partial_x u \\ &\frac{\bar{m}}{\bar{h}'} \ddot{u}^+ + \sigma^+ = 0 \\ &\ddot{u}^- = \ddot{u}_g^-(t) \ . \end{aligned} \tag{3.61}$$

The definitions of the parameters in the governing equations of the effective modulus theory, i.e., in Eqs. (3.61), are the same as those given for the mixture model.

Equations (3.61) can be put in a discrete form by following the procedure outlined in Section 3.3, to yield

in the frequency domain:

$$(-\omega^2 M_{11} + i\omega C_{11} + K_{11})y^F = \omega^2 M'_{11} u_g^F \tag{3.62}$$

in the time domain:

$$M_{11}\ddot{y} + C_{11}\dot{y} + K_{11}y = -M'_{11}\ddot{u}_g \tag{3.63}$$

with M_{11}, M'_{11}, C_{11}, K_{11} and y as defined previously by Eqs. (3.48 and 3.41). 3.41).

The expressions relating displacement and force distributions in the wall to the variable y of the discrete effective modulus model can be derived by using the procedure followed in Section 3.4. They are

displacement distribution:

$$u - u_g = \frac{1}{2}(\bar{x} + 1)y \tag{3.64}$$

force distribution:

$$V = (K_{11}y + C_{11}\dot{y} + \bar{x}\frac{f_{11}}{4}\ddot{y}) + \bar{x}\frac{f_{11}}{2}\ddot{u}_g \quad . \tag{3.65}$$

4. THEORETICAL AND EXPERIMENTAL RESPONSE FUNCTIONS

In this chapter, theoretical response functions are derived from the mixture and effective modulus theories, and the procedure for obtaining the experimental response function is presented. The parameters appearing in the theoretical models will be determined through optimization analysis by matching theoretical and experimental response functions of the wall in the following chapters. First, we define the response function for a general system and review very briefly its basic properties (for a more complete discussion see references [13-17]).

A response function, in general, is a function relating the output of a system at a specified location to a given input. When the system is linear and the input x and output y are functions of time, x and y are related by the convolution integral

$$y(t) = \int_{-\infty}^{\infty} h(\tau)x(t - \tau)d\tau \quad . \tag{4.1}$$

The corresponding relation in the frequency domain is

$$Y(f) = H(f) \cdot X(f) \tag{4.2}$$

where $Y(f)$, $H(f)$ and $X(f)$ are the Fourier transforms of $y(t)$, $h(t)$ and $x(t)$, respectively, and the frequency f is related to the angular frequency ω by $f = \omega/2\pi$. The response function $h(t)$ in the time domain is called the impulse response function whereas the response function $H(f)$ in the frequency domain is called the complex frequency response function (CFRF) of the system. The absolute value of CFRF, $|H(f)|$, describes the amplification of the input and $\tan^{-1}(H_I(f) / H_R(f))$ gives the phase angle difference between the output and input. Here H_I and H_R denote imaginary and real parts of CFRF, respectively.

In the evaluation of theoretical and experimental response functions of the wall, the base and top accelerations are chosen to be, respectively, the input and output of the wall. This choice is dictated by the fact that, because of the rigidity of the walls, reliable and sensitive measurements in experiments are obtained only from accelerometers. Since in this study, for reasons discussed later, the optimization analysis is carried out in frequency space rather than in time space, in what follows the response functions (relating base and top accelerations of the wall) are evaluated in frequency space only.

4.1 Theoretical Response Functions

In Chapter 3, two different mathematical models, namely the mixture and effective modulus models, were proposed to determine the theoretical response of masonry walls. Here, CFRF's based on these models are derived by using the relation

$$H_u^t = \frac{(\ddot{u}^+)^F}{(\ddot{u}_g)^F} = \frac{u^{+F}}{u_g^F} \tag{4.3}$$

in accordance with the definition given in Eq. (4.2), where H_u^t is the CFRF; and $(\ddot{u}^+)^F$ and $(\ddot{u}_g)^F$ are the transforms of the top and base accelerations, respectively. The last term of Eq. (4.3) follows since $(\ddot{g})^F = -\omega^2 g^F$ for any function $g(t)$.

4.1.1 Response Function for the Mixture Model

Dividing the governing equation of the mixture model in the frequency domain, Eq. (3.47), by M_{11} gives

$$\left(-\omega^2 \begin{bmatrix} 1 & m' \\ m' & \alpha \end{bmatrix} + 2i\xi\omega\bar{\omega} \begin{bmatrix} 1 & \gamma' \\ \gamma' & \alpha' \end{bmatrix} + \bar{\omega}^2 \begin{bmatrix} 1 & \gamma \\ \gamma & p \end{bmatrix}\right) \begin{bmatrix} y^F \\ r^F \end{bmatrix} = \omega^2 q' \begin{bmatrix} 1 \\ \ell \end{bmatrix} u_g^F \tag{4.4}$$

where $\bar{\omega}^2=K_{11}/M_{11}$; ξ is the damping coefficient defined by $\xi = C_{11}/2M_{11}\bar{\omega}$ and

$$\alpha = \frac{M_{22}}{M_{11}} ; \qquad m' = \frac{M_{12}}{M_{11}}$$

$$\alpha' = \frac{C_{22}}{C_{11}} ; \qquad \gamma' = \frac{C_{12}}{C_{11}} \tag{4.5}$$

$$p = \frac{K_{22}}{K_{11}} ; \qquad \gamma = \frac{K_{12}}{K_{11}}$$

$$q' = \frac{M'_{11}}{M_{11}} ; \qquad \ell = \frac{M'_{12}}{M'_{11}} \quad .$$

It should be noted that the constants α, m', α', γ', p, γ, q' and ℓ are nondimensional. Solving Eq. (4.4), which is a system of linear algebraic equations, for y^F; then substituting $u^{+F} = y^F + u_g^F$ in Eq. (4.3), gives

$$H_u^t = \frac{q'z^2}{D}(a_{22} - a_{12}\ell) + 1 \tag{4.6}$$

where z is the nondimensional frequency defined by $z = \omega/\bar{\omega}$ and

$$D = a_{11}a_{22} - a_{12}^2$$

$$a_{11} = 1 + 2\xi iz - z^2$$

$$a_{22} = p + 2\alpha'\xi iz - \alpha z^2 \tag{4.7}$$

$$a_{12} = \gamma + 2\gamma'\xi iz - m'z^2 \quad .$$

Although the number of parameters appearing in the mixture model is 11 (M_{11}, $\bar{\omega}$, α, m', ξ, α', γ', p, γ, q', ℓ), some of the parameters have pre-assigned values and do not enter into the optimization analysis as unknowns.

The values of these parameters can be computed from the physical and geometric properties of the wall specimen stated below

$$n_1 = 0.20 \quad ; \quad n_2 = 0.80$$

$$\rho_1^R = 1800 \text{ kg/m}^3 \quad ; \quad \rho_2^R = 1320 \text{ kg/m}^3 \tag{4.8}$$

$$b = 2.64 \text{ m} \quad ; \quad H = 1.52 \text{ m} \quad ;$$
$$M = 2304 \text{ kg} \quad ; \quad h' = 0.092 \text{ m} . \qquad \text{(4.8 Cont'd)}$$

In writing the value of ρ_2^R, the volume of the hole in the brick is taken into account, i.e., ρ_2^R is computed by dividing the mass of a brick by its total volume, including the holes in it. When the values of n_α and ρ_α^R are substituted from Eqs. (4.8) into Eqs. (3.15), taking into account the relation $\rho_\alpha = n_\alpha \rho_\alpha^R$ (α= 1,2; no summation on α), the following results are obtained.

$$e_{11} = 1 \quad ; \; e_{12} = -0.60 \quad ; \; e_{22} = 0.36$$
$$\rho_1 = 360 \text{ kg/m}^3 \quad ; \quad \rho_2 = 1056 \text{ kg/m}^3 \qquad (4.9)$$
$$\rho = 1416 \text{ kg/m}^3 \quad ; \quad s = -696 \text{ kg/m}^3 .$$

Substitution of these values, and the values of b, h', H from Eqs. (4.8) into Eqs. (3.48) gives

$$f_{11} = 523 \text{ kg} \quad ; \; f_{12} = -257 \text{ kg}$$
$$M_{11} = 2435 \text{ kg} \quad ; \; M_{12} = -1447 \text{ kg} \qquad (4.10)$$
$$M'_{11} = 2566 \text{ kg} \quad ; \; M'_{12} = -1511 \text{ kg} .$$

Then using the definitions of m', q' and ℓ in Eqs. (4.5), their values can be computed as

$$m' = -0.59 \quad ; \quad q' = 1.05 \quad ; \quad \ell = -0.59 . \qquad (4.11)$$

Since the values of the model parameters M_{11}, m', q' and ℓ are assigned, there remain only the 7 parameters ($\bar{\omega}$, ξ, α, α', γ', p, γ) to be determined through optimization.

In addition to having preassigned values for some parameters (given by Eq. (4.11)) there are also some constraints to be satisfied by the model parameters. To establish these constraints, we note first that the matrices $\underline{M} = (M_{ij})$, $\underline{C} = (C_{ij})$ and $\underline{K} = (K_{ij})$ in Eq. (3.47) can be written in the forms

$$\underline{M} = M\underline{E} + \frac{bh'H}{4}\underline{A}'$$

$$\underline{C} = \frac{bh'}{H}\underline{c} + \frac{bh'H}{4}c\underline{B} \qquad (4.12)$$

$$\underline{K} = \frac{bh'}{H}\underline{k} + \frac{bh'H}{4}k\underline{B}$$

where $\underline{E}$, $\underline{A}'$ and $\underline{B}$ are given in Eqs. (3.39, 3.46) and $\underline{c} = (c_{ij})$, $\underline{k} = (k_{ij})$ where (c_{ij}, k_{ij}) were defined in Section 3.2. It was stated in Section 3.2 that the matrices $\underline{A}'$, $\underline{k}$, and $\underline{c}$ are positive definite and the constants k and c are positive. Moreover, the matrices $\underline{E}$ and $\underline{B}$ are semi positive definite in view of their definitions. Hence, it follows from Eq. (4.12) that the matrices $\underline{M}$, $\underline{C}$, and $\underline{K}$ are positive definite. This, in turn, implies that the matrices appearing in Eq. (4.4) are also positive definite, and leads to the constraints

$$\alpha - m'^2 > 0 \; ; \; \alpha' - \gamma'^2 > 0 \; ; \; p - \gamma^2 > 0 \qquad (4.13)$$

on the model parameters.

4.1.2 Response Function for the Effective Modulus Model

The theoretical response function associated with the effective modulus model can be obtained by following the procedure outlined in Section 4.1.1.

Dividing Eq. (3.62) by M_{11} and using the definitions of $\bar{\omega}$, ξ, q' and z in the previous section, H_u^t can be obtained as

$$H_u^t = \frac{q'z^2}{1 + 2\xi iz - z^2} + 1 \quad . \qquad (4.14)$$

The effective modulus model contains only two parameters to be determined by optimization, namely $\bar{\omega}$ and ξ.

The CFRF of the effective modulus model can also be derived from the CFRF of the mixture model (Eq. (4.6)) by simply setting the parameters m', γ, α' and γ' equal to zero.

4.2 Experimental Response Functions

The experimental CFRF's based on experiments are evaluated by using the simple relation

$$H_u^e(f_j) = \frac{u_e^F(f_j)}{u_g^F(f_j)} \tag{4.15}$$

where H_u^e is the experimental CFRF, u_e^F and u_g^F are the Fourier transforms (spectra) of the acceleration records taken from accelerometers at the top and base of each wall of the test specimen during experiments, and f_j is the j th discrete frequency component. During each run of the experiments, the input and output acceleration histories are recorded at a set of equally spaced data points with a constant time increment Δt (0.00988 sec.) and a data record length of ND (number of data points). Fourier transforms of such discrete records in the time domain can be determined by using Discrete Fourier Transform techniques (DFT). The Fast Fourier Transform (FFT) is the algorithm chosen in the present study to determine the Fourier transforms of the discrete acceleration records. Detailed discussions of DFT, in particular the FFT, can be found in references [17-21].

The FFT gives the complex valued ordinates of the transformed records in the frequency domain at a set of equally spaced points, increment $\Delta f = 1/T$, for NF = ND/2 + 1 data points. Here, T is the time length of the original record in the time domain, defined by $T = ND \cdot \Delta t$ and NF is related to the cut off (aliasing) frequency f_c by $f_c = NF \cdot \Delta f$. The record length ND is varied at each run depending on the type of input motion.

As mentioned in Chapter 2 the wall specimen is composed of two parallel walls with identical instrumentation. These two walls will be referred to as walls A and B in the study. The specimen is subjected to two types of base excitation, classified in Chapter 2 as "periodic input" (in horizontal and vertical directions) and "modified El Centro input". In

the sections which follow, the experimental CFRF's obtained by using the experimental data associated with these two types of input are presented and discussed separately.

4.2.1 CFRF Derived from the Periodic Runs

The wall specimen is subjected to two different types of periodic base excitation, one being parallel and the other being perpendicular to the horizontal layering. The time lengths of all periodic runs are about 2.5 seconds, which corresponds to a record length of 256 data points.

The periodic inputs have approximately sinusoidal variations in time. If their variations were perfectly sinusoidal, the Fourier transform of each input should contain a Dirac delta function at its associated frequency. However, because of its not being perfectly sinusoidal, the Fourier transform of a periodic input remains finite for all frequencies; it reaches a maximum (in absolute value) at a certain frequency, then decreases rapidly and approaches zero, in both directions from that frequency. The frequency corresponding to the maximum value is designated as the "driving frequency" of that input. In harmony with the terminology used in the analysis of random processes, the variation described above will be called "narrow banded spectral density distribution" (NBSD). The time variation of an input-output pair is given in Fig. 7, for the driving frequency of 18.58 Hz. The associated distribution in the Fourier domain is presented in Fig. 10. From this figure it is apparent that the input-output pair has a NBSD with a band width of about 0.6 Hz, centered at the driving frequency 18.58 Hz.

The procedure for obtaining the experimental CFRF is now presented. This procedure is valid for both the horizontal and vertical periodic motions. Now let $\bar{f}_j$ (j = 1 - N) be the driving frequency of the j th input-

output pair, where N is the number of periodic runs. It must be noted that, for the j th run the spectral density distribution has a narrow banded structure centered at $\bar{f}_j$. Then it is clear from Eq. (4.15) that the experimental CFRF can be reliably found only in that narrow band, because the denominator of this equation fluctuates about zero outside the narrow band. Obviously, it has the most reliable value at $\bar{f}_j$. Accordingly the experimental value of CFRF at each $\bar{f}_j$ (j = 1 - N) is obtained by dividing the Fourier transform of output by that of input of the j th run at $\bar{f}_j$, i.e., using the relation given by Eq. (4.15) for the j th run at $\bar{f}_j$. Thus each periodic run gives a single value of CFRF at the driving frequency of that run. We note that in the experiments the driving frequencies of the periodic inputs varied from 3 Hz. to 30 Hz.

A last comment regarding the procedure outlined above is now in order. It is clear that, using the j th run it is possible to determine experimental values of CFRF not only at $\bar{f}_j$ but also in the neighborhood of $\bar{f}_j$, provided that the frequencies remain in the narrow band. However, CFRF values obtained at these frequencies will not provide additional information because all these frequencies would be closely packed about $\bar{f}_j$.

The driving frequencies, and the real and imaginary parts of the experimental CFRF's evaluated at these frequencies, derived from the horizontal runs, are given in Table 2 for each of the walls A and B. CFRF's obtained from the vertical periodic runs are presented in Table 3 for each of the walls. Graphical representations of these CFRF's are shown in Figs. 13,14 and 17,18, respectively, for the horizontal and vertical runs.

4.2.2 CFRF Derived from the Modified El Centro Runs

The base acceleration records used in the experiments which are derived from the El Centro 1940 ground acceleration records possess both

Table 2

Driving frequencies of periodic runs; real and imaginary parts of the experimental complex frequency response functions (CFRF's) of walls A and B (horizontal motion)

f (Hz)	WALL A		WALL B	
	Re (Hu)	Im (Hu)	Re (Hu)	Im (Hu)
3.56	+ 1.009	+ 0.015	+ 1.007	+ 0.019
6.32	+ 1.072	- 0.029	+ 1.062	- 0.014
12.26	+ 1.342	- 0.109	+ 1.317	- 0.043
15.42	+ 2.276	- 0.556	+ 2.025	- 0.404
16.61	+ 3.619	- 2.240	+ 2.900	- 1.535
17.40	+ 3.323	- 5.022	+ 2.504	- 3.241
18.58	- 0.562	- 5.951	+ 0.120	- 3.917
19.37	- 3.330	- 3.611	- 1.205	- 2.028
20.56	- 3.497	- 1.485	- 0.876	- 1.067
21.75	- 2.833	- 0.432	- 0.050	- 0.500
22.54	- 2.512	+ 0.451	+ 0.618	- 0.643
23.72	- 1.268	+ 2.146	+ 1.090	- 2.334
24.51	+ 0.360	+ 0.766	- 1.516	- 1.656
25.70	+ 0.319	+ 0.246	- 1.314	- 0.229
27.68	+ 0.050	- 0.0211	- 0.229	+ 0.040
30.84	+ 0.222	- 0.004	+ 0.175	+ 0.045

Table 3

Driving frequencies of periodic runs; real and imaginary parts of the experimental complex frequency response functions of walls A and B (vertical motion)

f (Hz)	WALL A		WALL B	
	Re (Hu)	Im (Hu)	Re (Hu)	Im (Hu)
3.56	+ 0.999	+ 0.005	+ 0.990	- 0.022
6.32	+ 1.023	+ 0.044	+ 1.012	- 0.012
9.49	+ 1.047	+ 0.032	+ 1.016	+ 0.026
12.26	+ 1.053	+ 0.014	+ 1.002	- 0.050
15.42	+ 1.110	+ 0.023	+ 1.016	- 0.050
16.61	+ 1.199	- 0.019	+ 1.010	- 0.037
17.40	+ 1.386	- 0.045	+ 1.050	- 0.027
18.58	+ 1.544	- 0.554	+ 1.041	- 0.078
19.77	+ 0.331	- 0.196	+ 1.004	- 0.091
20.56	+ 0.706	- 0.002	+ 0.958	- 0.053
21.75	+ 0.868	- 0.006	+ 0.974	- 0.067
24.51	+ 0.821	- 0.046	+ 1.037	- 0.006
27.68	+ 0.926	+ 0.020	+ 1.035	- 0.076
30.84	+ 0.985	+ 0.069	+ 1.039	- 0.094

horizontal and vertical acceleration components. However, analysis of readings of the vertical components did not lead to meaningful results because of their having negligibly small values compared with the horizontal components. Accordingly, only the records obtained from horizontal component accelerometers are considered and used in the analysis.

Time lengths of the modified El Centro runs obtained from the El Centro 1940 record depend on the time scale factor s, defined and explained in Section 2.3.3. For s = 1.0, 2.45, 3.46 and 7.7 the time lengths of the El Centro runs are 28, 11.4, 8, and 3.6 seconds, respectively. The corresponding data record lengths of these runs are ND = 2384, 1158, 819, and 368.

The input and output accelerations recorded during modified El Centro runs have similar spectral density distributions in Fourier space. The Fourier transforms of input-output acceleration pairs indicate that they all have "wide banded spectral density distributions" (WBSD): their Fourier transforms in absolute values have well-defined values over a wide frequency band, gradually decrease towards the ends and then fluctuate around zero outside the band. The widths of the bands depend on the s factors of the runs. The lower limits of the bands are 2 Hz for all runs, the upper limits are approximately 7, 9, 11 and 15 Hz for the runs with s factors of 1.0, 2.45, 3.46 and 7.7, respectively. The Fourier transform of the input acceleration for s = 7.7 is given in absolute values in Fig. 11. The WBSD structure of the input can be clearly observed in this figure.

The experimental CFRF may be obtained for the modified El Centro runs by taking the Fourier transform of an input-output acceleration pair and using Eq. (4.15). But, because of the reasons stated in Section 4.2.1, the CFRF obtained in this way would have reliable values only in the frequency band of its associated input-output pair. Thus, from the previous paragraph

it is clear that this interval, which will be called the "reliable frequency band" (RFB), is $(2 \leq f \leq 15)$ Hz for the run with s = 7.7, which is the widest of the El Centro runs. Consequently, only this run is considered in the analysis.

The CFRF's of the walls A and B derived from the modified El Centro run with s = 7.7 are presented graphically in Figs. 20 and 21. The figures show clearly that the CFRF's have relatively smooth behavior over their RFB $(2 \leq f \leq 15)$ Hz. Outside the RFB the experimental points defining the CFRF's exhibit very large scattering with unacceptable variances about their expected values.

4.2.3 Discussions on the Experimental CFRF's

In the previous two sections the experimental CFRF's are derived for the walls A and B, using the periodic and the modified El Centro runs. The CFRF's relating the vertical input and output accelerations are obtained only from the periodic runs, but the CFRF's relating the horizontal ones are obtained from both types of excitation.

The discrete points defining the CFRF's obtained from the horizontal periodic runs are spaced in a frequency interval of $(3 \leq f \leq 32)$ Hz with frequency increments of 1 or 3 Hz. Those obtained from the horizontal component of the modified El Centro run with s = 7.7 define the horizontal CFRF's in the RFB of s = 7.7, $(2 \leq f \leq 15)$ Hz, at more closely spaced frequency points, with a constant frequency increment of 0.198 Hz.

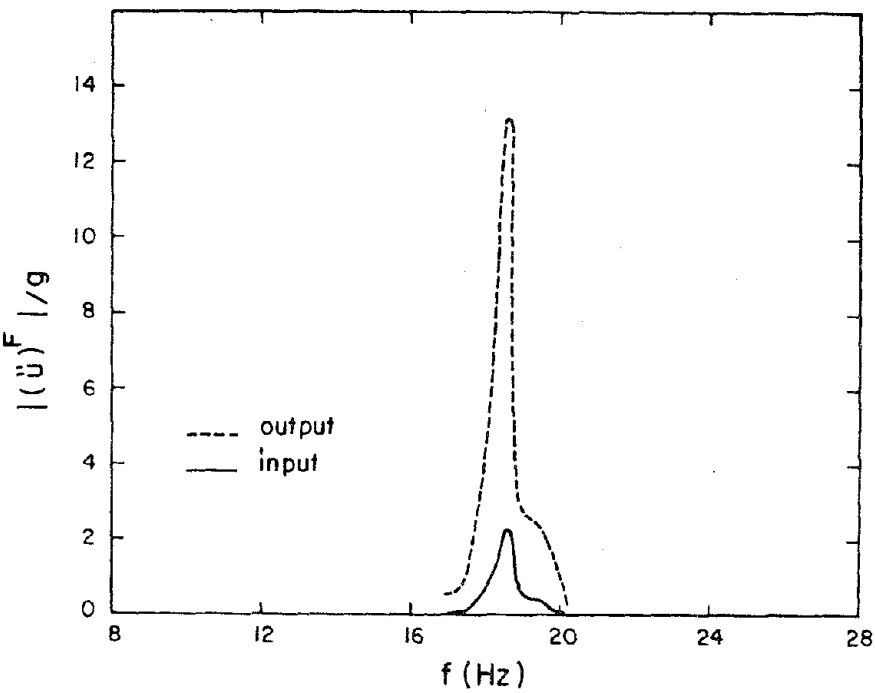

Figure 10. Amplitude spectrum of a periodic input-output acceleration pair (driving frequency = 18.58 Hz)

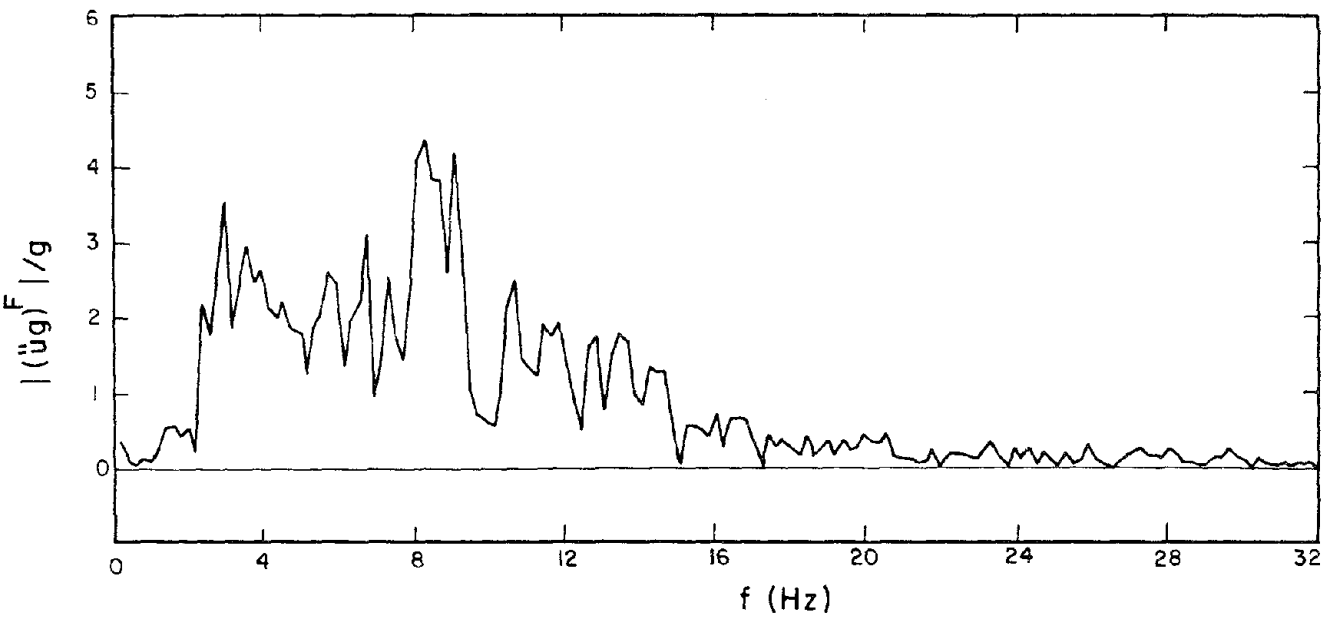

Figure 11. Amplitude spectrum of an El Centro input acceleration (time scale factor = 7.7)

Taking into account the rigidity of masonry walls, the resonance phenomena for the walls in the test specimen can be expected to occur at high frequencies. In fact, information obtained from the horizontal periodic runs shows that the first resonance occurs at about 16 - 18 Hz (see Figs. 13, 14). Hence, it is clear that even the widest RFB of the CFRF obtained from the El Centro run with s = 7.7 does not contain the first resonance frequency. This means that the El Centro run with s = 7.7 can provide experimental data only in the low frequency range. To have data from the El Centro runs in the high frequency range, it is necessary to increase the value of the scaling factor s. Unfortunately experiments were not performed for s values greater than 7.7. Therefore the experimental data obtained from the periodic runs which accommodate both the low and high frequency behavior of the wall, are considered in the optimization analysis presented in the next chapter.

In Fig. 12 the horizontal CFRF's derived from the horizontal periodic and El Centro runs are compared in the frequency interval ($2 \leq f \leq 15$) Hz for the wall A. The very close agreement shown between these two CFRF's indicates that the response of the wall during the experiments is in the linear range. This justifies the use of linear models in the optimization analysis.

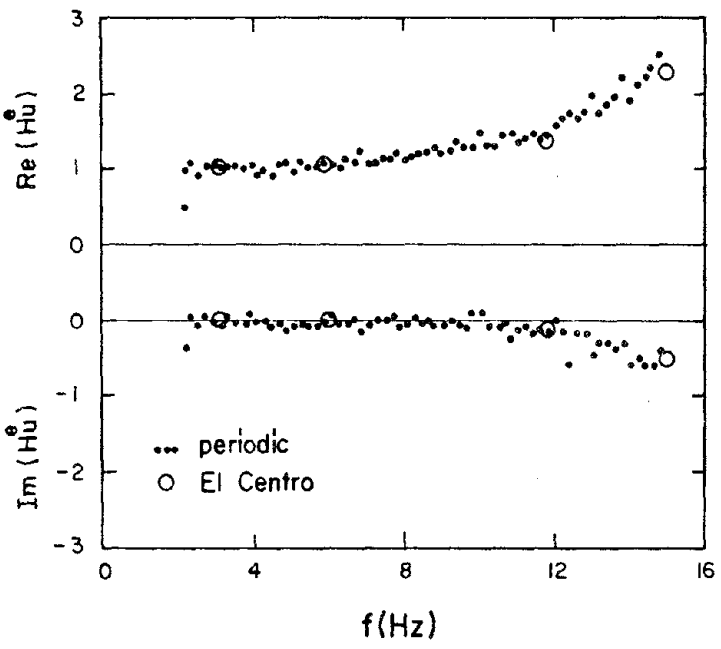

Figure 12. Comparison of horizontal complex frequency response functions (experimental) derived from the periodic and El Centro runs for wall A

5. OPTIMIZATION ANALYSIS

Optimization analysis involves three main steps:(a) choosing a suitable mathematical model describing the behavior of a given system;(b) introducing an objective function measuring the goodness of the match between theoretical and experimental responses and(c) finding the unknown parameters or functions appearing in the theoretical model by minimizing the objective function with the aid of an optimization algorithm.

The most important step among these three is deciding on the mathematical model. On one hand, the model should be capable of predicting the experimental behavior of the system and should accommodate its desired characteristics but on the other it should be as simple as possible. A logical way of constructing the mathematical model might involve the following phases. First, starting from physical laws and considerations, the equations of the model should be established in a general form which can accommodate all the observed characteristics of the experimental response. Then the model should be simplified as much as possible, by discarding the model parameters or functions which have very little influence on the response, by taking into account the specific frequency or time interval considered in the optimization analysis, etc. It must be emphasized again that the choice of an appropriate theoretical model is crucial. In fact, starting the analysis with a bad model would rarely lead to a good match even for optimum model parameters or functions.

The other two steps involve mathematical analysis and are of less significance in optimization than the first. The objective function can be considered as a norm for the error measuring the goodness of the match between the experimental and theoretical responses. It must be selected in such a way that it would be zero if and only if the theoretical and

experimental values coincide at all points considered in the optimization analysis. Moreover, the theoretical response could be obtained in terms of unknown model parameters or functions, then the objective function would be a function or functional of these unknowns. The last step involves finding the model parameters or functions by minimizing the objective function with the aid of an optimization algorithm. Various algorithms exist for different types of optimization problems [22-27]; these are mostly based on iterative schemes derived from the approximation of the error surface by a simpler analytical surface in the neighborhood of the minimum point. Selection of a suitable algorithm for a given problem depends on the structure of the objective function (i.e., on whether it is a function or functional of unknowns), on whether the problem has any constraints or not, etc.

In the present study a two phase parametric model is chosen to predict the dynamic behavior of masonry walls. The equations of this model have already been established in Chapter 3. To complete the optimization analysis, it remains now to select both an appropriate objective function, and an optimization algorithm for minimizing the objective function. This is done in the following two sections. Before proceeding to these two sections, it is important to note the use of frequency space in the analysis. The optimization analysis is carried out by matching experimental and theoretical CFRF's in frequency space. The CFRF governs the response of the wall through Eq. (4.3) or Eq. (4.15) and, consequently, matching the CFRF's leads to matching the responses. Carrying out the optimization in frequency space rather than in time space has various advantages. First it determines the frequency range over which the model is valid. Then by studying the Fourier spectrum of a given input, we can determine in advance whether or not the model predicts adequately the response in time space for that given input. For example, if the major portion of the spectral density of input is

contained in the frequency region over which the model is valid, then we would know immediately that the model would predict the response to that input correctly. Secondly, the analysis indicates that the matching of CFRF's in frequency space is very crucial and can be used as a criterion for the goodness of the model. Thirdly, working in frequency space simplifies the optimization analysis. This is because the equations are simpler and there are less data points in frequency space compared with those in time space. In fact, in this study, to determine the theoretical response it is necessary to solve differential equations (Eq. 3.49) in time space whereas simple algebraic equations in frequency space (Eqs. 3.47).

5.1 The Objective Function

The objective function is expressed as the integrated least squares error between the theoretical and experimental CFRF's over the frequency interval $[0, \hat{f}]$, which can be written as

$$J(\underline{\beta}) = \int_0^{\hat{f}} (H_u^t - H_u^e)(H_u^t - H_u^e)^* df \quad . \tag{5.1}$$

Here, $\underline{\beta}^T = (\alpha, m', \bar{\omega}, p, \gamma, \xi, \alpha', \gamma')$ is the vector of model parameters, $(\cdot)^*$ denotes the complex conjugate of $(\cdot)$ and $[0, \hat{f}]$ is the interval considered in the analysis. J is a scalar quantity which is a function of $\underline{\beta}$ since H_u^t in Eq. (5.1) is a function of the model parameters $\underline{\beta}$.

Because H_u^e is a discrete function of frequency as defined in Chapter 4, integration in Eq. (5.1) must be performed numerically. This is done by using the trapezoidal rule. Thus, denoting the argument of the integral at the frequency point $f = f_j$ by c_j,

$$J(\underline{\beta}) = \frac{1}{2} \sum_{j=1}^{N-1} (c_j + c_{j+1})(f_{j+1} - f_j) \tag{5.2}$$

where N is the number of frequency points for which H_u^e has defined values. Eq. (5.2) can be written in a more suitable form for optimization as

$$J(\underline{\beta}) = \sum_{j=1}^{N} w_j[(r_j - \bar{r}_j)^2 + (s_j - \bar{s}_j)^2] \ . \qquad (5.3)$$

In this equation, w_j denotes the weight for the j th frequency point f_j, defined by $w_j = (f_{j+1} - f_{j-1})/2$ $(j = 2 - (N-1))$, $w_1 = (f_2 - f_1)/2$, $w_N = (f_N - f_{N-1})/2$ and (r_j, s_j) and $(\bar{r}_j, \bar{s}_j)$ are (real, imaginary) parts of the values of H_u^t and H_u^e at f_j, respectively.

The j th term in Eq. (5.3) is associated with the frequency point f_j. In the analysis f_j will be taken as the driving frequency of the j th run for periodic inputs, and the j th discrete frequency point in the reliable frequency band (RFB) for El Centro inputs.

It is important to note that the number of data points in Eq. (5.3) defining an objective function in frequency space is much less than in a comparable objective function that can be defined in time space. This can be seen very clearly by considering the periodic runs for which the number of data points in Eq. (5.3) is equal to the number of periodic runs, say M, whereas the objective function defined in time space for the same periodic runs would have (M x ND) data points, where ND is the number of time points in each periodic run.

5.2 Optimization Algorithm

The objective function $e = J(\underline{\beta})$ describes an error surface of an n+1 dimensional space $(\beta_1, \beta_2, \ldots, \beta_n, e)$ where n is the number of model parameters and e is the value of J at $\underline{\beta}$. Each set of parameters $\underline{\beta}$ defines a different point on the error surface with coordinates $(\underline{\beta}, J(\underline{\beta}))$. The first element of $(\underline{\beta}, J(\underline{\beta}))$ gives the projection of that point on the $\underline{\beta}$-plane. In optimization analysis the object is to determine that set of parameters for which the error surface has a minimum. Such a set is called the optimum

set. In the present study, the optimum set will be found by using an optimization algorithm based on an iterative scheme. Before discussing the specific algorithm chosen in the study, it is useful to comment on some aspects common to all iterative algorithms. In an iterative algorithm, first an initial approximation $\underline{\beta}_0$ to the optimum $\underline{\beta}$ is chosen. Then a sequence $\{\underline{\beta}_0, \underline{\beta}_1, \underline{\beta}_2, \ldots\}$ is generated by using a recurrence formula of the form

$$\underline{\beta}_{i+1} = \underline{\beta}_i + \Delta\underline{\beta}_i \qquad (i = 0,1,2,\ldots) \tag{5.4}$$

where $\underline{\beta}_{i+1}$ designates the updated set at the i th iteration. The expression defining $\Delta\underline{\beta}_i$ has different forms for different iterative algorithms. If the optimization algorithm generates a convergent sequence, the error e decreases at each iteration, i.e.,

$$J(\underline{\beta}_{i+1}) < J(\underline{\beta}_i) \tag{5.5}$$

and reaches its minimum value, within a limit of certain accuracy, in a finite number of iterations. In the neighborhood of a local minimum, the rate of convergence slows down. Iterations are stopped when a certain criterion for convergence is satisfied. The most commonly used convergence criterion is based on the relative change of either the error e or the set $\underline{\beta}$ and has the form

$$\frac{|e_{i+1} - e_i|}{e_i} < \varepsilon \tag{5.6}$$

or

$$\frac{||\Delta\beta_i||}{||\beta_i||} < \varepsilon \tag{5.7}$$

where ε is a prescribed positive small number and $||(\underline{\cdot})||$ designates the maximum norm of a vector quantity $(\underline{\cdot})$.

The initial estimate of the optimum set is an important stage of the analysis. Starting the iterations with a poor initial estimate, which

defines a point on the error surface far away from the minimum, may lead to divergence of the sequence, or convergence only after a large number of iterations. To make a good guess for the initial estimate $\underline{\beta}_0$ it is first necessary to establish a feasible region for $\underline{\beta}$. This can be done by taking into account the parameters which have preassigned values, and by considering the conditions to be imposed on the parameters by physical and geometric constraints of the problem. Then, by gaining some insight into the physical aspects of the problem under consideration, an appropriate $\underline{\beta}_0$ can be chosen in the feasible region of $\underline{\beta}$.

The incremental set $\Delta\underline{\beta}_i$ in Eq. (5.4) defines an improvement to $\underline{\beta}_i$ satisfying the inequality in Eq. (5.5). An optimization algorithm,in general, generates $\Delta\underline{\beta}_i$ at each iteration. Such an algorithm can be modified to increase the rate of convergence as follows. Let $\underline{d}_i$ be the increment generated by the algorithm and $\Delta\underline{\beta}_i$ be the increment modified as

$$\Delta\underline{\beta}_i = \lambda_i \, \underline{d}_i \quad \text{(no sum on i)} \tag{5.8}$$

where λ_i is the modification factor. It is to be noted that Eq. (5.8) with $\lambda_i = 1$ gives the unmodified increment. λ_i is to be determined at each iteration i in such a way that the error e becomes a minimum along the descent direction $\underline{d}_i$. This procedure for determining λ_i is called a "line search".

The algorithm used in the present study to find the increment $\underline{d}_i$ in Eq. (5.8) is Newton's method which is discussed briefly in the next section, and followed by a description of the line search algorithm. A full discussion of Newton's method and other multivariable or single variable optimization methods can be found in references [22-27].

5.2.1 Newton's Method

Newton's method which is also referred to as the second order gradient method in the literature, is based on Taylor's expansion of the objective function around a set $\underline{\beta}$, i.e.,

$$J(\underline{\beta} + \underline{d}) = J(\underline{\beta}) + \underline{G}^T\underline{d} + \frac{1}{2}\,\underline{d}^T\underline{H}\,\underline{d} + \text{higher order terms} \qquad (5.9)$$

where $\underline{G}$ is the gradient vector, $\underline{H}$ is the Hessian matrix, both evaluated at $\underline{\beta}$, and $\underline{d}$ is an incremental vector. The elements of the gradient vector (G_k) and the Hessian matrix ($H_{k\ell}$) are defined by the relations

$$G_k = \frac{2J(\underline{\beta})}{\partial\beta_k}\ ; \quad H_k = \frac{\partial^2 J(\underline{\beta})}{\partial\beta_k\partial\beta_\ell} \qquad (k,\ell=1\text{-}n). \qquad (5.10)$$

Let $\underline{\beta}$ in Eq. (5.9) be an approximation to the optimum set $\underline{\beta}_{min}$ and $||\underline{d}||$ be small, then the expansion in Eq. (5.9), when higher order terms are neglected, takes the form

$$J(\underline{\beta} + \underline{d}) \simeq J(\underline{\beta}) + \underline{G}^T\underline{d} + \frac{1}{2}\,\underline{d}^T\,\underline{H}\,\underline{d} = Q(\underline{d})\ . \qquad (5.11)$$

The object is to determine $\underline{d}$ so that $\underline{\beta} + \underline{d} = \underline{\beta}_{min}$. For fixed $\underline{\beta}$ and variable $\underline{d}$, $e = Q(\underline{d})$ defines a quadratic surface approximating the error surface in the neighborhood of the point $(\underline{\beta}, J(\underline{\beta}))$. We know that at the minimum point $(\underline{\beta}_{min}, J(\underline{\beta}_{min}))$ the slope of the error surface must be zero. This is approximately satisfied if the derivative of $Q(\underline{d})$ with respect to $\underline{d}$ vanishes. Thus, from Eq. (5.11),

$$\underline{G} + \underline{H}\,\underline{d} = \underline{0}$$

or

$$\underline{d} = -\underline{H}^{-1}\,\underline{G}\ . \qquad (5.12)$$

Because the error surface is approximated by a quadratic surface, the increment $\underline{d}$ determined by Eq. (5.12) would be approximate, unless the error

surface is actually quadratic. Therefore ($\underline{\beta} + \underline{d}$) determines the next approximation to $\underline{\beta}_{min}$. The repeated use of this improvement procedure gives the Newton recurrence relation

$$\underline{\beta}_{i+1} = \underline{\beta}_i + d_i \qquad (i = 0,1,\ldots) \tag{5.13}$$

with

$$\underline{d}_i = -H^{-1}(\underline{\beta}_i)\ \underline{G}(\underline{\beta}_i) \ . \tag{5.14}$$

Computation of $\underline{d}_i$ from Eq. (5.14) requires the inversion of the Hessian. Alternatively, $\underline{d}_i$ can be found by solving the linear algebraic equations

$$H(\underline{\beta}_i)\underline{d}_i = -\underline{G}(\underline{\beta}_i) \tag{5.15}$$

with the aid of an elimination technique which is more suitable for computer use than the inversion of the Hessian.

Evaluation of $\underline{G}$ and $\underline{H}$ for the Present Problem

The objective function in this study is given by Eq. (5.3). Hence, the elements of $\underline{G}$ and $\underline{H}$ are obtained by substituting Eq. (5.3) into Eqs. (5.10). This results in

$$G_k = 2 \sum_{j=1}^{N} w_j \left[(r_j - \bar{r}_j) \frac{\partial r_j}{\partial \beta_k} + (s_j - \bar{s}_j) \frac{\partial s_j}{\partial \beta_k} \right] \tag{5.16}$$

$$H_{k\ell} = 2 \sum_{j=1}^{N} w_j \left[\frac{\partial r_j}{\partial \beta_k} \frac{\partial r_j}{\partial \beta_\ell} + \frac{\partial s_j}{\partial \beta_k} \frac{\partial s_j}{\partial \beta_\ell} + (r_j - \bar{r}_j) \frac{\partial^2 r_j}{\partial \beta_k \partial \beta_\ell} + (s_j - \bar{s}_j) \frac{\partial^2 s_j}{\partial \beta_k \partial \beta_\ell} \right] . \tag{5.17}$$

The Hessian matrix may be estimated by neglecting terms with second order partial derivatives (see [22]). This gives

$$H_{k\ell} \simeq H'_{k\ell} = 2 \sum w_j \left[\frac{\partial r_j}{\partial \beta_k} \frac{\partial r_j}{\partial \beta_\ell} + \frac{\partial s_j}{\partial \beta_k} \frac{\partial s_j}{\partial \beta_\ell} \right] . \tag{5.18}$$

The approximate Hessian $\underline{H}'$ approaches the Hessian $\underline{H}$ as $\underline{\beta} \to \underline{\beta}_{min}$. To evaluate $\underline{H}'$ it is not necessary to determine the second partial derivatives of r_j and

s_j, so the procedure is simplified. From Eqs. (5.16) and (5.18) it follows that the first order derivatives $\partial r_j/\partial \beta_k$ and $\partial s_j/\partial \beta_k$ are sufficient to find both $\underline{G}$ and $\underline{H}'$. These derivatives, called sensitivity coefficients, are evaluated and presented in Appendix B. The modified version of Newton's method in which $\underline{H}$ is approximated by $\underline{H}'$, is referred to as the Gauss-Newton method.

5.2.2 Line Search Algorithm

Let $\underline{\beta}$ and $\underline{d}$ be, respectively, the approximation and increment found in a particular, say i th, iteration. Then, $(\underline{\beta} + \underline{d})$ determines the approximation in the next iteration. It was stated earlier (see Eq. (5.8)) that the convergence can be improved by modifying the increment $\underline{d}$ to $\lambda \underline{d}$, where λ is a modification factor to be determined by a "line search". For fixed $\underline{\beta}$ and $\underline{d}$ and variable λ, the equation

$$e = J(\underline{\beta} + \lambda \underline{d}) \tag{5.19}$$

describes a profile of the error surface along a line L (in the $\underline{\beta}$ plane) passing through the point $\underline{\beta}$ and having the direction $\underline{d}$. By searching along the line L the minimum of the profile is located. The value of λ corresponding to this minimum determines the value of λ to be used in the i th iteration. It should be noted that λ has a different value in each iteration.

In the present study a simple line search algorithm is used in the analysis. Its derivation is based on the approximation of the error profile along L by a second order interpolating polynomial reproducing the three function values

$$e_0 = J(\underline{\beta}) \quad ; \quad e_1 = J(\underline{\beta} + \underline{d}) \quad ; \quad e_2 = J(\underline{\beta} + 2\underline{d}) \tag{5.20}$$

at $\lambda = 0,1,2$, respectively. Then the value of λ associated with the minimum point of the approximate profile may be found easily. It is

$$\lambda = \frac{e_2 - 4e_1 + 3e_0}{2(e_2 - 2e_1 + e_0)} \tag{5.21}$$

which involves evaluation of three error values in each iteration.

A value of λ close to 1 in a certain iteration indicates that the point on the error surface corresponding to $\underline{\beta}$ in that iteration is near the minimum and, consequently, the error surface in the neighborhood of that point is approximately quadratic. Accordingly, the value of λ associated with a selected initial approximation $\underline{\beta}_0$ gives a rough indication of whether the sequence $\{\underline{\beta}_0, \underline{\beta}_1, \ldots\}$ will converge or diverge.

5.2.3 The Iterative Algorithm

The method of optimization used in this study is presented and discussed in detail in the previous sections. The iterative algorithm is now summarized step by step:

1. Find an initial estimate $\underline{\beta}_0$ to $\underline{\beta}_{min}$, set $i = 0$
2. Evaluate $e_i = J(\underline{\beta}_i)$ [Eq. (5.3)]
3. Evaluate $\underline{G}(\underline{\beta}_i)$, $\underline{H}'(\underline{\beta}_i)$ [Eqs. (5.16),(5.18)]
4. Solve $\underline{H}'(\underline{\beta}_i)\underline{d}_i = -\underline{G}(\underline{\beta}_i)$ for $\underline{d}_i$ [Eq. (5.15)]
5. Determine λ_i [Eqs. (5.20),(5.21)]
6. Find the modified increment $\Delta\underline{\beta}_i = \lambda_i \underline{d}_i$ [Eq. (5.8)]
7. Obtain the next approximation by using $\underline{\beta}_{i+1} = \underline{\beta}_i + \Delta\underline{\beta}_i$ [Eq. (5.4)]
8. Evaluate $e_{i+1} = J(\underline{\beta}_{i+1})$ [Eq. (5.3)]
9. Check convergence [Eqs. (5.6) or (5.7)]
10. If not converged, set $i = i+1$, go to step 3.

6. NUMERICAL RESULTS AND DISCUSSIONS

Two theoretical models, namely the mixture and the effective modulus models, have been developed (Chapter 3) and their associated CFRF's obtained (Chapter 4), containing seven and two parameters, respectively. These models (CFRF's) are valid for both horizontal and vertical directions of motion. Therefore, associated with each model there are two sets of parameters to be determined through optimization, one for the horizontal and the other for the vertical response of the wall.

A general purpose computer program was developed to determine the model parameters through optimization and, together with its flowchart, is presented in Appendix C. The program, which is based on the Gauss-Newton method, is general in the sense that it has two features explained below.

(a) The program has the flexibility of varying the values of an arbitrary number of parameters in the set $\underline{\beta}$ while fixing the values of the remaining ones. This property can be used effectively to facilitate the optimization analysis as described below. (i) It may be used for shortening the computations. In fact, this property of the program makes it possible to examine, at any point on the error surface, the sensitivity of the error to changes in each parameter separately. If it is observed that the sensitivity of the error to a particular parameter is small compared with that of the others in the feasible region of $\underline{\beta}$, then the value of that parameter can be fixed during optimization, so that the number of variables is reduced. (ii) It gives control over the convergence and an appropriate initial estimate leading to a convergent sequence can be chosen. When convergence cannot be achieved by releasing all of the parameters, a sequential procedure may be tried. Optimization is started by releasing only the parameters having stable characteristics, say $\underline{\beta}^*$, with the number of

elements $n^* < 7$. Upon convergence, the next step is to release one more parameter and to choose an initial estimate composed of the converged values of $\underline{\beta}^*$ found in the previous step and an estimate for the new parameter. Also, when necessity arises, the effect of one parameter on another can be observed by releasing these two only.

(b) The program can be used for evaluating parameters appearing in both the mixture and the effective modulus models. This generality is introduced into the program because the effective modulus model may be obtained from the mixture model as its special case. To compute the optimum values of the parameters $\bar{\omega}$ and ξ in the effective modulus model, zero values are assigned to α', γ', γ and m', and two fixed dummy values to α and p.

The optimization program is used first to determine the parameters associated with the horizontal, then with the vertical response of the masonry walls.

6.1 Parameters for Horizontal Response

The parameters of the effective modulus and mixture models are determined by minimizing the objective function defined in Eq. (5.1), where H_u^t and H_u^e are, respectively, the theoretical and experimental CFRF's associated with the horizontal motion of the walls. The H_u^e values in this expression are obtained from the periodic runs rather than from the El Centro runs, for the reasons stated in Chapter 4. The El Centro data are used for comparison only.

First, the simplest of the two models, the effective modulus model, is considered. Then, the information and experience gained from the study of this model is used to analyze the more complicated mixture model.

6.1.1 Effective Modulus Model

The effective modulus model contains only two parameters, namely $\underline{\beta} = (\bar{\omega},\xi)$. Selection of the initial approximation $\underline{\beta}_0$ is rather straight forward for this model. The parameters $\bar{\omega}$ and ξ can be interpreted, respectively, as the undamped angular frequency and the nondimensional damping coefficient of the fundamental mode. An estimate for $\bar{\omega}$ can be obtained from the first intercept of $Re[H_u^e]$ on the frequency axis or by the frequency where $Im[H_u^e]$ has the first peak. From Figs. 13 and 14 $\bar{\omega}$ is estimated as about 113 rads (18 Hz) for wall A and 119 rads (19 Hz) for wall B. A short survey made on the error surface by using these values for $\bar{\omega}$ and varying ξ showed that ξ is roughly about 0.08 for wall A and 0.12 for wall B, and that the error surface is approximately quadratic in the neighborhood of the points defined by these estimated values. With the initial approximations $\underline{\beta}_0$ = (113, 0.08) for wall A and (119, 0.12) for wall B, the sequence generated by the program converged to the optimum values in 3 iterations for wall A and 6 iterations for wall B. The results are presented in Table 4, where the relative error is defined by

$$e \Big/ \sum_{j=1}^{N} (\bar{r}_j^2 + \bar{s}_j^2).$$

As seen from the table, the optimum value of ξ for wall B is larger than that for wall A. This is expected because (see Figs. 15 and 16) the dissipation for wall B appears to be greater than that for wall A. The theoretical CFRF's obtained using the optimum values of $\bar{\omega}$ and ξ are compared with the experimental CFRF's in Figs. 13 to 16. The two CFRF's match fairly well for both walls A and B in the low frequency range, up to the first modal frequency. The model has no ability to predict the high frequency response of masonry walls.

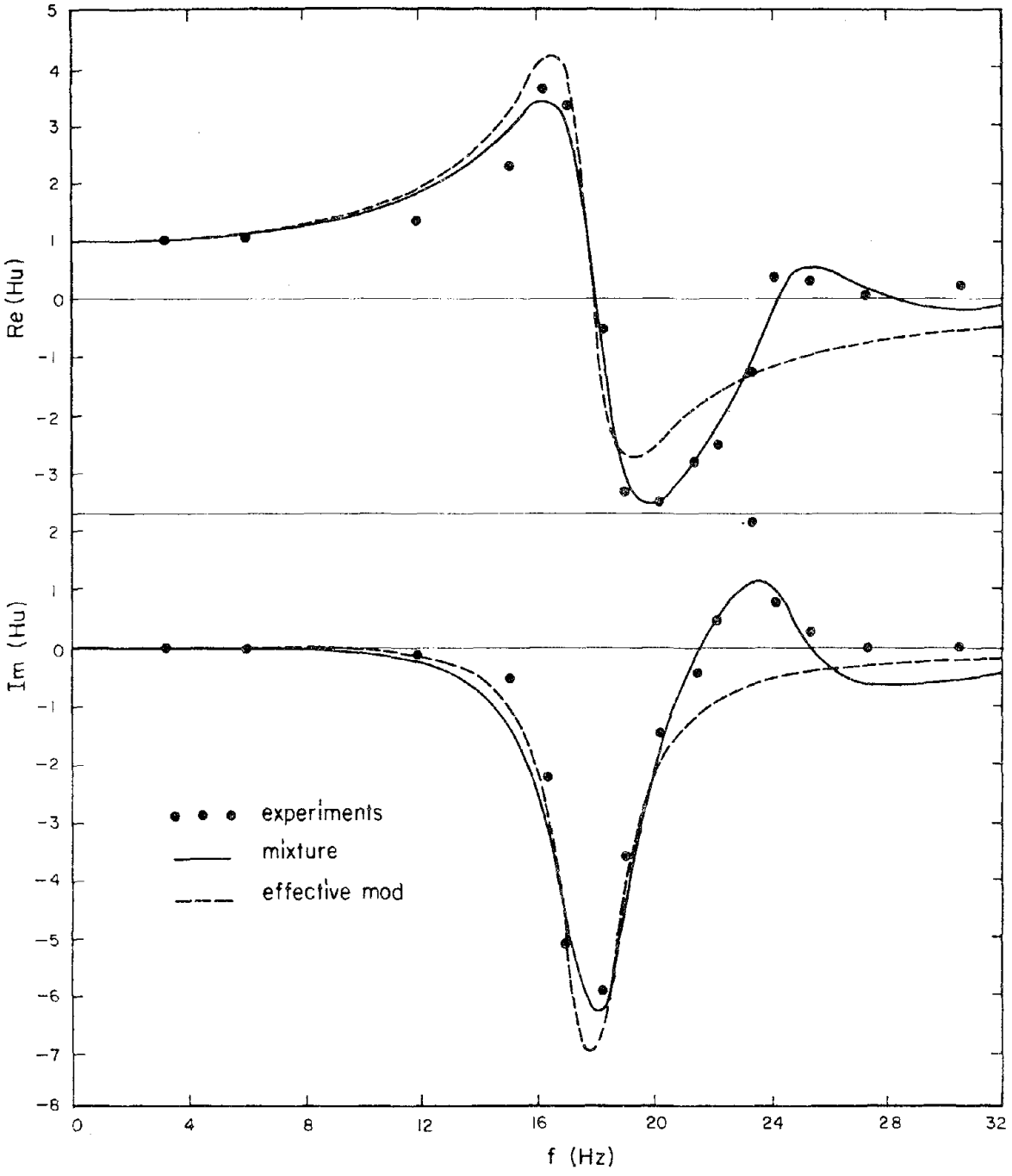

Figure 13. Theoretical and experimental complex frequency response functions (CFRF's) for horizontal motions of wall A (periodic data)

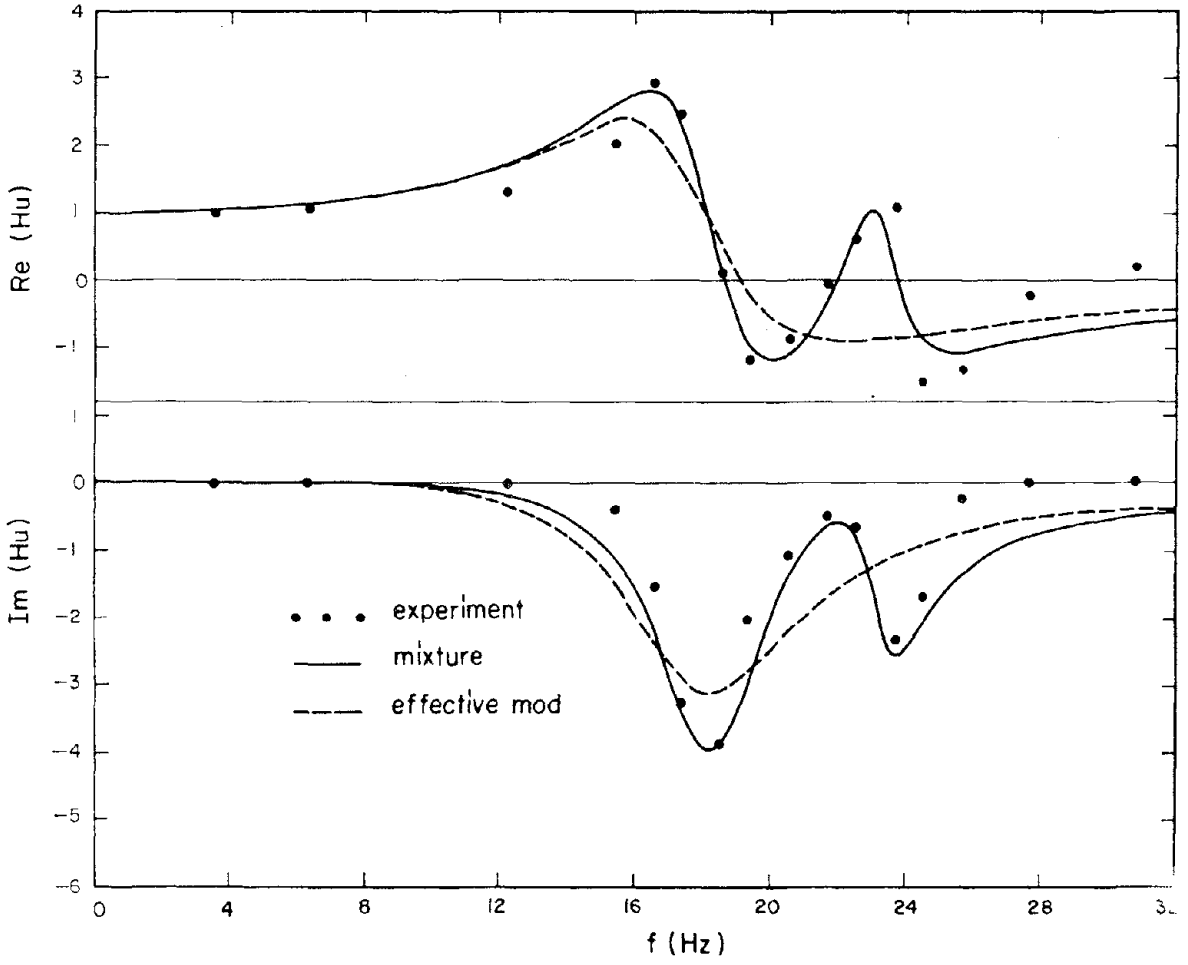

Figure 14. Theoretical and experimental CFRF's for horizontal motion of wall B (periodic data)

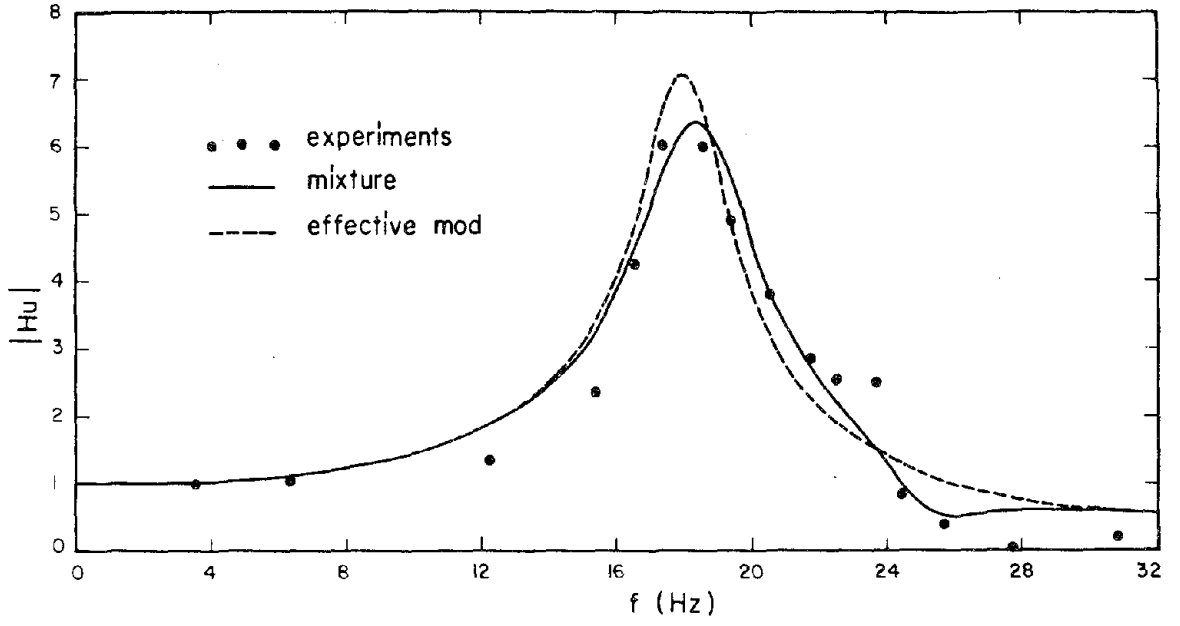

Figure 15. Theoretical and experimental amplification spectra for horizontal motion of wall A (periodic data)

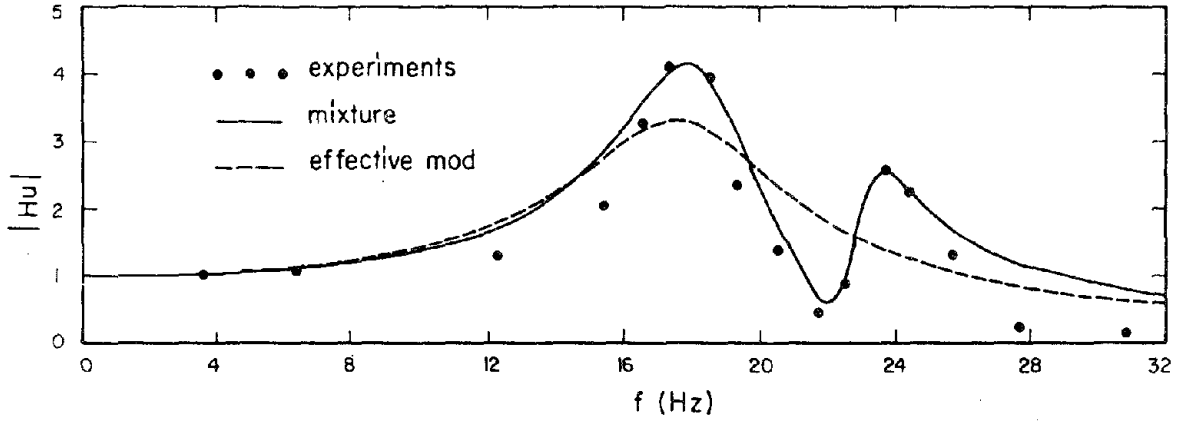

Figure 16. Theoretical and experimental amplification spectra for horizontal motion of wall B (periodic data)

6.1.2 Mixture Model

Finding a reasonable initial approximation which leads to convergence when all of the seven parameters are released is almost impossible for this model. A rational way to proceed is, first to establish a feasible region for the parameter set $\underline{\beta}$, then to start the optimization with a set of three or four released parameters and to increase the number of released parameters sequentially, upon convergence of each set. The set $(\bar{\omega},\xi)$ is taken here as as basis for starting the analysis, because the optimum values of these parameters in the mixture model are expected to be approximated by those predicted by the effective modulus model, and the sensitivity of the error to these parameters is similar for both models.

To establish a feasible region, it is necessary to determine the bounds for each parameter. In view of the definitions in Eqs. (3.48), (3.15) and (4.8 to 4.10), the parameter α defined in Eq. (4.5) is only dependent on the term q describing linear momentum interaction between the phases of the wall. For the two extreme values of q, which are zero (no interaction) and ρ (complete interaction), α assumes the values 0.40 and 0.60. These values establish a feasible interval for α ($0.40 \leq \alpha \leq 0.60$) which also meets the constraint condition stated in Eq. (4.13). On the other hand, the restrictions on the other parameters (p,γ) and (α', γ'), representing the elastic and viscous coefficients, respectively, come only from the constraint conditions in Eq. (4.13). However, these restrictions are not sufficient to determine well defined bounds for these parameters. The sequential procedure used in the analysis is explained below step by step. The arguments given are valid for both walls.

In the first step the released set is chosen to be composed of $\bar{\omega}$, ξ and the elastic parameters p, γ. The fixed parameter α is assumed to take an average value of 0.5, and zero is assigned to α' and γ', which is the

value of these parameters in the effective modulus model. The initial estimates $(\bar{\omega}_0,\xi_0)$ for $(\bar{\omega},\xi)$ are taken as their optimum values predicted by the effective modulus model, γ_0 is estimated to be -0.5 by assuming that brick is stiffer than mortar and p_0 is taken to be 1.0. Optimization of the released parameters with these initial estimates gives the desired result. The minimized relative error for both walls decreases by about 30% compared with that of the effective modulus model and no difficulty arises in convergence. There is no significant change in $(\bar{\omega},\xi)$ as expected, γ remains near its estimated value and the converged value of p is between 0.5 and 1. In the second step, the parameters $\bar{\omega}$, ξ, α' and γ' are varied while fixing the remaining parameters α, p, γ to the values $\alpha = 0.5$ and (p,γ) = their converged values obtained in the first step. The initial estimates of the released parameters are chosen to be $\alpha'_0 = \gamma'_0 = 0$ and $(\bar{\omega}_0,\xi_0)$ = their converged values in the first step. The convergence is again achieved in a few iterations, improving the minimum relative error. The converged values of the parameters are similar in magnitude and sign for both walls. In the third step all of the parameters except α, which is fixed to the value $\alpha = 0.5$ are released, with the initial estimates (p_0,γ_0) = their converged values in the first step and $(\bar{\omega}_0,\xi_0,\alpha'_0,\gamma'_0)$ = their converged values in the second step. The converged values of the parameters and the associated relative error obtained in this step are presented in Table 4. As a last step, all of the seven parameters are released, by estimating the initial values of parameters to be those given in the table; but in this case, the sequence of parameter sets diverges after a few iterations for both walls.

The same sequential procedure is repeated for the other feasible values of α, α = 0.45 and 0.55, and the same convergence phenomenon is observed at the third step. The converged values of the parameters for these α's are presented in Table 5 for both walls A and B. As seen from the

Table 4

Comparison of the converged values of model parameters determined through optimization with periodic and El Centro data (horizontal motion)

Type of Experiment	Wall	Type of Model	α	m'	$\bar{\omega}$	p	γ	ξ	α'	γ'	Relative Error
Periodic	A	Mixture	0.5	-0.59	115.21	0.6638	-0.6184	0.0802	0.2110	-0.2663	0.0482
		Effective Mod	—	—	113.84	—	—	0.0753	—	—	0.1629
	B	Mixture	0.5	-0.59	115.15	0.5621	-0.5637	0.1122	0.3368	-0.5239	0.1346
		Effective Mod	—	—	113.32	—	—	0.1696	—	—	0.2623
El Centro	A	Mixture	0.5	-0.59	112.56	0.6478	-0.5499	0.1050	0.2110	-0.2663	0.2527
	B	Mixture	0.5	-0.59	115.00	0.5339	-0.4776	0.1466	0.3368	-0.5239	0.2402

Table 5

Comparison of the converged values of model parameters for different values of α (horizontal motion)

Type of Experiment	Wall	Type of Model	α	m'	$\bar{\omega}$	p	γ	ξ	α'	γ'	Relative Error
Periodic	A	Mixture	0.45	-0.59	115.66	0.561	-0.612	0.0831	0.263	-0.385	0.04822
			0.50		115.21	0.664	-0.618	0.0802	0.211	-0.266	0.04822
			0.55		114.73	0.768	-0.623	0.0786	0.156	-0.140	0.04822
Periodic	B	Mixture	0.45	-0.59	115.13	0.491	-0.572	0.1111	0.338	-0.542	0.1346
			0.50		115.15	0.562	-0.564	0.1122	0.337	-0.524	0.1346
			0.55		115.26	0.632	-0.556	0.1130	0.333	-0.504	0.1346

table, the relative errors of the three parameter sets with α = 0.45, 0.50, 0.55 are identical. The computations indicate that the three sets, furthermore, lead to an identical match between theoretical and experimental CFRF's. The theoretical CFRF's the same for the three α's are shown for walls A and B in Figs. 13, 15 and 14, 16, respectively.

The arguments presented above indicate the existence of a uniqueness problem regarding the parameter α. However this problem does not cause any major inconvenience for the following reasons. First, for extreme values of the linear momentum interaction coefficient q, the parameter α varies over a narrow interval, $0.40 \leq \alpha \leq 0.60$, in which the parameters change smoothly and slowly. Moreover, the value of q is at most about 0.30 for layered composites (see reference [8]). Because of these observations, the parameters for α = 0.45, which corresponds to q = 0.26, are suggested for practical purposes. The set associated with α = 0.45 is named as the optimum set of the mixture model. In order to be more precise about the value of α, additional observations should be made at intermediate locations of the wall and the associated readings should be included in the analysis. Unfortunately, in the present study the measurements were made only at the top and bottom ends of the wall because of the limited number of available accelerometers.

Comparison of the experimental and theoretical CFRF's presented in Figs. 13 to 16 suggests that the mixture model is capable of predicting not only low frequency, but also high frequency response of the walls.

6.2 Parameters for Vertical Response

The experimental CFRF's associated with the vertical excitations of the walls A and B are presented in Figs. 17 and 18, respectively. It may be observed that there are some marked differences between these CFRF's and those for the horizontal response. Before presenting the analysis, it is

appropriate to examine a characteristic of the experimental CFRF's for the vertical response. In Figs. 17, 18 it can be seen that $Re[H_u^e]$ and $Im[H_u^e]$ have approximately constant values of about one and zero, respectively, except for a narrow frequency interval where they deviate slightly from these constant values. This implies that the wall will behave rigidly when it is subjected to vertical periodic base excitation with a frequency not contained in the narrow interval. This peculiar behavior may be attributed partly to the fact that masonry walls constitute a highly dissipative medium for vertical excitations, resulting in damping out of the vertical amplification.

The function $H_u^e(f_j)$ for wall A has better defined values than for wall B and gives a rough idea at least about the response of the wall around the first modal frequency. For this reason, the parameters of wall A will be determined first. A procedure similar to that outlined in the previous section is used in the analysis. Because the high frequency response of the wall is very uncertain after the first modal frequency, there is difficulty in choosing the released parameters. Through the search, the most suitable released parameter set leading to a convergent sequence is found to be $(\bar{\omega}, \xi, \alpha', \gamma)$. Using the optimization program, the converged values of the released parameters are determined for fixed values of α, p, γ'. A survey based on the feasible values of p and γ' yields as the most suitable values, 0.35 for p and zero for γ'.

It is found that the uniqueness problem regarding the parameter α exists also for the vertical case. Three different sets of parameters are obtained for the three fixed values of α, α = 0.45, 0.50 and 0.55, and are presented in Table 7. Similar to the horizontal case, these three sets give identical relative errors and identical CFRF's.

After determining the optimum set of parameters for wall A, the parameters for wall B are found by choosing an initial set which is, except ξ, equal to the optimum set for wall A. ξ_o is modified because an increased value is expected for it. The result of optimization supported this expectation: the optimum ξ of wall B is found to be about eight times that of wall A.

The values of parameters for both walls are presented in Table 6, for $\alpha = 0.5$. The theoretical CFRF's of the two walls A and B obtained using the optimum parameters are compared with the experimental CFRF's in Figs. 17 and 18. A comparison of the theoretical and experimental CFRF's in absolute values is given in Fig. 19 for wall A.

6.3 Coefficients

The coefficients appearing in the governing equations of the mixture model, Eq. (3.48), can be determined in terms of the model parameters considered in the optimization analysis. The relations between the model parameters and these coefficients are given in Eqs. (4.5). Using the relations $\bar{\omega}^2 = K_{11}/M_{11}$; $\xi = C_{11}/2M_{11}\bar{\omega}$, and taking into account the definitions given in Eqs. (4.10), the coefficients M_{ij}, C_{ij} and K_{ij} (i,j=1,2) associated with both horizontal and vertical responses are computed for walls A and B. The results are presented in Tables 8 and 9. If it is desired, the corresponding coefficients appearing in the effective modulus model, Eq. (3.62), can be obtained by following the same procedure.

6.4 Discussion

The results obtained in the previous sections and their implications are now discussed in detail. The discussion is essentially based on comparison of the experimental and theoretical responses in the frequency and time spaces, and on the relative participation of the brick and mortar constituents

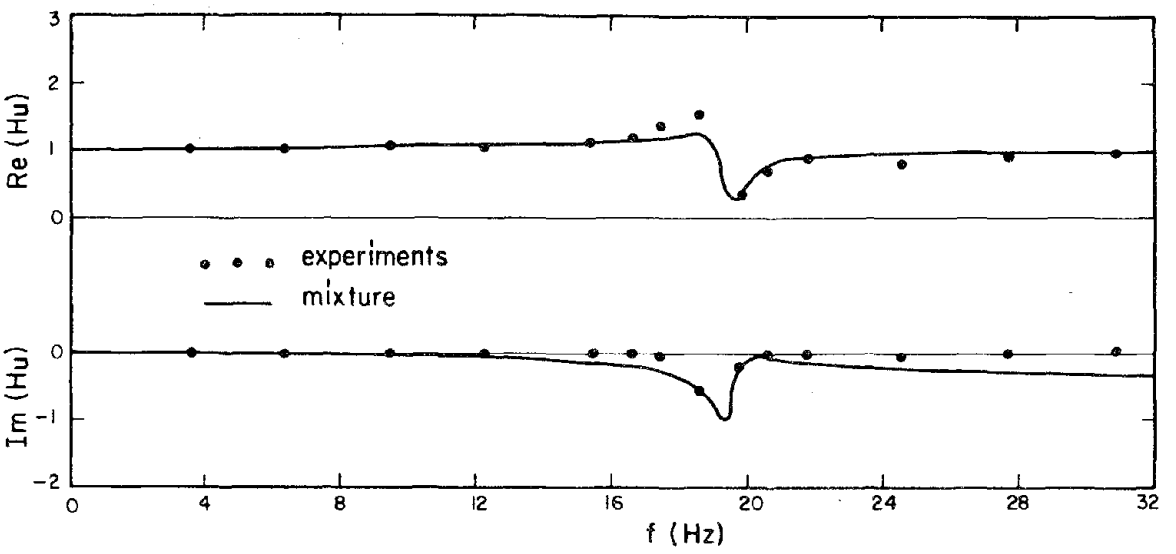

Figure 17. Theoretical and experimental CFRF's for vertical motion of wall A (periodic data)

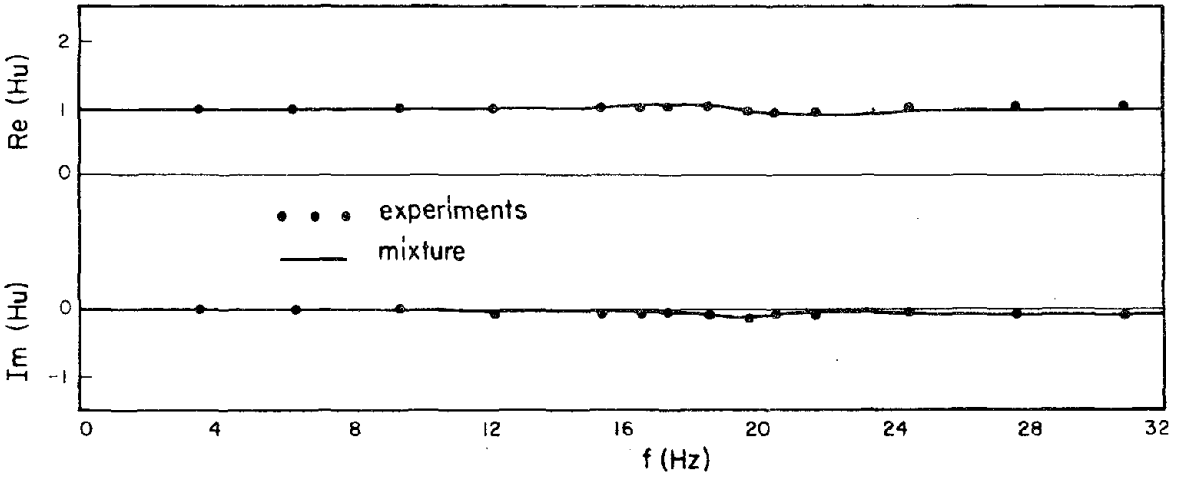

Figure 18. Theoretical and experimental CFRF's for vertical motion of wall B (periodic data)

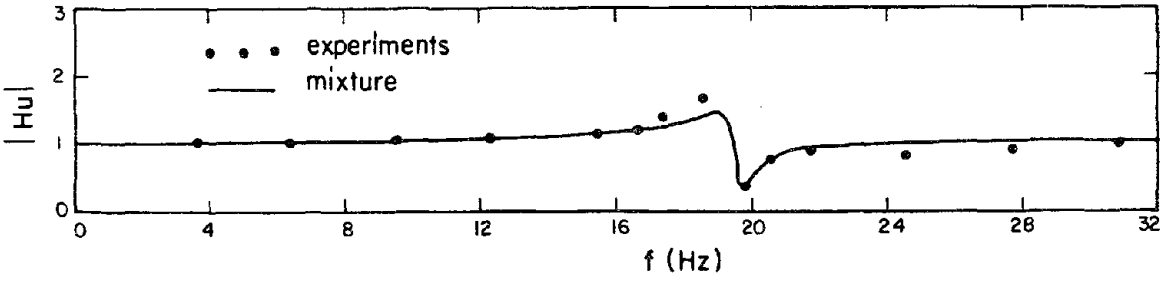

Figure 19. Theoretical and experimental amplification spectra for vertical motion of wall A (periodic data)

Table 6

Comparison of the converged values of model parameters determined through optimization with periodic data (vertical motion)

Type of Experiment	Wall	Type of Model	α	m'	$\bar{\omega}$	p	γ	ξ	α'	γ'	Relative Error
Periodic	A	Mixture	0.5	-0.59	146.01	0.350	-0.3841	0.5708	0.0130	0.0	0.03524
Periodic	B	Mixture	0.5	-0.59	147.17	0.340	-0.4060	4.2716	0.0062	0.0	0.00035

Table 7

Comparison of the converged values of model parameters for different values of α (vertical motion)

Type of Experiment	Wall	Type of Model	α	m'	$\bar{\omega}$	p	γ	ξ	α'	γ'	Relative Error
Periodic	A	Mixture	0.45	-0.59	145.52	0.330	-0.420	0.387	0.0113	0.0	0.03569
			0.50		146.00	0.350	-0.384	0.571	0.0130	0.0	0.03524
			0.55		154.41	0.345	-0.336	0.582	0.0129	0.0	0.03538

Table 8

Optimum values of coefficients in the mixture model (horizontal motion)

Type of Experiment	Wall	Type of Model	M_{11}	M_{22}	M_{12}	$K_{11}/10^6$	$K_{22}/10^6$	$K_{12}/10^6$	$C_{11}/10^4$	$C_{22}/10^4$	$C_{12}/10^4$	M'_{11}	M'_{12}
			kg			N/m			N. sec / m			kg	
Periodic	A	Mixture	2435.	1217.5	-1446.7	32.32	21.46	-19.99	4.5	0.95	-1.2	2566.	-1511.
	B	Mixture	2435.	1217.5	-1446.7	32.29	18.17	-18.20	6.3	2.12	-3.3	2566.	-1511.

Table 9

Optimum values of coefficients in the mixture model (vertical motion)

Type of Experiment	Wall	Type of Model	M_{11}	M_{22}	M_{12}	$K_{11}/10^6$	$K_{22}/10^6$	$K_{12}/10^6$	$C_{11}/10^4$	$C_{22}/10^4$	$C_{12}/10^4$	M'_{11}	M'_{12}
			kg			N/m			N. sec / m			kg	
Periodic	A	Mixture	2435.	1217.5	-1446.7	51.91	18.17	-19.94	40.6	0.53	0.0	2566.	-1511.
	B	Mixture	2435.	1217.5	-1446.7	52.74	17.93	-21.41	306.1	1.89	0.0	2566.	-1511.

in the dynamic response of the masonry walls. Since the mixture model is a more refined model than the effective modulus model, only the results obtained from the former model will be considered in the discussions.

6.4.1 Comparison of the Parameters Obtained from Periodic and El Centro Data

In this section, the optimum values of the parameters are computed using the El Centro data and these values are compared with those already determined from the periodic data.

The experimental CFRF's derived from the El Centro runs were found in Chapter 4 for the horizontal response, and presented in Figs. 20 and 21, respectively, for walls A and B. They are truncated at f = 24 Hz because of large fluctuations after f = 24 Hz (caused by the unreliability of the El Centro data at higher frequencies). These CFRF's are used in the optimization analysis to determine the values of parameters associated with the El Centro data. The lack of information in the neighborhood of and after the second modal frequency in the El Centro data necessitate fixing $(\alpha, \alpha', \gamma')$ to achieve convergence. The fixed values of $(\alpha, \alpha', \gamma')$ and the initial values of the released parameters $(\bar{\omega}, \xi, p, \gamma)$ are chosen to be $\alpha = 0.50$; $(\alpha', \gamma', \bar{\omega}_0, \xi_0, p_0, \gamma_0)$ = their converged values found from the periodic data with $\alpha = 0.5$

The results of the optimization analysis are presented in Table 4 together with the corresponding relative errors. When the two sets of parameters computed from the periodic and the El Centro data are compared in this table, some small differences for $(\bar{\omega},p)$ and relatively large differences for (ξ,γ) may be observed for both of the walls. These differences are expected for the following reasons. First, the frequency interval considered in the optimization analysis is different for the periodic data and the El Centro data. In fact, it is $0 \leq f \leq 32$ Hz for the periodic data and

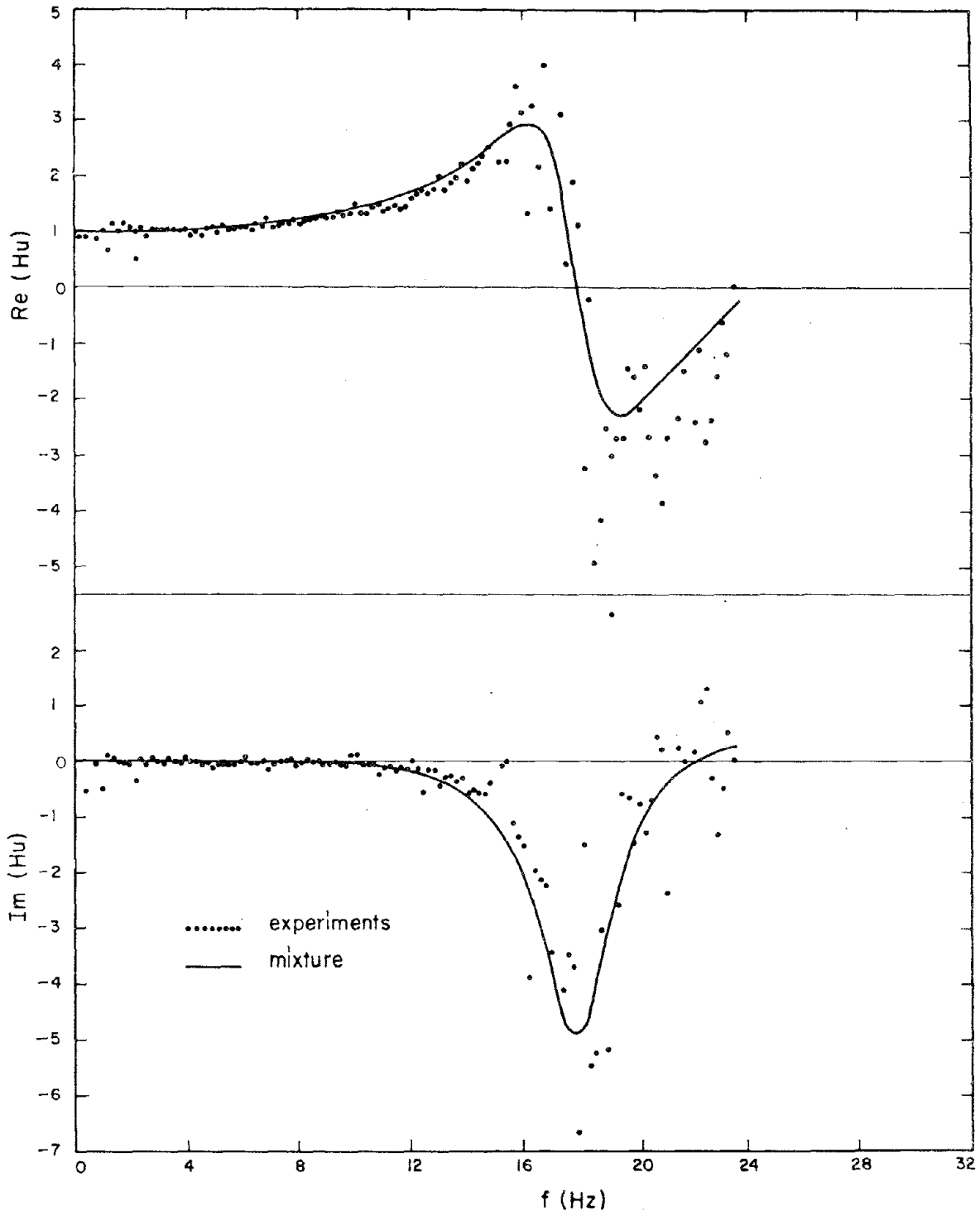

Figure 20. Theoretical and experimental CFRF's for horizontal motion of wall A (El Centro data)

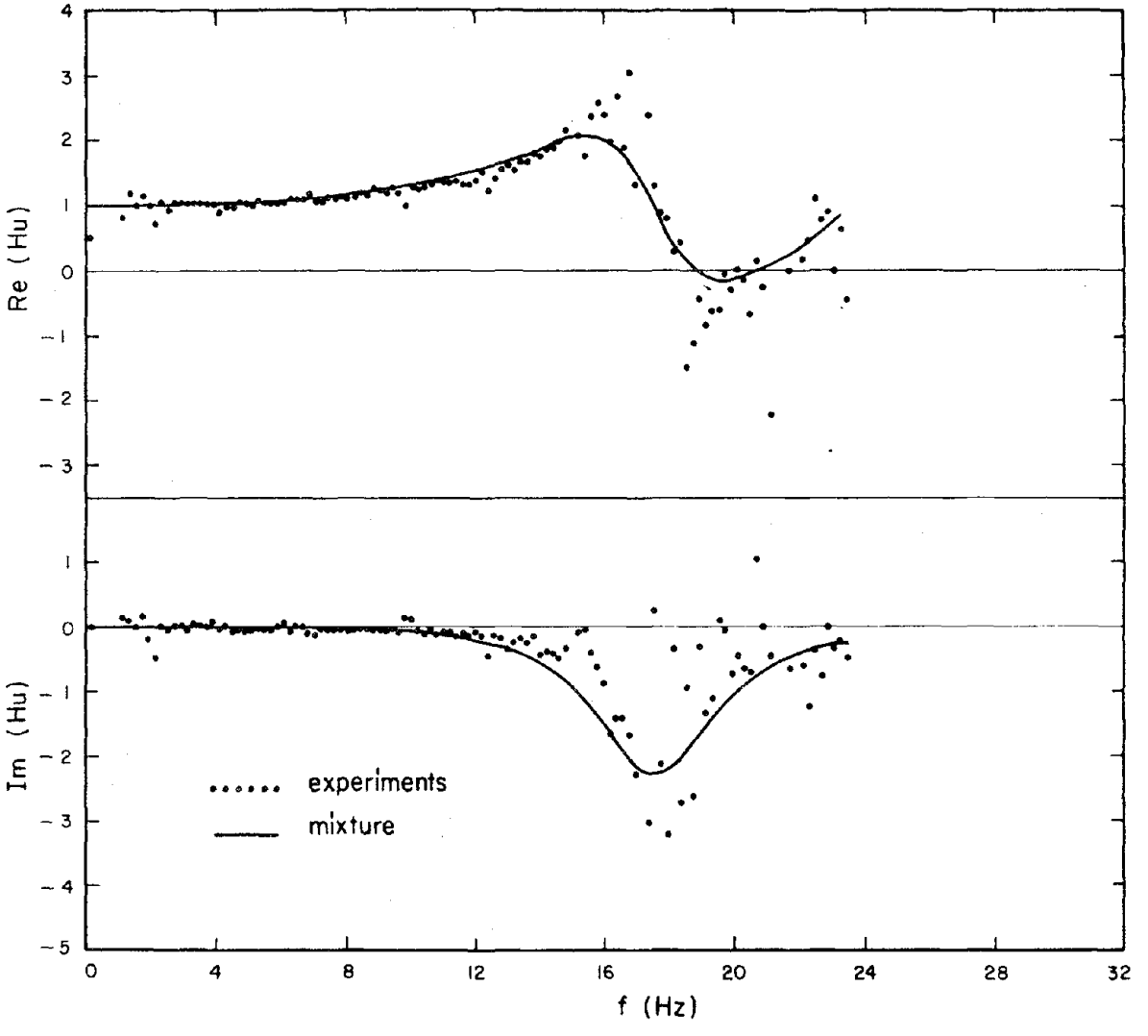

Figure 21. Theoretical and experimental CFRF's for horizontal motion of wall B (El Centro data)

$0 \leq f \leq 24$ Hz for the El Centro data. Secondly, the H_u^e obtained from the periodic and from the El Centro data differ considerably outside the interval $2 \leq f \leq 15$ Hz (which is the reliable frequency band (RFB) of H_u^e computed from the El Centro data).

The H_u^t are computed using the parameters obtained from the El Centro data and are compared with the experimental values in Figs. 20 and 21 for walls A and B, respectively.

6.4.2 Comparison of Response in Time Space

Comparisons are presented for the horizontal top acceleration $\ddot{u}^+(t)$ and the base shear force $V^-(t)$. The experimental $\ddot{u}^+$ used for comparison is the acceleration output recorded during the El Centro run with s = 7.7 (the maximum amplitude of the input acceleration $\ddot{u}_g$ for this run is 0.236 g). The theoretical $\ddot{u}^+$ is obtained as follows: the Fourier transform of the input acceleration $(\ddot{u}_g)^F$ is multiplied by the theoretical CFRF H_u^t computed using the parameters presented in Table 4 (obtained from the periodic data). From Eq. (4.2) the resulting quantity determines $(\ddot{u}^+)^F$ which is the Fourier transform of the output acceleration; its inverse transform gives the theoretical $\ddot{u}^+$. The experimental and theoretical $\ddot{u}^+$ are compared in Figs. 22 and 23 for walls A and B, respectively. The figures indicate that the two $\ddot{u}^+$ time histories match fairly well. This good match is anticipated because, as seen from Figs. 13 and 14, H_u^t matches H_u^e closely in the frequency band (FB) ($2 \leq f \leq 15$ Hz) of the input acceleration.

A general comment will be made now regarding the advantage of optimization using the CFRF. The match of H_u^t and H_u^e only in the frequency band of the input governs the goodness of the match between the experimental and theoretical outputs. The match of the outputs is not affected by differences in H_u^t and H_u^e at frequencies outside this band. If the optimization is based

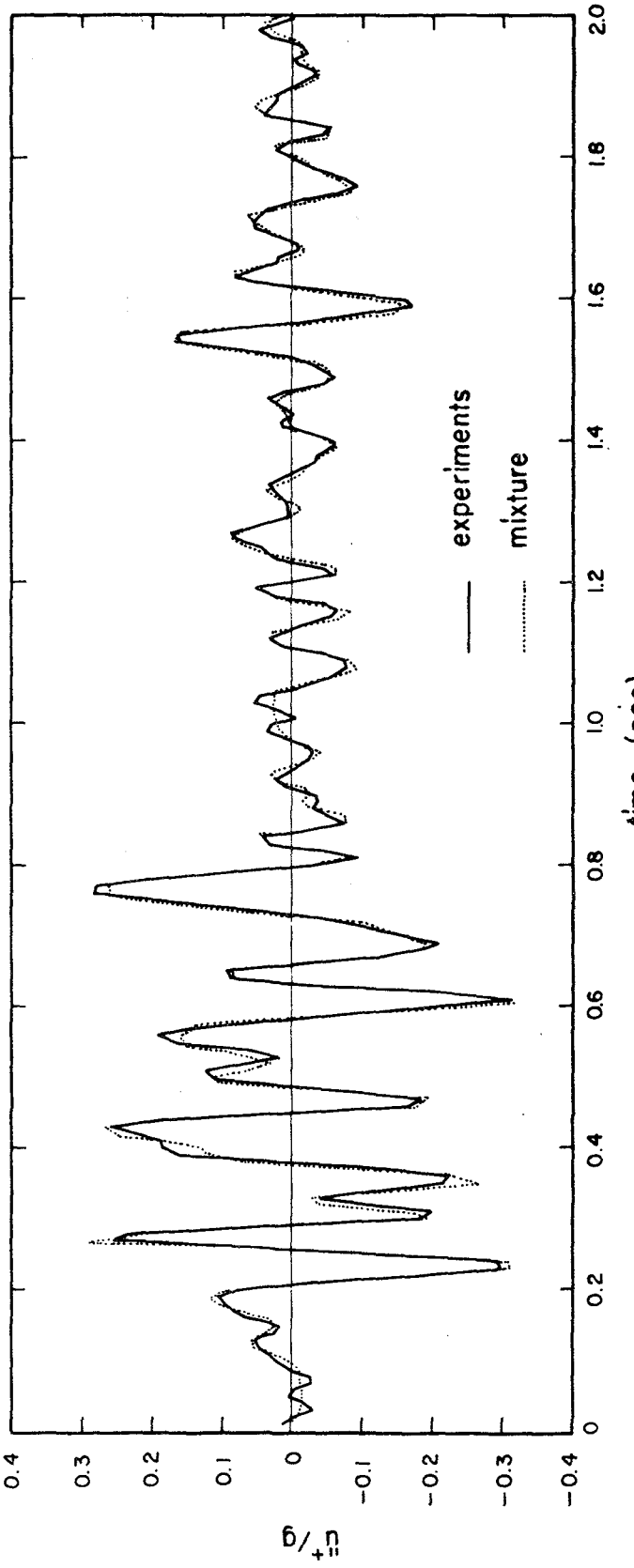

Figure 22. Comparison of time histories of theoretical and experimental top acceleration responses for wall A (for El Centro input)

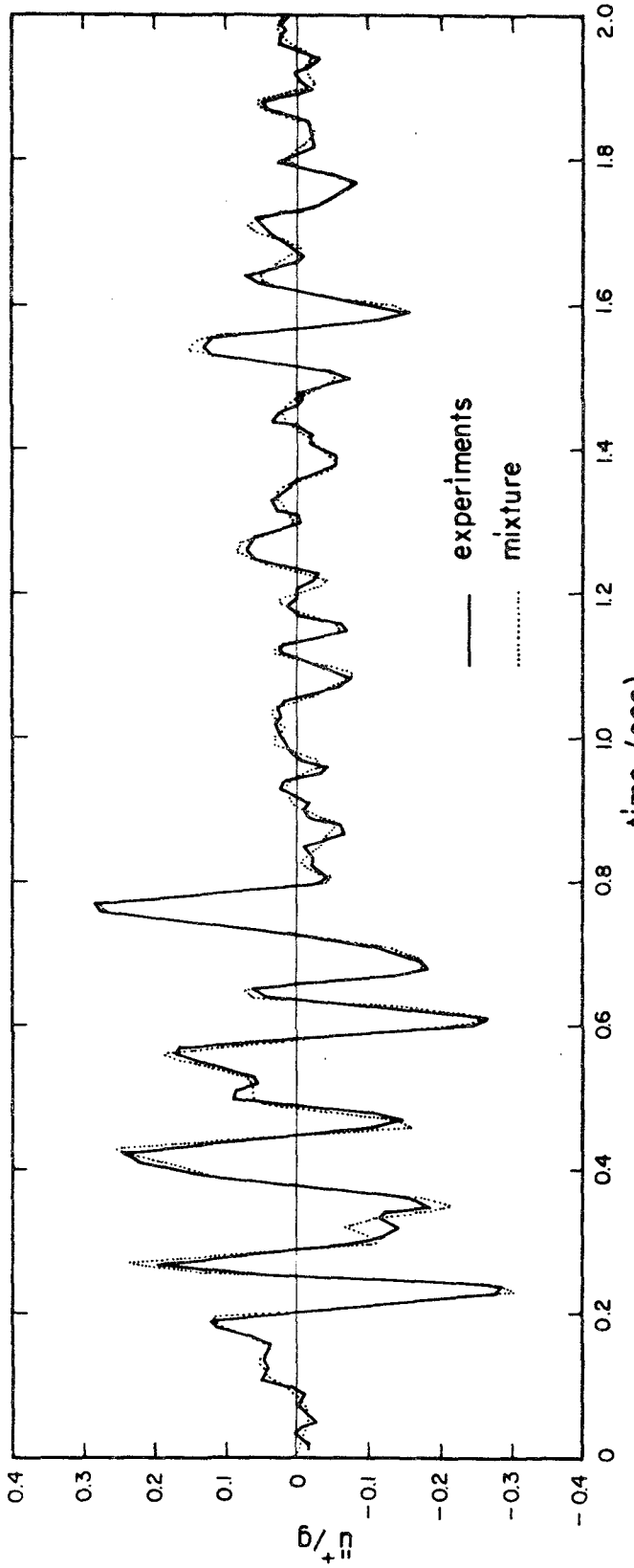

Figure 23. Comparison of time histories of theoretical and experimental top acceleration responses for wall B (for El Centro input)

on matching CFRF's, then a study of the match of the H_u in the FB of a given input could determine in advance whether or not the model would predict adequately the response to that input. A good match in time space associated with a certain input is not a reliable indicator for the goodness of the model. It shows only that the model predicts the response correctly for the excitations with FB's contained in the FB of that input.

Although the shear force at the base of the wall is not measured during the tests, it can be computed from a free body analysis of the wall by using the horizontal base and top acceleration records, and by assuming a linear acceleration distribution over the height of the wall. The theoretical base shear force can be found in frequency space by using Eq. (3.59) with $\bar{x} = -1$. The coefficients in this equation are listed in Table 8. Transformation from frequency to time space yields the theoretical $V^-(t)$. The experimental (computed) and the theoretical V^- are obtained for the El Centro run with $s = 7.7$ (having the maximum $\ddot{u}_g$ of 0.236 g). The results are compared in Figs. 24 and 25 for walls A and B, respectively. The close match in these figures can be attributed to the good agreement between the $\ddot{u}^+$. This can be seen more clearly by comparing Fig. 24 with Fig. 22 and Fig. 25 with Fig. 23.

6.4.3 Comparison of the Responses of Walls A and B

The horizontal response of the walls is governed by their CFRF's shown in Figs. 13 and 14. It is clear from these figures that the low frequency behaviors of the walls A and B are similar and their first modal frequencies are close (18 Hz for wall A and 18.5 Hz for wall B). The only marked difference in the first mode is in the amount of amplification, which is greater in wall A than in wall B. This difference is certainly due to different energy dissipation in the two walls. The second modal frequencies of walls

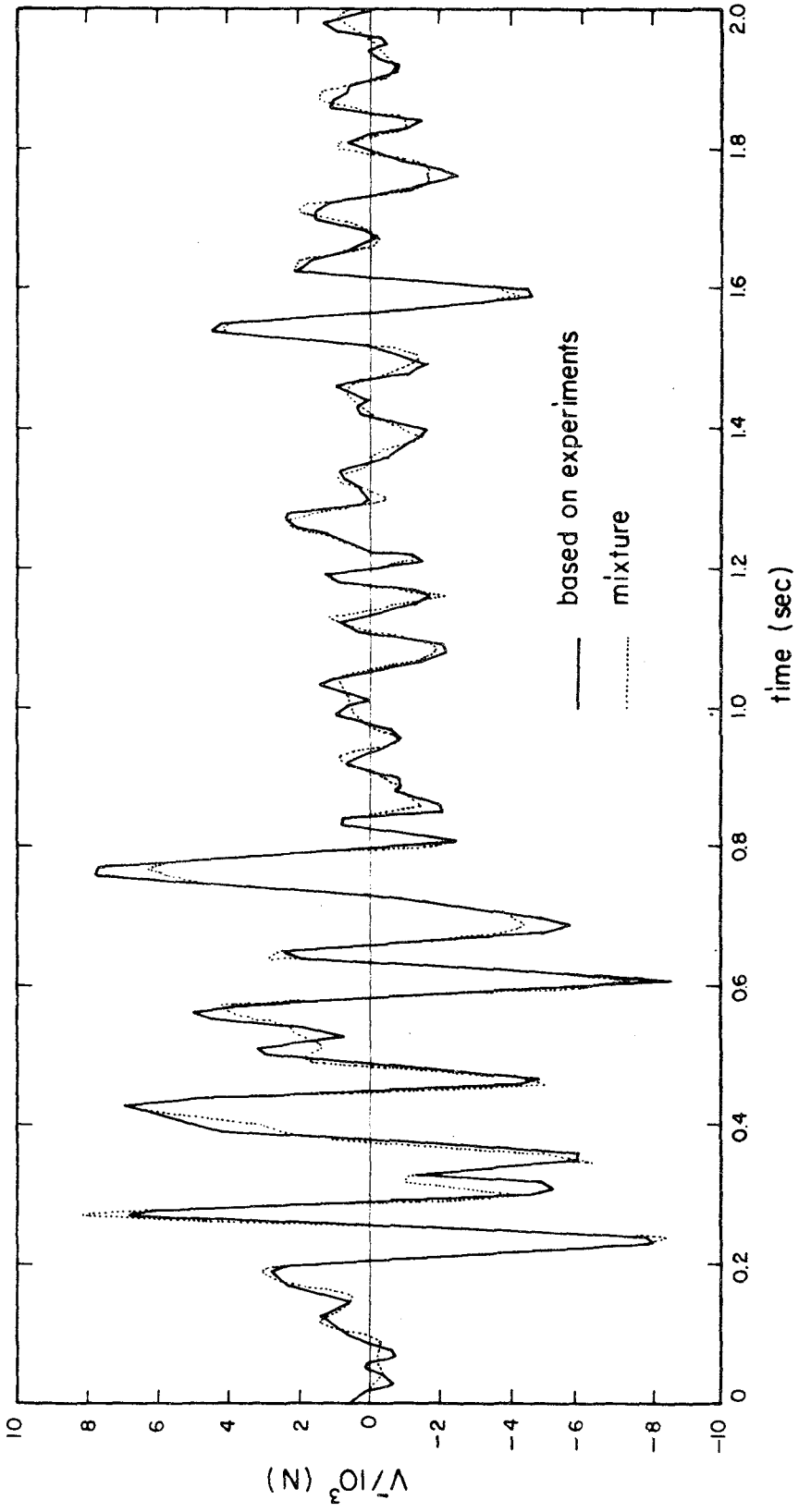

Figure 24. Comparison of time histories of theoretical and experimental base shear force for wall A (for El Centro input)

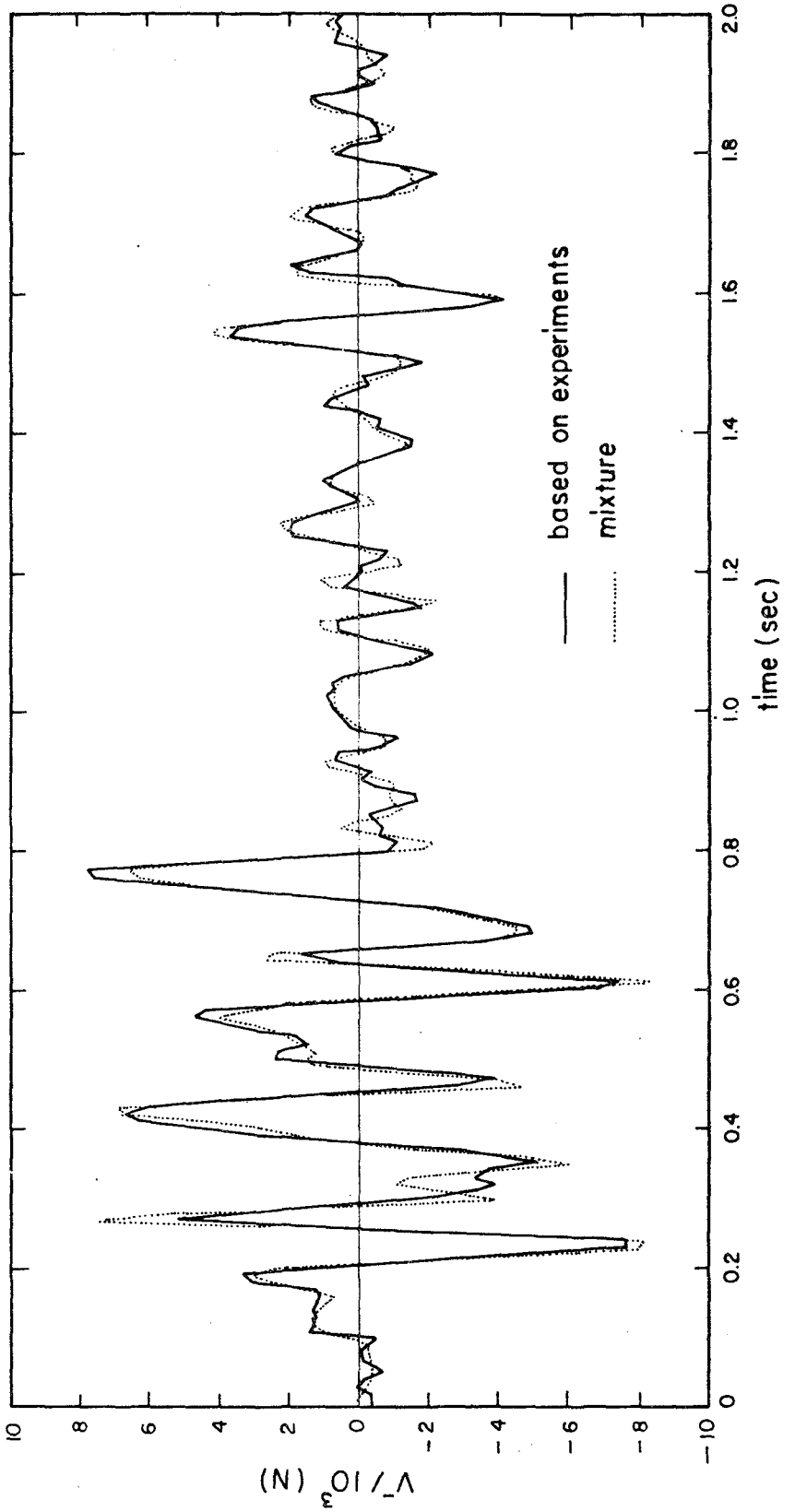

Figure 25. Comparison of time histories of theoretical and experimental base shear force for wall B (for El Centro input)

A and B are also close (~ 23.5 Hz for both walls), but their behaviors after the first modal frequency are completely different: the second peak values of the $Im[H_u]$ have opposite signs, and the second and third intercepts of the $Re[H_u]$ with the frequency axis are different for walls A and B. These differences are due to different micro slip distributions in the two walls. A detailed discussion of slip phenomenon is given in the next Chapter. It is remarkable that the mixture model is able to predict the response of both walls in spite of their having very different CFRF's.

CFRF's for the vertical response were presented in Figs. 17 and 18 for walls A and B, respectively. A comparison of the figures indicates that the difference in the vertical responses of the two walls stems from the amount of dissipated energy which is extremely high for wall B compared with that for wall A. The optimum values of the parameters for walls A and B support this observation (Table 6) where, among all of the parameters, only the value of the damping coefficient ξ differs considerably for the two walls.

6.4.4 Horizontal Response of the Constituents

CFRF's for the horizontal response of the brick and mortar constituents are obtained theoretically for walls A and B by using the mixture model with the optimum parameters given in Table 5. These CFRF's relating the horizontal top accelerations of the constitutents to the horizontal base acceleration are found using the equation

$$Hu_\alpha = \frac{(\ddot{u}_\alpha^+)^F}{(\ddot{u}_g)^F} = \frac{u_\alpha^{+F}}{u_g^F} \qquad (\alpha = 1,2) \qquad (6.1)$$

and by taking into account Eqs. (3.11, 3.40, 3.47). The results are shown in Figs. 26, 27 and 28, 29 for walls A and B, respectively. (The subscripts 1 and 2 designate mortar and brick constituents, respectively, in these figures).

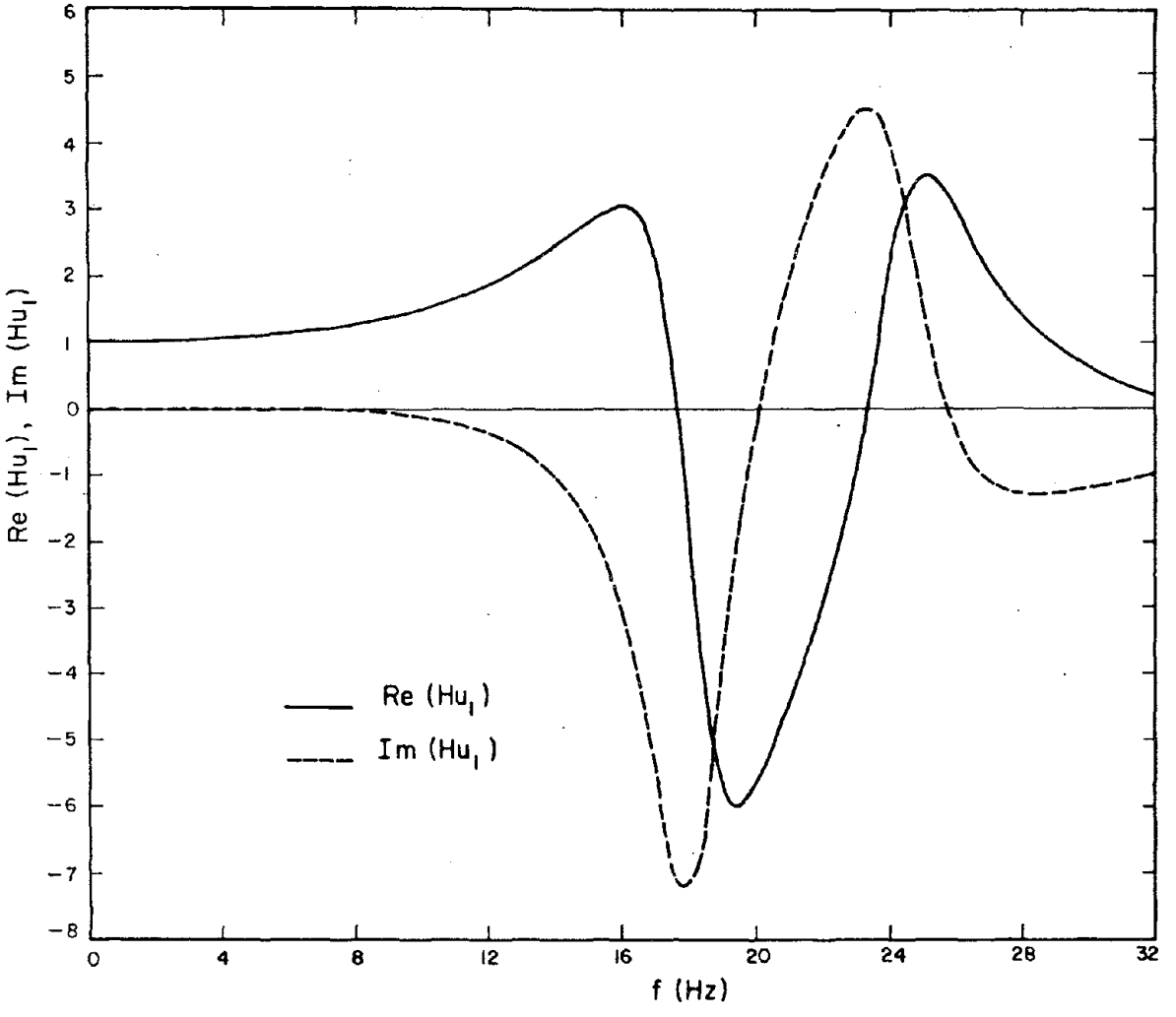

Figure 26. CFRF for mortar constituent of wall A (horizontal motion)

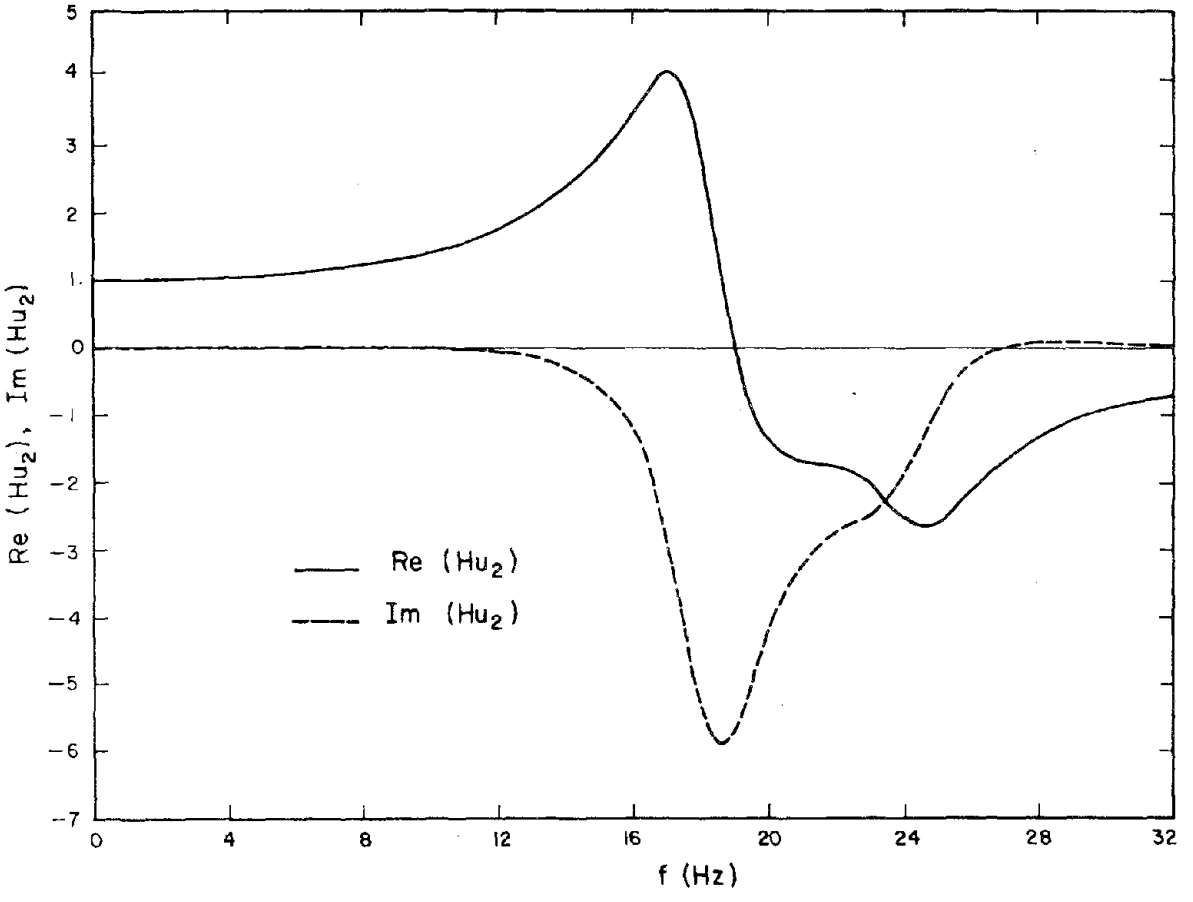

Figure 27. CFRF for brick constituent of wall A (horizontal motion)

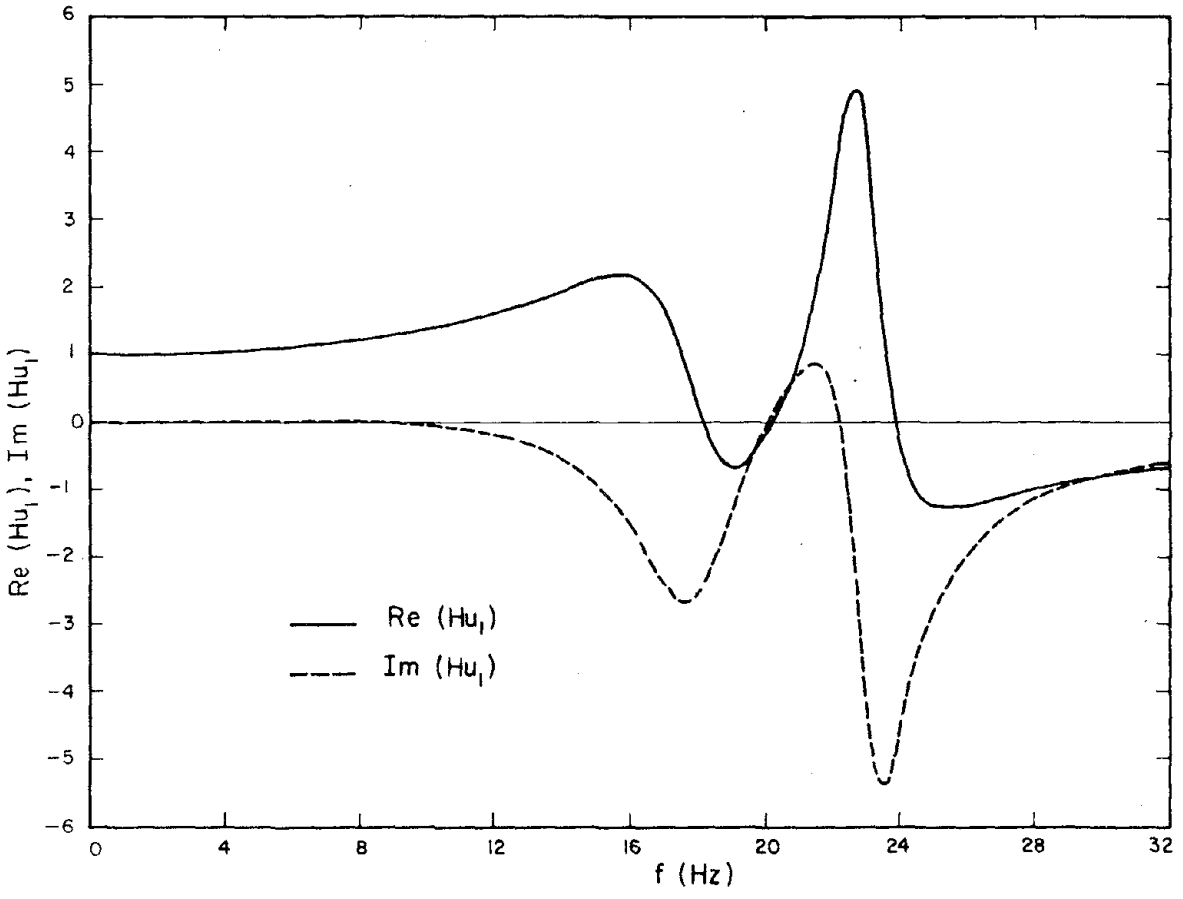

Figure 28. CFRF for mortar constituent of wall B (horizontal motion)

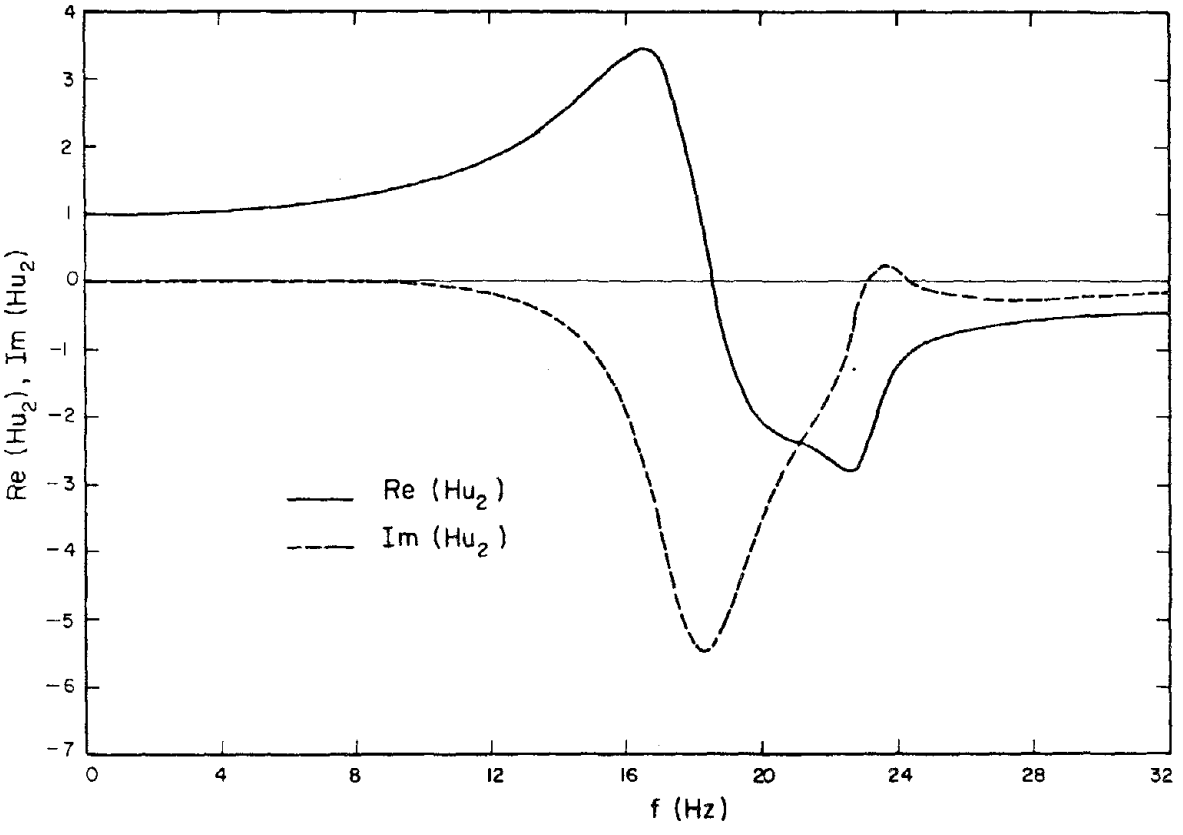

Figure 29. CFRF for brick constituent of wall B (horizontal motion)

When the theoretical CFRF's of the constitutents in walls A and B are compared, it is found that the response of brick is similar for both walls whereas the response of mortar is completely different. To understand the dynamic behavior of the constituents more clearly, their amplifications $|Hu_j|$ and phase angles $\alpha_i = \tan^{-1}\{Im[Hu_i] / Re[Hu_i]\}$ are obtained separately. The amplification and phase spectra are shown in Figs. (30 to 33) for the constituents of walls A and B. The angle α_i in the figures designates the phase shift of the top acceleration of the i th constituent with respect to the base acceleration, and is measured counterclockwise from the $Re[Hu_i]$ axis in the complex Hu_i plane with the range $0 \leq \alpha_i \leq 2\pi$.

In Fig. 30 the amplification curves for the brick and mortar constituents of wall A are approximately parallel throughout the frequency range under consideration. The phase difference between constituent top accelerations, designated by $(\alpha_2 - \alpha_1)$ in Fig. 31, is zero at $f = 0$ and then, varying slowly, reaches a value of about $\pi/4$ at the first modal frequency. Afterwards it increases more rapidly between the two modal frequencies and assumes an average value of about π in the high frequency range. In view of these observations we conclude that the top accelerations of the two constituents are "in phase" in the low frequency range and "out of phase" in the high frequency range. The amplification of mortar is greater than that of brick by 18% in the first mode and by 30% in the second mode.

The situation is rather different for wall B (see Figs. 32, 33). The constituent accelerations are almost in phase in the first mode. The phase difference $(\alpha_2 - \alpha_1)$ suddenly jumps from $\pi/8$ to π at $f \simeq 20$ Hz, which is between the two modal frequencies, then reaches a value of about $3\pi/2$ in the second mode (out of phase). An interesting situation is observed at $f \simeq 20$ Hz for the mortar constituent. Around this frequency the amplification curve passes through a minimum while its phase shift suddenly decreases

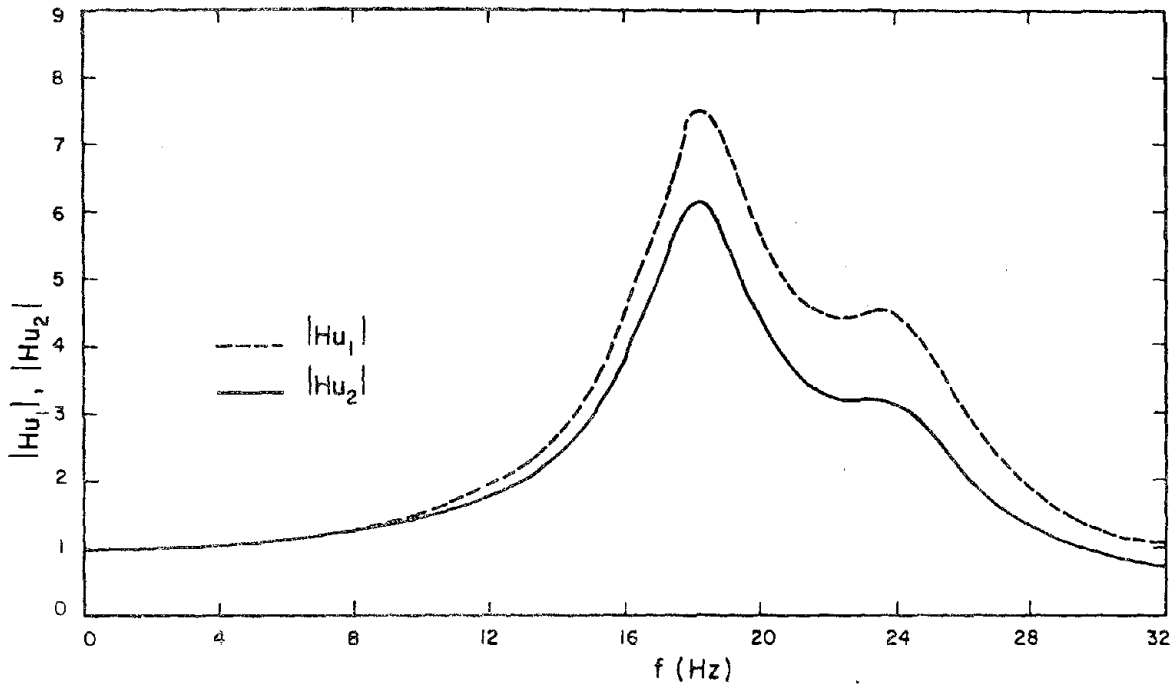

Figure 30. Amplification spectra for mortar and brick constituents of wall A (horizontal motion)

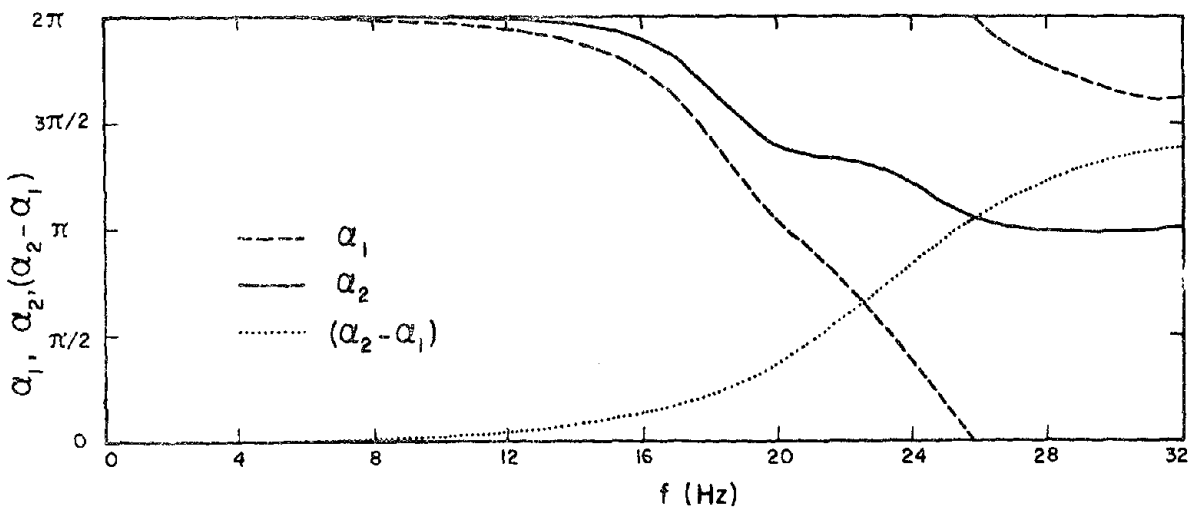

Figure 31. Phase spectra for mortar and brick constituents of wall A (horizontal motion)

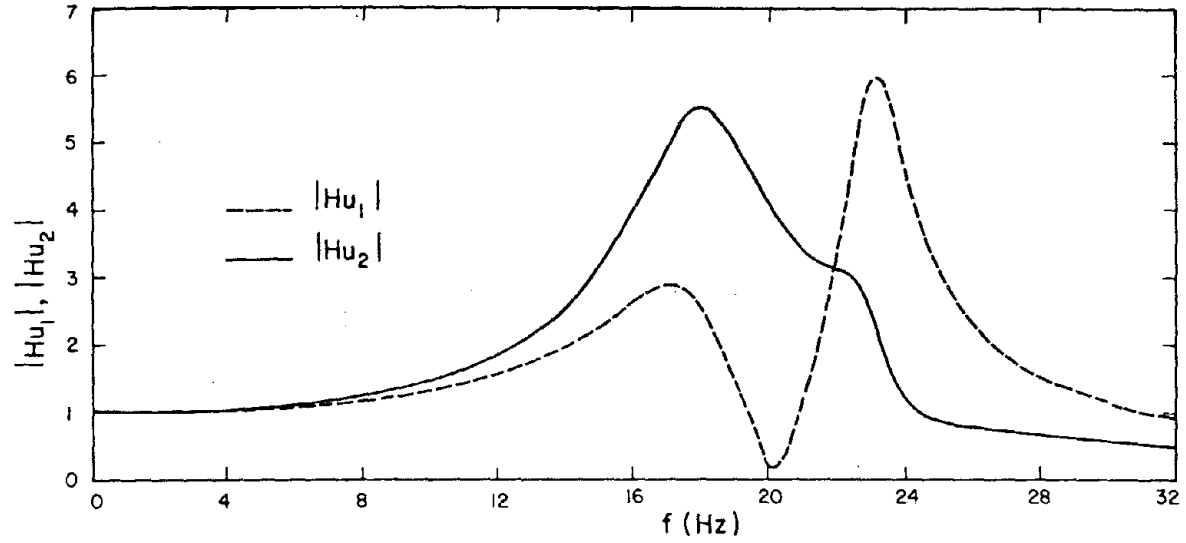

Figure 32. Amplification spectra for mortar and brick constituents of wall B (horizontal motion)

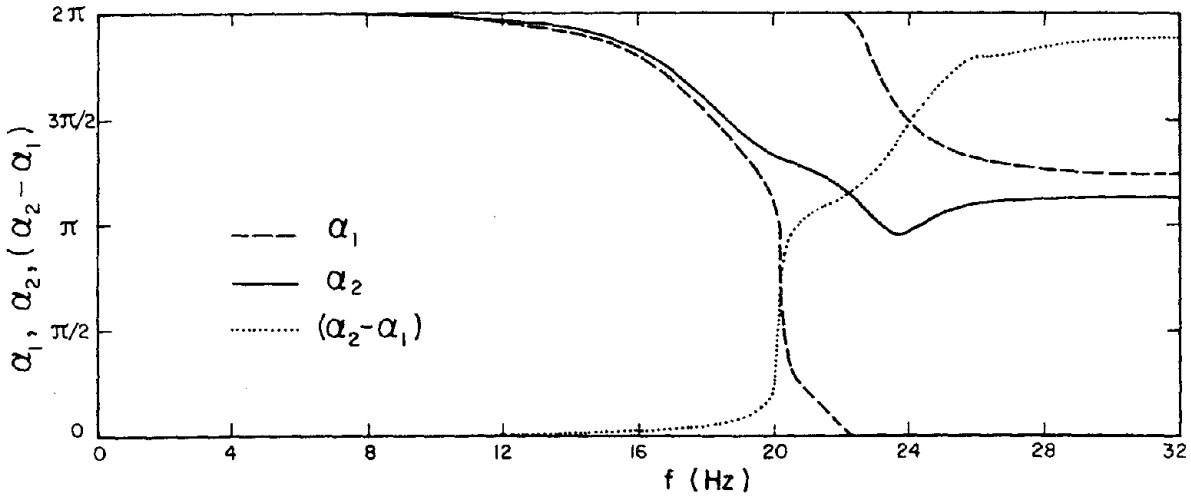

Figure 33. Phase spectra for mortar and brick constituents of wall B (horizontal motion)

from 1.2π to 0.3π. This singular behavior of the mortar around $f \simeq 20$ Hz is probably due to the propagation (initiated at this frequency) of micro cracks which might be present initially between the mortar and brick layers. Micro cracks may exist in a wall because of imperfections in its structure. The peculiar behavior at $f \simeq 20$ Hz is observed only for wall B, not for wall A. This is probably due to a higher density of micro cracks in wall B than in wall A.

7. ASSESSMENT OF THE PROPOSED MODELS

In the following sections the results obtained in the previous chapter are discussed and interpreted further, and the dynamic stiffness matrix for a wall element is presented to appraise the models used in the study. Suggestions are also made regarding research areas that need to be investigated in the future.

7.1 Comments on Closely Spaced Modal Frequencies

In the present study a two-phase model was chosen to study the dynamic behavior of masonry walls. This choice was dictated by experimental observation. As can be seen from Figs. 13 and 14, the first two resonance frequencies of the wall predicted by experiment are close to each other. It may be expected on physical grounds that the closeness of these two frequencies is due to the strong interaction between the brick and mortar phases of the wall, and accordingly that this interaction could be taken into account only by a model that differentiates the two phases of the wall. The results obtained in Chapter 6 verify this expectation. The mixture model yields a CFRF which duplicates closely the experimental CFRF up to a frequency which is well above the second modal frequency, whereas the effective modulus model gives satisfactory results only up to the first model frequency (see Figs. 13-16).

7.2 Comments on the Effect of Debonding in the Behavior of Masonry Walls

In the previous chapter, it was observed that the CFRF's of walls A and B were very different and this difference was attributed to different densities of micro crack distributions in the two walls. Some further remarks follow regarding the influence of micro cracks on the wall behavior.

Slip and debonding phenomena in elastic composites have been studied by many researchers (see, for example [28-31]). In references [30] and [31]

the mixture and effective modulus theories are proposed for layered composites. The incorporation of slip (along constituent interfaces) in the formulation does not change the form of the equations of the mixture or effective modulus theory for perfectly bonded constituents, but the model parameters appearing in these equations become dependent on the slip coefficient.

The form of the equations of the mixture theory, Eqs. (3.1 to 3.3), used in this study to analyze the dynamic behavior of masonry walls was established in references [8 to 11] by assuming that the constituents were perfectly bonded. However, in view of the findings mentioned in the previous paragraph, it is anticipated that this form could be used also to determine the response of the wall when slip and debonding are present between brick and mortar constituents. In fact, the results obtained in the previous chapter support this expectation. There, it was found that the mixture model could predict the response of both walls A and B each having very different debonding and slip characteristics.

Much work remains to be done to establish the debonding and slip phenomena in walls more rigorously. Developments in this direction could follow the steps outlined below. First, parameters describing the debonding characteristics must be chosen. The selection of slip coefficient and the density of micro crack (separation) distribution seem reasonable for this purpose. Secondly, the type of dependence of the parameters of the mixture model on the slip parameters should be established from a theoretical analysis. Finally, the type of experiments necessary to evaluate the slip parameters must be ascertained; and, with the aid of such experiments, the values of the slip parameters should be determined through optimization.

7.3 Dynamic Stiffness Matrix for a Wall Element

In this section, a dynamic stiffness matrix relating the forces to displacements, at the lower and upper ends of a wall element, is developed using the mixture theory. To this end, Eqs. (3.29) and (3.37) will be re-written in matrix form

$$\begin{bmatrix} \underline{f}^{+F} \\ \underline{f}^{-F} \end{bmatrix} = \begin{bmatrix} 0 & \frac{2}{H}\bar{\underline{S}} \\ -\frac{H}{2}\underline{A} & \underline{0} \end{bmatrix} \begin{bmatrix} \underline{W}^{+F} \\ \underline{W}^{-F} \end{bmatrix} \tag{7.1}$$

where

$$\underline{f}^{\mp F} = \begin{bmatrix} R^{\mp F} & T^{\mp F} \end{bmatrix}^T \; ; \; \underline{W}^{\mp F} = \begin{bmatrix} \bar{\underline{S}}^{\mp F} & \Psi^{\mp F} \end{bmatrix}^T \; . \tag{7.2}$$

From the definitions in Eqs. (3.20),

$$\begin{bmatrix} \underline{f}^{+F} \\ \underline{f}^{-F} \end{bmatrix} = \begin{bmatrix} 1 & 1 \\ 1 & -1 \end{bmatrix} \begin{bmatrix} \underline{g}^{+F} \\ \underline{g}^{-F} \end{bmatrix}$$

$$\begin{bmatrix} \underline{w}^{+F} \\ \underline{w}^{-F} \end{bmatrix} = \begin{bmatrix} 1 & 1 \\ 1 & -1 \end{bmatrix} \begin{bmatrix} \underline{j}^{+F} \\ \underline{j}^{-F} \end{bmatrix} \tag{7.3}$$

where

$$\underline{g}^{\mp F} = \begin{bmatrix} \sigma^{\mp F} & \tau^{\mp F} \end{bmatrix}^T \; ; \; \underline{j}^{\mp F} = \begin{bmatrix} u^{\mp F} & \Psi^{\mp F} \end{bmatrix}^T \; . \tag{7.4}$$

Substitution of Eqs. (7.3) into Eq. (7.1), solving for $[\underline{g}^{+F} \;\; \underline{g}^{-F}]^T$ and multiplying the resulting equation by bh' give

$$\begin{bmatrix} \underline{F}^{+F} \\ \underline{F}^{-F} \end{bmatrix} = \begin{bmatrix} \underline{D}^1 & -\underline{D}^2 \\ \underline{D}^2 & -\underline{D}^1 \end{bmatrix} \begin{bmatrix} \underline{j}^{+F} \\ \underline{j}^{-F} \end{bmatrix} \tag{7.5}$$

where

$$\underline{F}^{\mp F} = \begin{bmatrix} V^{\mp F} & \Delta^{\mp F} \end{bmatrix}^T \; . \tag{7.6}$$

with

$$V^{\mp F} = bh'\sigma^{\mp F} \quad , \quad \Delta^{\mp F} = bh'\tau^{\mp F} \quad \text{and}$$

$$D^1_{11} = K_{11} + i\omega C_{11} - \omega^2 \frac{f_{11}}{4}$$

$$D^1_{12} = D^1_{21} = K_{12} + i\omega C_{12} - \omega^2 \frac{f_{12}}{4} \tag{7.7}$$

$$D^1_{22} = K_{22} + i\omega C_{22} - \omega^2 \frac{f_{22}}{4}$$

and

$$D^2_{11} = K_{11} + i\omega C_{11} + \omega^2 \frac{f_{11}}{4}$$

$$D^2_{12} = D^2_{21} = K_{12} + i\omega C_{12} + \omega^2 \frac{f_{12}}{4} \tag{7.8}$$

$$D^2_{22} = K'_{22} + i\omega C'_{22} + \omega^2 \frac{f_{22}}{4} \quad .$$

In Eqs. (7.8)

$$K'_{22} = \frac{bh'k_{22}}{H} - \frac{bh'Hk}{4} \; ; \quad C'_{22} = \frac{bh'c_{22}}{H} - \frac{bh'Hc}{4} \; ; \tag{7.9}$$

all of the coefficients in Eqs. (7.7) and (7.8) are defined in Eqs. (3.48).

The 4 x 4 matrix

$$D = \begin{bmatrix} \underline{D}^1 & -\underline{D}^2 \\ \underline{D}^2 & -\underline{D}^1 \end{bmatrix} \tag{7.10}$$

is the dynamic stiffness matrix which is being sought. It may be noted that the discrete form of the governing equations of the mixture model, Eq. (3.47), could be derived also from the dynamic stiffness relation, Eq. (7.5), by taking into account the boundary conditions, Eqs. (3.27).

Study of Eqs. (7.7 to 7.9) indicates that all of the elements except D^2_{22} in the dynamic stiffness matrix $\underline{D}$ could be computed using the optimum values of parameters determined in Chapter 6. From Eq. (7.8) , and from the comparison of the relations defining (K_{22}, C_{22}) and K'_{22}, C'_{22}) in Eqs. (3.48) and (7.9) it is clear that D^2_{22} could also be evaluated if the non-dimensional parameters $\bar{K}$ and $\bar{C}$ defined by

$$\bar{K} = \frac{bh'Hk}{K_{11}}, \qquad \bar{C} = \frac{bh'Hc}{C_{11}} \tag{7.11}$$

are known. Unfortunately, the experimental data used in this study were not sufficient to determine these two parameters through optimization.

The values of $\bar{K}$ and $\bar{C}$ could perhaps be estimated theoretically. Such analysis might be very complicated but could be simplified by taking into account the periodicity of the wall, and consequently basing the analysis on a unit cell of the wall. This could involve the use of certain hypotheses regarding deformation modes of the unit cell. The determination of $\bar{K}$ and $\bar{C}$ in this way remains to be done in a later study.

It should be noted that some intervals with well defined lower and upper bounds exist for $\bar{K}$ and $\bar{C}$. Since k and c are positive (see Section 3.2), the lower bound for $\bar{K}$ and $\bar{C}$ is zero. The limiting situation $|\underline{k}| = 0$, $|\underline{c}| = 0$ of $\underline{k} = (k_{ij})$ and $\underline{c} = (c_{ij})$ establishes the upper bounds of $\bar{K}$ and $\bar{C}$, which can be computed using the optimum values of parameters presented in Chapter 6. For example, associated with the horizontal motion of wall A, they are found to be 0.744 and 0.460 for $\bar{K}$ and $\bar{C}$, respectively. The use of the rough estimate $\bar{K} = \bar{C} = 0$ is suggested here for practical purposes, until a better estimate is found through either experimental or theoretical analysis.

Finally, it may be observed that knowing $\bar{K}$ and $\bar{C}$, in addition to the parameters already determined in Chapter 6, is sufficient to compute the values of all the coefficients appearing in the equations of the continuum (mixture) model, Eqs. (3.12, 3.13).

REFERENCES

1. Mayes, R. L. and Clough, R. W., "State-of-the-Art in Seismic Shear Strength of Masonry-An Evaluation and Review", EERC Report No. 72/21, University of California, Berkeley, California (1975).

2. Mayes, R.L., Omote, Y. and Clough, R.W., "Cyclic Shear Tests of Masonry Piers, Volume I-Test Results", EERC Report No. 76/8, University of California, Berkeley, California (1976).

3. Mayes, R. L., Omote, Y. and Clough, R.W., "Cyclic Shear Tests of Masonry Piers, Volume II-Analysis of Test Results", EERC Report No. 76/16, University of California, Berkeley, California (1976).

4. Hidalgo, P.A., Mayes, R.L., McNiven, H.D. and Clough, R.W., "Cyclic Loading Tests of Masonry Single Piers, Volume 3-Height to Width Ratios of 0.5", EERC Report No. 79/12, University of California, Berkeley, California (1979).

5. Gülkan, P., Mayes, R.L. and Clough, R.W., "Shaking Table Study of Single-Story Masonry Houses-Volume I, Test Structures 1 and 2", EERC Report No. 79/23, University of California, Berkeley, California (1979).

6. Gülkan, P., Mayes, R.L. and Clough, R.W., "Shaking Table Study of Single-Story Masonry Houses-Volume 2, Test Structures 3 and 4", EERC Report No. 79/24, University of California, Berkeley, California (1979).

7. Rytov, S.M., "Acoustical Properties of a Thinly Laminated Medium", Soviet Physics-Acoustics, Vol. 2, 68-80 (1955).

8. Mengi, Y. and McNiven, H.D., "A Mathematical Model of Masonry for Predicting its Linear Seismic Response Characteristics", EERC Report No. 79/04, University of California, Berkeley, California (1979).

9. Mengi, Y. and McNiven, H.D., "A Mathematical Model for the Linear Dynamic Behavior of Two Phase Periodic Materials", International Journal of Solids and Structures, Vol. 15, 271-280 (1979).

10. Mengi, Y. and McNiven, H.D., "A Mixture Theory for Elastic Laminated Composites", International Journal of Solids and Structures, Vol. 15, 281-302 (1979).

11. Mengi, Y. and McNiven, H.D., "Propagation of Transient Waves in Elastic Laminated Composites", International Journal of Solids and Structures, Vol. 15, 303-318 (1979).

12. Mengi, Y., "A New Approach for Developing Dynamic Theories for Structures", Vol. 16, 1155-1168 (1980).

13. Cooper, R.G. and McGillem, C.D., "Methods of Signal and System Analysis", Holt, Rinehart and Winston, Inc. (1967).

14. Crandall, S.H. and Mark, W.D., "Random Vibration in Mechanical Systems", Academic Press, Inc. (1963).

15. Champeney, D.C., "Fourier Transforms and Their Physical Applications", Academic Press, Inc. (London) Ltd. (1973).

16. Sneddon, I.N., "Fourier Transforms", McGraw-Hill Book Company, Inc. (1951).

17. Bendat, J.S. and Piersol, A.G., "Measurement and Analysis of Random Data", John Wiley and Sons, Inc. (1971).

18. Cooley, J.W., Lewis, P.A.W. and Welch, P.D., "The Fast Fourier Transform and Its Applications", IEEE Transactions on Education, Vol. 12, 27-34 (1969).

19. Welch, P.D., "The Use of Fast Fourier Transform for the Estimation of Power Spectra: A Method Based on Time Averaging Over Short, Modified Periodograms", IEEE Transactions on Audio and Electroacoustics, Vol. AU-15, 70-73 (1967).

20. Bergland, G.D., "A Guided Tour of the Fast Fourier Transform", IEEE Spectrum, Vol. 6, 41-52 (1969).

21. Brigham, E.O., "The Fast Fourier Transform", Prentice-Hall, Inc., Englewood Cliffs, N.J. (1974).

22. Adby, P.R. and Dempster, M.A.H., "Introduction to Optimization Methods", Chapman and Hall, London (1974).

23. Luenberger, D.G., "Introduction to Linear and Nonlinear Programming", Addison-Wesley Publishing Company (1973).

24. Jacoby, S.L.S., Kowalik, J.S. and Pizzo, J.T., "Iterative Methods for Nonlinear Optimization Problems", Prentice-Hall, Inc., N.J. (1972).

25. Kowalik, J. and Osborne, M.R., "Methods for Unconstrained Optimization Problems", American Elsevier Publishing Company, Inc., N.Y. (1968).

26. Wilde, J.D. and Beightler, C.S., "Foundations of Optimization", Prentice-Hall, Inc., N.J. (1967).

27. Pierre, D.A., "Optimization Theory with Applications", John Wiley and Sons, Inc.(1969).

28. Drumheller, D.S. and Norwood, F.R., "On the Behavior of Stress Waves in Composite Materials - I. A Universal Set of Boundary Conditions", International Journal of Solids and Structures, Vol. 11, 53-73 (1975).

29. Gurtman, G.A. and Hegemier, G.A., "A Mixture Theory for Wave Guide-Type Propagation and Debonding in Laminated Composites", International Journal of Solids and Structures, Vol. 11, 973-984 (1975).

30. Benveniste, Y. and Aboudi, J., "A Mixture Theory for Wave Propagation in a Laminated Medium with Debonding", Journal of Sound and Vibration, Vol. 46, 473-482 (1976).

31. Lene, F. and Leguillon, D., "Homogenized Constitutive Law for a Partially Cohesive Composite Material", to be published in International Journal of Solids and Structures.

APPENDIX A

VERIFICATION OF $||(H^2/12)\bar{\underline{S}}^{-1}\,\underline{A}|| < 1$

The verification will be presented only for the horizontal motion of wall A and for the frequency range that is considered in the analysis.

Let the matrix $\underline{G}'$ denote the matrix whose norm is to be evaluated:

$$\underline{G}' = \frac{H^2}{12}\,\bar{\underline{S}}^{-1}\,\underline{A} \tag{A.1}$$

where $\underline{A}$ and $\bar{\underline{S}}$ are given in Eqs. (3.34) and H is the height of the wall. When the numerator and denominator of the right hand side of Eq. (A.1) is multiplied by bh', $\underline{G}'$ can be expressed as

$$\underline{G}' = \frac{1}{12}\,\frac{H}{bh'}\,\bar{\underline{S}}^{-1}\,\underline{B}' \tag{A.2}$$

where b, h' are defined in Chapter 4 and

$$\underline{B}' = \omega^2\underline{F} - bh'H\bar{Q}'\underline{B}\ . \tag{A.3}$$

In Eq. (A.3), ω is angular frequency, $\bar{Q}'$ is defined in Chapter 3, $\underline{F} = (f_{ij})$ with f_{ij} given in Eqs. (3.48), and $\underline{B}$ is defined in Eqs. (3.46). Some manipulation of Eq. (A.3) yields a more suitable form for $\underline{B}'$:

$$\underline{B}' = K_{11}\{z^2\underline{F}' - (\bar{K} + 2\xi iz\bar{C})\underline{B}\}\ . \tag{A.4}$$

In Eq. (A.4), $z = \omega/\bar{\omega}$, $\bar{\omega}^2 = K_{11}/M_{11}$, $\xi = C_{11}/2M_{11}\bar{\omega}$ and

$$\underline{F}' = (f'_{ij}) = \frac{1}{M_{11}}\,(f_{ij})\ ;\ \ (i,j = 1,2),\ \ \bar{K} = \frac{K}{K_{11}}\ ,\ \ \bar{C} = \frac{C}{C_{11}} \tag{A.5}$$

where K_{11}, M_{11}, C_{11} are defined in Chapter 3, and $bh'H\bar{Q}' = K + i\omega C$. Substitution of $\underline{B}'$ from Eq. (A.4) into Eq. (A.2) gives

$$\underline{G}' = \frac{1}{12}\,\frac{H}{bh'}\,\bar{\underline{S}}^{-1}\,K_{11}\,\{z^2\underline{F}' - (\bar{K} + 2\xi iz\bar{C})\underline{B}\}\ . \tag{A.6}$$

Let the matrix $(H/bh')\bar{\underline{S}}^{-1} K_{11}$ in Eq. (A.6) be designated by $\underline{J}$, which can be written after some manipulation as

$$\underline{J} = \frac{1}{\Delta} \begin{bmatrix} S_{22}^* & -S_{12}^* \\ -S_{12}^* & S_{11}^* \end{bmatrix} \tag{A.7}$$

where

$$\Delta = S_{11}^* \; S_{22}^* - S_{12}^{*2} \; ;$$

$$S_{11}^* = 1 + 2\xi i z \quad ; \quad S_{12}^* = \gamma + 2\xi i z\gamma' \quad ; \quad S_{22}^* = \bar{p} + 2\xi i z\bar{\alpha}' \quad ; \tag{A.8}$$

$$p = \frac{\bar{K}_{22}}{K_{11}} \quad ; \quad \bar{\alpha}' = \frac{\bar{C}_{22}}{C_{11}} \quad ; \quad (\bar{K}_{22}, \bar{C}_{22}) = \frac{bh'}{H} (k_{22}, c_{22})$$

In Eq. (A.8) γ, γ' are defined in Eqs. (4.5), and k_{22} and c_{22} in Chapter 3.

From discussion given in Chapter 7, $\bar{K}$ and $\bar{C}$ are taken to be $\bar{K} = \bar{C} = 0$, which implies $\bar{\alpha}' = \alpha'$ and $\bar{p} = p$ (where the parameters α' and p are defined in Eqs. (4.5)). Then Eq. (A.6) becomes

$$\underline{G}' = \frac{z^2}{12} \; \underline{J} \; \underline{F}' \tag{A.9}$$

which is a function of ω. From this equation it is clear that the maximum norm of $\underline{G}'$, i.e., $||\underline{G}'||$, is zero at $\omega = 0$ and increases with ω. In the calculations, $f = \omega/2\pi$ is chosen to be 25 Hz which is well above the second modal frequency. $||\underline{G}'||$ is computed by using this value of ω and the optimum values of the parameters with $\alpha = 0.45$ listed in Table 5. (For the definition of α see Eqs. (3.48, 4.5).) The maximum norm of $||G'||$ is found to be

$$||\underline{G}'|| = 0.319,$$

which is less than one. In the computation of $\underline{F}'$, the values of M (top mass) and M_{11} given in Eqs. (3.48, 4.8) and Eqs. (3.48, 4.5, 4.9 to 4.11) are used.

APPENDIX B

SENSITIVITY COEFFICIENTS

In the present problem the number of parameters to be determined through optimization is seven for the mixture model and two for the effective modulus model. Let them be ordered so that

$$(\beta_1, \beta_2, \ldots, \beta_7) = (\bar{\omega}, \alpha, \xi, \alpha', \xi', p, \gamma) \tag{B.1}$$

for the mixture model, and

$$(\beta_1, \beta_3) = (\bar{\omega}, \xi) \tag{B.2}$$

for the effective modulus model.

First, the evaluation of the sensitivity coefficients of the mixture model will be presented.

In Section 5.1 the theoretical CFRF is written in the form

$$H_u^t(f_j) = r_j + is_j \tag{B.3}$$

where (r_j, s_j) are the (real, imaginary) parts of H_u^t at $f = f_j$, respectively. Differentiation of Eq. (B.3) with respect to β_k yields

$$\frac{\partial H_u^t(f_j)}{\partial \beta_k} = \frac{\partial r_j}{\partial \beta_k} + i \frac{\partial s_j}{\partial \beta_k} \quad . \tag{B.4}$$

The aim here is to evaluate the sensitivity coefficients $\partial r_j/\partial \beta_k$, $\partial s_j/\partial \beta_k$ which appear as real and imaginary parts of $\partial H_u^t(f_j)/\partial \beta_k$ in Eq. (B.4). To this end, H_u^t defined in Eq. (4.6) is differentiated with respect to β_k taking into account the definitions in Eq. (4.7). Thus,

$$\frac{\partial H_u^t}{\partial \beta_k} = \frac{q'z^2}{D^2}\left[\frac{\partial}{\partial \beta_k}(a_{22} - a_{12}^{\ell})D - (a_{22} - a_{12}^{\ell})\frac{\partial D}{\partial \beta_k}\right] + \frac{2q'z}{D}\left[\frac{\partial z}{\partial \beta_k}(a_{22} - a_{12}^{\ell})\right] \tag{B.5}$$

where

$$\frac{\partial D}{\partial \beta_k} = a_{22} \frac{\partial a_{11}}{\partial \beta_k} + a_{11} \frac{\partial a_{22}}{\partial \beta_k} - 2a_{12} \frac{\partial a_{12}}{\partial \beta_k} \tag{B.6}$$

and $\partial z/\partial \beta_1 = -z/\bar{\omega}$, $\partial z/\partial \beta_k = 0$ for $k \neq 1$ since z depends only on the parameter $\bar{\omega}$ through $z = \omega/\bar{\omega}$. To evaluate $\partial H_u^t/\partial \beta_k$ in Eq. (B.5) it is necessary to determine the derivatives of a_{11}, a_{12} and a_{22} with respect to β_k. Using the expressions defining a_{11}, a_{12} and a_{22}, these derivatives are evaluated at $f = f_j$ and presented in Table B.1. In the preparation of this table the definition $z_j = 2\pi f_j/\bar{\omega}$ is used. Once the right hand side of Eq. (B.5) is evaluated at $f = f_j$, its real and imaginary parts give the sensitivity coefficients $\partial r_j/\partial \beta_k$ and $\partial s_j/\partial \beta_k$, respectively.

The sensitivity coefficients of the effective modulus model are the real and imaginary parts of $\partial H_u^t/\partial \bar{\omega}$ and $\partial H_u^t/\partial \xi$, where H_u^t is the CFRF defined by Eq. (4.14). They can be evaluated using Eq. (B.5) with (k = 1,3) by setting the parameters m', α', γ', γ in Eqs. (4.6, 4.7) and in Table B.1 equal to zero.

Table B.1 Derivatives of a_{ij} (i,j = 1,2) with respect to model parameters at $f = f_j$.

a_{ij} \ $\frac{\partial}{\partial \beta_k}$	$\frac{\partial}{\partial \beta_1}$	$\frac{\partial}{\partial \beta_2}$	$\frac{\partial}{\partial \beta_3}$	$\frac{\partial}{\partial \beta_4}$	$\frac{\partial}{\partial \beta_5}$	$\frac{\partial}{\partial \beta_6}$	$\frac{\partial}{\partial \beta_7}$
a_{11}	$\frac{2z_j}{\bar{\omega}}(z_j - i\xi)$	0	$2iz_j$	0	0	0	0
a_{12}	$\frac{2z_j}{\bar{\omega}}(m'z_j - i\gamma'\xi)$	0	$2i\gamma' z_j$	0	$2i\xi z_j$	0	1
a_{22}	$\frac{2z_j}{\bar{\omega}}(\alpha z_j - i\alpha'\xi)$	$-z_j^2$	$2i\alpha' z_j$	$2i\xi z_j$	0	1	1

APPENDIX C

COMPUTER PROGRAM

The FORTRAN program consists of a main program and six subprograms with a total of 188 statements. The compilation time with the G compiler of the IBM 370/145 computer is about 28 seconds. Execution takes 3.20 seconds when periodic data are used and convergence is achieved in eight iterations.

Flowcharts are presented only for the MAIN program and subroutine SUM. The other subprograms complement the computations performed in SUM and MAIN. A listing of the computer program and the output for a sample problem (involving the evaluation of the optimum values of the parameters of wall A using horizontal periodic data) are included at the end of this Appendix.

The symbols used in the flowcharts are defined in Chapter 5.

MAIN PROGRAM

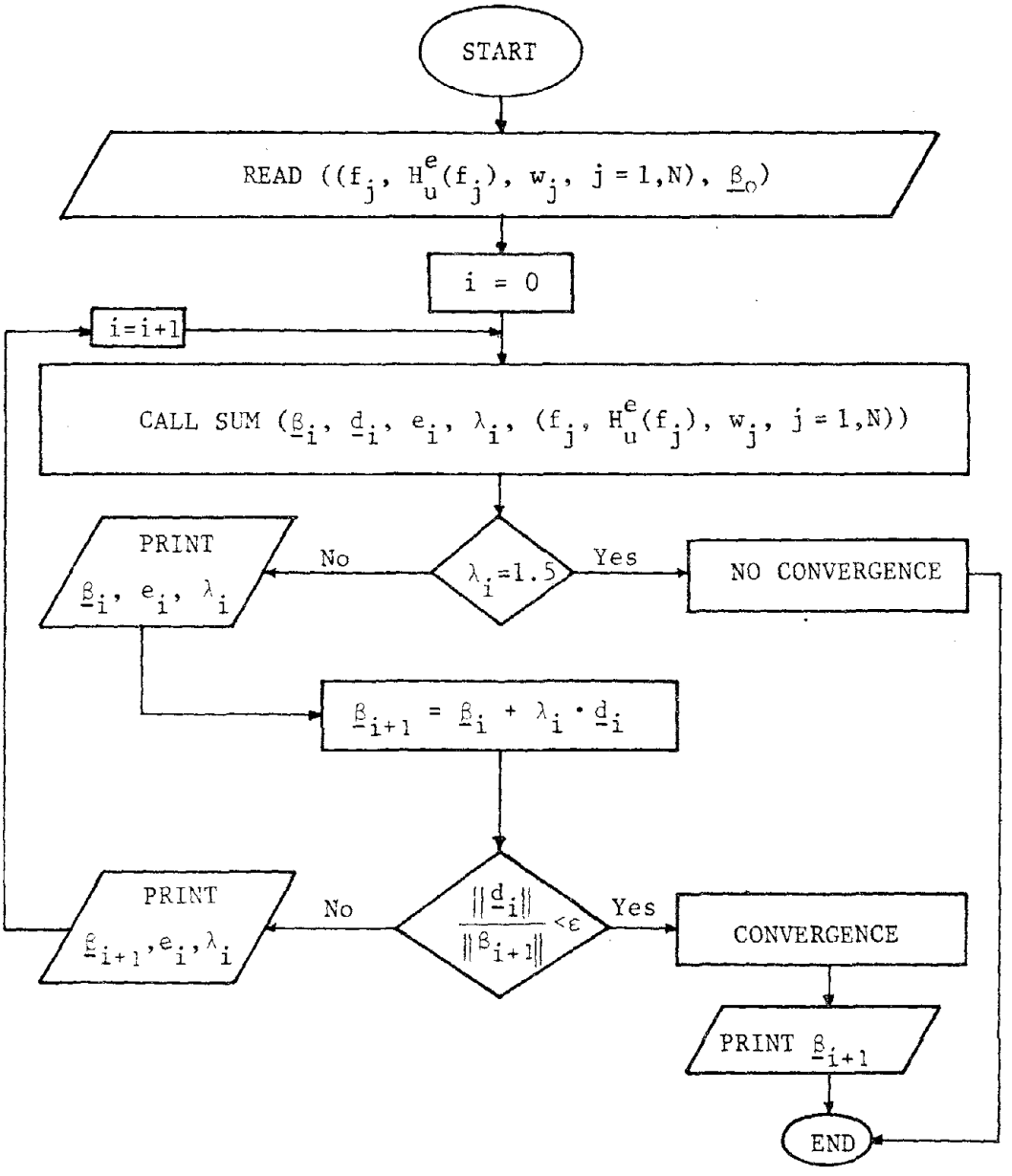

i : Iteration no.

N : Number of data points

SUBROUTINE SUM

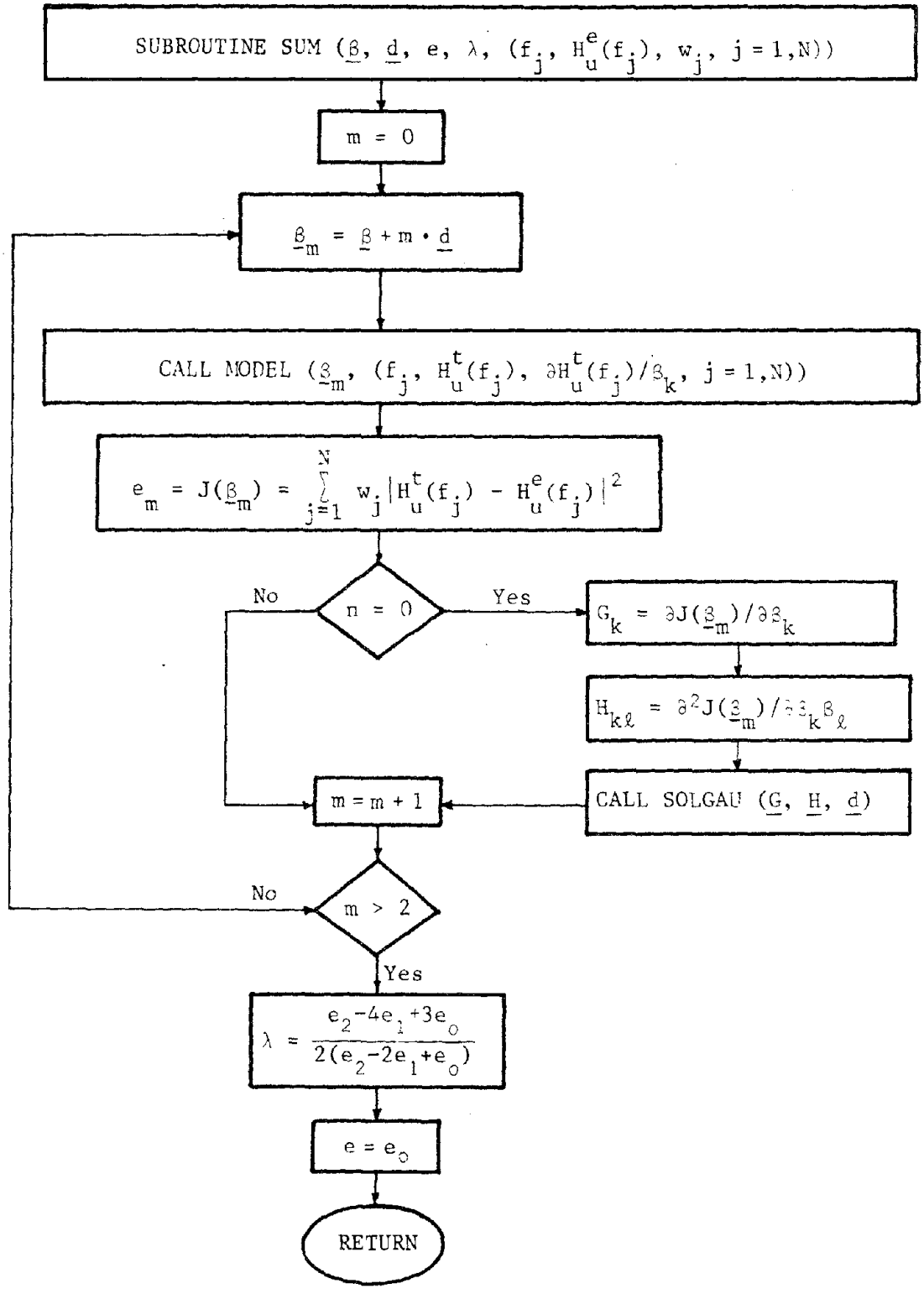

β_k: k th element of $\underline{\beta}$

k, ℓ = 1 - n ; n is the number of released parameters in $\underline{\beta}$

```
C
C
C     A COMPUTER PROGRAM TO DETERMINE THE OPTIMUM PARAMETERS OF AN
C     ANALYTICAL MODEL SIMULATING THE DYNAMIC RESPONSE OF MASONRY WALLS
C
C
C     R(I),S(I)      : REAL AND IMAGINARY PARTS OF THE EXPERIMENTAL
C                      RESPONSE FUNCTION AT THE I'TH FREQUENCY
C     FX(I)          : FREQUENCY(HZ) OF THE I'TH EXPERIMENTAL
C                      RESPONSE QUANTITY
C     XX             : VECTOR OF PARAMETERS INITIALLY ESTIMATED
C                      AND CURRENTLY CALCULATED DURING ITERATIONS
C     DX             : INCREMENTAL PARAMETER VECTOR
C     IP             : A VECTOR TO IDENTIFY RELEASED AND FIXED PARAMETERS
C     M              : NUMBER OF RELEASED PARAMETERS
C     NN             : NUMBER OF DATA
C
      DIMENSION FX(20),R(20),S(20),DX(8),WT(20),XX(8),D(8),AC(8),IP(8)
      READ(5,101)PI,NN,M,IP
      READ(5,101)AC
      DO 110 I=1,NN
  110 READ(5,200)FX(I),R(I),S(I),WT(I)
  200 FORMAT(3F10.0,20X,F10.0)
 1000 READ(5,101)XX
      IF(XX(1).LT.0.001)GO TO 500
      WRITE(6,302)M
      WRITE(6,302)XX
      WRITE(6,209)
C
C     ***  START OF ITERATIONS  ***
C
      ITE=0
 1011 ITE=ITE+1
      CALL SUM( IP,PI,XX,NN,M,DX,ER,RER,DL,FX,R,S,WT,AC)
      DO 6 I=1,3
    6 DX(I)=DX(I)*AC(I)
      WRITE(6,300)ITE,XX,ER,RER,DL
      IF(DL.LT.1.501.AND.DL.GT.1.499)GO TO 1000
      DO 7 I=1,3
      XX(I)=XX(I)+DL*DX(I)
      IF(IP(I).EQ.0) GO TO 7
      D(I)=ABS(DX(I)/XX(I))
    7 CONTINUE
      IF(ITE.GT.10)GO TO 20
```

```
C
C       **  CHECK FOR CONVERGENCE  **
C
        DO 8 I=1,8
        IF(D(I).GT.0.005) GO TO 1011
    8   CONTINUE
   20   WRITE(6,301)
        WRITE(6,302)XX
        GO TO 1000

  100   FORMAT(F10.0,1015)
  101   FORMAT(3F10.0)
  299   FORMAT(///2X,'ITE',6X,'X1',10X,'X2',10X,'X3',10X,'X4',10X,'X5',10X
     *,'X6',10X,'X7',10X,'X3',8X,'ERROR',6X,'REL ERROR',2X,'LAMDA')
  300   FORMAT(/2X,I2,2X,10E12.4,F8.3)
  301   FORMAT(///10X,'** CONVERGED PARAMETERS **'/)
  302   FORMAT(10X,'X1=',E15.7,/10X,'X2=',E15.7,/10X,'X3=',E15.7,/10X,'X4=
     *',E15.7/10X,'X5=',E15.7/10X,'X6=',E15.7/10X,'X7=',E15.7/10X,'X8=',
     *E15.7)
  303   FORMAT(///10X,'NO OF PARAMETERS=',I2//10X,'** INITIAL ESTIMATES **
     *'/)
  500   STOP
        END
```

```
      SUBROUTINE SUM( IP,PI,Y,NN,M,DX,ER,RER,DL,FX,R,S,WT,AC)
C
C     CALCULATES THE ERROR QUANTITY AND THE INCREMENTAL PARAMETER VECTOR
C     DURING THE CURRENT ITERATION. PERFORMS LINE SEARCH
C     ALONG THE DESCENT DIRECTION
C
C     ER              : ERROR
C     RER             : RELATIVE ERROR
C     DL              : LINE SEARCH PARAMETER
C
      DIMENSION FX(120),R(120),S(120),WT(120)
      DIMENSION H(8,8),G(8),DX(8),DR(8),DS(8),Y(8),X(8),EE(3),AC(8)
      DIMENSION YY(8),DDR(8),DDS(8),DDX(8),IP(8),AAC(8)
      M1=M+1
      DO 5 I=1,M
      G(I)=0.0
      DDX(I)=0.0
      DO 5 J=1,M
    5 H(I,J)=0.0
      DO 20 I=1,3
      E=0.0
      II=I-1
      DO 6 L=1,3
    6 X(L)=Y(L)+II*DX(L)*AC(L)
      RM=0.0
      DO 10 J=1,NN
      W=2.*PI*FX(J)
      CALL MODEL(I,M,W,X,RB,SB,DR,DS,IP)
      RR=RB-R(J)
      SS=SB-S(J)
      E=E+WT(J)*(RR*RR+SS*SS)
      IF(I.NE.1)GO TO 10
      CALL TRANS(DR,DDR,IP,+1)
      CALL TRANS(DS,DDS,IP,+1)
      CALL TRANS(AC,AAC,IP,+1)
      DO 9 K=1,M
      G(K)=G(K)+2.*(RR*DDR(K)+SS*DDS(K))*WT(J)*AAC(K)
      DO 9 L=1,M
    9 H(K,L)=H(K,L)+2.*(DDR(K)*DDR(L)+DDS(K)*DDS(L))*WT(J)*AAC(K)*AAC(L)
      RM=RM+(R(J)**2+S(J)**2)*WT(J)
   10 CONTINUE
      IF(I.NE.1)GO TO 15
      EP=E
      RER=E/RM
      DO 11 K=1,M
   11 H(K,M1)=-G(K)
      CALL SOLSAL(M,M1,H,DX)
      CALL TRANS(DX,DDX,IP,-1)
   15 EE(I)=E
   20 CONTINUE
      DL=0.5*(EE(3)-4.*EE(2)+3.*EE(1))/(EE(3)-2.*EE(2)+EE(1))
      RETURN
      END
```

```
      SUBROUTINE MODEL(I,M,W,X,RB,SB,DR,DS,IP)
C
CC    CALCULATES THE COMPLEX FREQUENCY RESPONSE FUNCTION AT A GIVEN FREQUENCY
CC    AND ITS FIRST DERIVATIVES WITH RESPECT TO THE RELEASED PARAMETERS
C
      DIMENSION X(8),DR(8),DS(8),IP(8)
      COMPLEX H(8),DB(8),DD(8),B,D,HH
      DATA EQ/1.054/
      EL=X(2)
      Z=W/X(3)
      RD=(Z**4)*(X(1)-X(2)*X(2))-Z*Z*(X(4)+X(1)+2.*X(5)*X(2)+4.*X(6)*
     2X(6)*(X(7)-X(8)*X(8)))+X(4)-X(5)*X(5)
      DI=2.*X(6)*Z*(-Z*Z*(X(7)+X(1)+2.*X(2)*X(8))+X(7)+X(4)-2.*X(5)*X(8)
     3)
      D=CMPLX(RD,DI)
      BR=EQ*Z*Z*(Z*Z*(X(2)*EL-X(1))+X(4)+EL*X(5))
      BI=2.*EQ*X(6)*(Z**3)*(X(7)+EL*X(8))
      B=CMPLX(BR,BI)
      IF(I.NE.1)GO TO 700
      DB(1)=CMPLX(-EQ*(Z**4),0.0)
      DB(2)=CMPLX(EQ*Z*Z*(2.*Z*Z*X(2)+X(5)),2.*EQ*X(6)*X(8)*(Z**3))
      DB(3)=CMPLX(-2.*EQ*Z*Z*(2.*Z*Z*(X(2)*EL-X(1))+X(4)+X(5)*EL)/X(3))
     3,(-6.*EQ*X(6)*(Z**3)*(X(7)+EL*X(8))/X(3)))
      DB(4)=CMPLX(EQ*Z*Z,0.0)
      DB(5)=CMPLX(EQ*EL*Z*Z,0.0)
      DB(6)=CMPLX(0.0,BI/X(6))
      DB(7)=CMPLX(0.0,2.*X(6)*EQ*(Z**3))
      DB(8)=DB(7)*EL
      A1=Z*Z*X(2)+X(5)
      A2=2.*X(6)*Z
      A3=Z*Z
      DD(1)=CMPLX(A3*(A3-1.),-A2*A3)
      DD(2)=CMPLX(-2.*A3*A1,-A2*A3*2.*X(8))
      DD(3)=CMPLX((2.*A3*(-2.*A3*(X(1)-X(2)*X(2))+X(4)+X(1)+2.*X(5)*X(2)
     2+4.*X(6)*X(6)*(X(7)-X(8)))/X(3)),(A2/X(3)*(3.*A3*(X(7)+X(1)+2.*X(2
     3)*X(8))-X(7)-X(4)+2.*X(5)*X(8))))
      DD(4)=CMPLX((1.-A3),A2)
      DD(5)=CMPLX(-2.*A1,-2.*A2*X(8))
      DD(6)=CMPLX(8.*A3*X(6)*(-X(7)+X(8)*X(8)),DI/X(6))
      DD(7)=CMPLX(-A2*A2,A2*(1.-A3))
      DD(8)=CMPLX(2.*X(3)*A2*A2,-2.*A2*A1)
      DO 600 L=1,8
      IF(IP(L).EQ.0) GO TO 600
      H(L)=(DB(L)*D-DD(L)*B)/(D*D)
      DR(L)=REAL(H(L))
      DS(L)=AIMAG(H(L))
600   CONTINUE
700   HH=B/D+1.
      RB=REAL(HH)
      SB=AIMAG(HH)
      RETURN
      END
```

```
      SUBROUTINE SOLGAU(N,M,A,Y)
C
C     SOLVES SYSTEM OF LINEAR EQUATIONS
C
      DIMENSION A(8,9),Y(8)
      L=N-1
      DO 12 K=1,L
      JJ=K
      AB=ABS(A(I,K))
      KP1=K+1
      DO 7 I=KP1,N
      BIG=ABS(A(K,L))
      IF(BIG-AB) 6,7,7
    6 BIG=AB
      JJ=I
    7 CONTINUE
      IF(JJ-K) 8,10,8
    8 DO 9 J=K,M
      TEMP=A(JJ,J)
      A(JJ,J)=A(K,J)
    9 A(K,J)=TEMP
   10 DO 11 I=KP1,N
      QUOT=A(I,K)/A(K,K)
      DO 11 J=KP1,M
   11 A(I,J)=A(I,J)-QUOT*A(K,J)
      DO 12 I=KP1,N
   12 A(I,K)=0.
      Y(M)=A(N,M)/A(N,N)
      DO 14 NN=1,L
      SUM=0.
      I=N-NN
      IP1=I+1
      DO 13 J=IP1,M
   13 SUM=SUM+A(I,J)*Y(J)
   14 Y(I)=(A(I,M)-SUM)/A(I,I)
      RETURN
      END


      SUBROUTINE TRANS(X,XX,IP,L)
C
C     GENERATES A VECTOR OF RELEASED PARAMETERS FROM THE
C     TOTAL PARAMETER VECTOR OR VICE VERCA
C
      DIMENSION X(8),XX(8),IP(8)
      J=0
      DO 100 I=1,8
      IF(IP(I).EQ.0) GO TO 100
      J=J+1
      IF(L.EQ.1) XX(J)=X(I)
      IF(L.EQ.-1) X(I)=XX(J)
  100 CONTINUE
      RETURN
      END
```

NO OF PARAMETERS= 6

** INITIAL ESTIMATES **

X1= 0.5000000E 00
X2= -0.5900000E 00
X3= 0.1160000E 03
X4= 0.6000000E 00
X5= 0.5000000E 00
X6= 0.5291930E-01
X7= 0.3000000E 00
X8= 0.3000000E 00

ITE	X1	X2	X3	X4	X5	X6	X7	X8	ERROR	REL ERROR	LAMDA
1	0.5000E 00	-0.5900E 00	0.1160E 03	0.6000E 00	0.5000E 00	0.1000E 00	0.3000E 00	0.3000E 00	0.3670E 02	0.2039E 00	0.656
2	0.5000E 00	-0.5900E 00	0.1141E 03	0.6712E 00	0.5791E 00	0.1055E 00	0.1533E 00	0.1636E 00	0.1578E 02	0.8766E-01	0.863
3	0.5000E 00	-0.5900E 00	0.1145E 03	0.6504E 00	0.6101E 00	0.8269E-01	0.1503E 00	0.7814E-01	0.9275E 01	0.5154E-01	1.305
4	0.5000E 00	-0.5900E 00	0.1149E 03	0.6795E 00	0.6121E 00	0.7893E-01	0.1822E 00	0.1641E 00	0.3967E 01	0.4983E-01	0.970
5	0.5000E 00	-0.5900E 00	0.1149E 03	0.6754E 00	0.6165E 00	0.7930E-01	0.1940E 00	0.1803E 00	0.8344E 01	0.4915E-01	0.894
6	0.5000E 00	-0.5900E 00	0.1150E 03	0.6717E 00	0.6148E 00	0.7932E-01	0.1906E 00	0.2100E 00	0.8771E 01	0.4874E-01	1.045
7	0.5000E 00	-0.5900E 00	0.1151E 03	0.6696E 00	0.6179E 00	0.7953E-01	0.2014E 00	0.2216E 00	0.8730E 01	0.4851E-01	0.991
8	0.5000E 00	-0.5900E 00	0.1151E 03	0.6677E 00	0.6166E 00	0.7996E-01	0.2001E 00	0.2378E 00	0.8705E 01	0.4837E-01	1.106
9	0.5000E 00	-0.5900E 00	0.1152E 03	0.6665E 00	0.6133E 00	0.7987E-01	0.2063E 00	0.2450E 00	0.8691E 01	0.4829E-01	0.883
10	0.5000E 00	-0.5900E 00	0.1152E 03	0.6656E 00	0.6175E 00	0.8009E-01	0.2056E 00	0.2529E 00	0.8685E 01	0.4826E-01	1.159
11	0.5000E 00	-0.5900E 00	0.1152E 03	0.6650E 00	0.6184E 00	0.8006E-01	0.2089E 00	0.2569E 00	0.8681E 01	0.4824E-01	0.880
12	0.5000E 00	-0.5900E 00	0.1152E 03	0.6646E 00	0.6190E 00	0.8017E-01	0.2086E 00	0.2604E 00	0.8679E 01	0.4823E-01	1.165
13	0.5000E 00	-0.5900E 00	0.1152E 03	0.6643E 00	0.6194E 00	0.8016E-01	0.2101E 00	0.2625E 00	0.8677E 01	0.4822E-01	0.926
14	0.5000E 00	-0.5900E 00	0.1152E 03	0.6641E 00	0.6192E 00	0.8021E-01	0.2100E 00	0.2644E 00	0.8678E 01	0.4822E-01	1.256

** CONVERGED PARAMETERS **

X1= 0.5000000E 00
X2= -0.5900000E 00
X3= 0.1152104E 03
X4= 0.6631237E 00
X5= 0.6189922E 00
X6= 0.8022461E-01
X7= 0.2101175E 00
X8= 0.2652942E 00

EARTHQUAKE ENGINEERING RESEARCH CENTER REPORTS

NOTE: Numbers in parentheses are Accession Numbers assigned by the National Technical Information Service; these are followed by a price code. Copies of the reports may be ordered from the National Technical Information Service, 5285 Port Royal Road, Springfield, Virginia, 22161. Accession Numbers should be quoted on orders for reports (PB --- ---) and remittance must accompany each order. Reports without this information were not available at time of printing. The complete list of EERC reports (from EERC 67-1) is available upon request from the Earthquake Engineering Research Center, University of California, Berkeley, 47th Street and Hoffman Boulevard, Richmond, California 94804.

UCB/EERC-77/01 "PLUSH - A Computer Program for Probabilistic Finite Element Analysis of Seismic Soil-Structure Interaction," by M.P. Romo Organista, J. Lysmer and H.B. Seed - 1977 (PB81 177 651)A05

UCB/EERC-77/02 "Soil-Structure Interaction Effects at the Humboldt Bay Power Plant in the Ferndale Earthquake of June 7, 1975," by J.E. Valera, H.B. Seed, C.F. Tsai and J. Lysmer - 1977 (PB 265 795)A04

UCB/EERC-77/03 "Influence of Sample Disturbance on Sand Response to Cyclic Loading," by K. Mori, H.B. Seed and C.K. Chan - 1977 (PB 267 352)A04

UCB/EERC-77/04 "Seismological Studies of Strong Motion Records," by J. Shoja-Taheri - 1977 (PB 269 655)A10

UCB/EERC-77/05 Unassigned

UCB/EERC-77/06 "Developing Methodologies for Evaluating the Earthquake Safety of Existing Buildings," by No. 1 - B. Bresler; No. 2 - B. Bresler, T. Okada and D. Zisling; No. 3 - T. Okada and B. Bresler; No. 4 - V.V. Bertero and B. Bresler - 1977 (PB 267 354)A08

UCB/EERC-77/07 "A Literature Survey - Transverse Strength of Masonry Walls," by Y. Omote, R.L. Mayes, S.W. Chen and R.W. Clough - 1977 (PB 277 933)A07

UCB/EERC-77/08 "DRAIN-TABS: A Computer Program for Inelastic Earthquake Response of Three Dimensional Buildings," by R. Guendelman-Israel and G.H. Powell - 1977 (PB 270 693)A07

UCB/EERC-77/09 "SUBWALL: A Special Purpose Finite Element Computer Program for Practical Elastic Analysis and Design of Structural Walls with Substructure Option," by D.Q. Le, H. Peterson and E.P. Popov - 1977 (PB 270 567)A05

UCB/EERC-77/10 "Experimental Evaluation of Seismic Design Methods for Broad Cylindrical Tanks," by D.P. Clough (PB 272 280)A13

UCB/EERC-77/11 "Earthquake Engineering Research at Berkeley - 1976," - 1977 (PB 273 507)A09

UCB/EERC-77/12 "Automated Design of Earthquake Resistant Multistory Steel Building Frames," by N.D. Walker, Jr. - 1977 (PB 276 526)A09

UCB/EERC-77/13 "Concrete Confined by Rectangular Hoops Subjected to Axial Loads," by J. Vallenas, V.V. Bertero and E.P. Popov - 1977 (PB 275 165)A06

UCB/EERC-77/14 "Seismic Strain Induced in the Ground During Earthquakes," by Y. Sugimura - 1977 (PB 284 201)A04

UCB/EERC-77/15 Unassigned

UCB/EERC-77/16 "Computer Aided Optimum Design of Ductile Reinforced Concrete Moment Resisting Frames," by S.W. Zagajeski and V.V. Bertero - 1977 (PB 280 137)A07

UCB/EERC-77/17 "Earthquake Simulation Testing of a Stepping Frame with Energy-Absorbing Devices," by J.M. Kelly and D.F. Tsztoo - 1977 (PB 273 506)A04

UCB/EERC-77/18 "Inelastic Behavior of Eccentrically Braced Steel Frames under Cyclic Loadings," by C.W. Roeder and E.P. Popov - 1977 (PB 275 526)A15

UCB/EERC-77/19 "A Simplified Procedure for Estimating Earthquake-Induced Deformations in Dams and Embankments," by F.I. Makdisi and H.B. Seed - 1977 (PB 276 820)A04

UCB/EERC-77/20 "The Performance of Earth Dams during Earthquakes," by H.B. Seed, F.I. Makdisi and P. de Alba - 1977 (PB 276 821)A04

UCB/EERC-77/21 "Dynamic Plastic Analysis Using Stress Resultant Finite Element Formulation," by P. Lukkunapvasit and J.M. Kelly - 1977 (PB 275 453)A04

UCB/EERC-77/22 "Preliminary Experimental Study of Seismic Uplift of a Steel Frame," by R.W. Clough and A.A. Huckelbridge 1977 (PB 278 769)A08

UCB/EERC-77/23 "Earthquake Simulator Tests of a Nine-Story Steel Frame with Columns Allowed to Uplift," by A.A. Huckelbridge - 1977 (PB 277 944)A09

UCB/EERC-77/24 "Nonlinear Soil-Structure Interaction of Skew Highway Bridges," by M.-C. Chen and J. Penzien - 1977 (PB 276 176)A07

UCB/EERC-77/25 "Seismic Analysis of an Offshore Structure Supported on Pile Foundations," by D.D.-N. Liou and J. Penzien 1977 (PB 283 180)A06

UCB/EERC-77/26 "Dynamic Stiffness Matrices for Homogeneous Viscoelastic Half-Planes," by G. Dasgupta and A.K. Chopra - 1977 (PB 279 654)A06

UCB/EERC-77/27 "A Practical Soft Story Earthquake Isolation System," by J.M. Kelly, J.M. Eidinger and C.J. Derham - 1977 (PB 276 814)A07

UCB/EERC-77/28 "Seismic Safety of Existing Buildings and Incentives for Hazard Mitigation in San Francisco: An Exploratory Study," by A.J. Meltsner - 1977 (PB 281 970)A05

UCB/EERC-77/29 "Dynamic Analysis of Electrohydraulic Shaking Tables," by D. Rea, S. Abedi-Hayati and Y. Takahashi 1977 (PB 282 569)A04

UCB/EERC-77/30 "An Approach for Improving Seismic - Resistant Behavior of Reinforced Concrete Interior Joints," by B. Galunic, V.V. Bertero and E.P. Popov - 1977 (PB 290 870)A06

UCB/EERC-78/01 "The Development of Energy-Absorbing Devices for Aseismic Base Isolation Systems," by J.M. Kelly and D.F. Tsztoo - 1978 (PB 284 978)A04

UCB/EERC-78/02 "Effect of Tensile Prestrain on the Cyclic Response of Structural Steel Connections, by J.G. Bouwkamp and A. Mukhopadhyay - 1978

UCB/EERC-78/03 "Experimental Results of an Earthquake Isolation System using Natural Rubber Bearings," by J.M. Eidinger and J.M. Kelly - 1978 (PB 281 686)A04

UCB/EERC-78/04 "Seismic Behavior of Tall Liquid Storage Tanks," by A. Niwa - 1978 (PB 284 017)A14

UCB/EERC-78/05 "Hysteretic Behavior of Reinforced Concrete Columns Subjected to High Axial and Cyclic Shear Forces," by S.W. Zagajeski, V.V. Bertero and J.G. Bouwkamp - 1978 (PB 283 858)A13

UCB/EERC-78/06 "Three Dimensional Inelastic Frame Elements for the ANSR-I Program," by A. Riahi, D.G. Row and G.H. Powell - 1978 (PB 295 755)A04

UCB/EERC-78/07 "Studies of Structural Response to Earthquake Ground Motion," by O.A. Lopez and A.K. Chopra - 1978 (PB 282 790)A05

UCB/EERC-78/08 "A Laboratory Study of the Fluid-Structure Interaction of Submerged Tanks and Caissons in Earthquakes," by R.C. Byrd - 1978 (PB 284 957)A08

UCB/EERC-78/09 Unassigned

UCB/EERC-78/10 "Seismic Performance of Nonstructural and Secondary Structural Elements," by I. Sakamoto - 1978 (PB81 154 593)A05

UCB/EERC-78/11 "Mathematical Modelling of Hysteresis Loops for Reinforced Concrete Columns," by S. Nakata, T. Sproul and J. Penzien - 1978 (PB 298 274)A05

UCB/EERC-78/12 "Damageability in Existing Buildings," by T. Blejwas and B. Bresler - 1978 (PB 80 166 978)A05

UCB/EERC-78/13 "Dynamic Behavior of a Pedestal Base Multistory Building," by R.M. Stephen, E.L. Wilson, J.G. Bouwkamp and M. Button - 1978 (PB 286 650)A08

UCB/EERC-78/14 "Seismic Response of Bridges - Case Studies," by R.A. Imbsen, V. Nutt and J. Penzien - 1978 (PB 286 503)A10

UCB/EERC-78/15 "A Substructure Technique for Nonlinear Static and Dynamic Analysis," by D.G. Row and G.H. Powell - 1978 (PB 288 077)A10

UCB/EERC-78/16 "Seismic Risk Studies for San Francisco and for the Greater San Francisco Bay Area," by C.S. Oliveira - 1978 (PB 81 120 115)A07

UCB/EERC-78/17 "Strength of Timber Roof Connections Subjected to Cyclic Loads," by P. Gülkan, R.L. Mayes and R.W. Clough - 1978 (HUD-000 1491)A07

UCB/EERC-78/18 "Response of K-Braced Steel Frame Models to Lateral Loads," by J.G. Bouwkamp, R.M. Stephen and E.P. Popov - 1978

UCB/EERC-78/19 "Rational Design Methods for Light Equipment in Structures Subjected to Ground Motion," by J.L. Sackman and J.M. Kelly - 1978 (PB 292 357)A04

UCB/EERC-78/20 "Testing of a Wind Restraint for Aseismic Base Isolation," by J.M. Kelly and D.E. Chitty - 1978 (PB 292 833)A03

UCB/EERC-78/21 "APOLLO - A Computer Program for the Analysis of Pore Pressure Generation and Dissipation in Horizontal Sand Layers During Cyclic or Earthquake Loading," by P.P. Martin and H.B. Seed - 1978 (PB 292 835)A04

UCB/EERC-78/22 "Optimal Design of an Earthquake Isolation System," by M.A. Bhatti, K.S. Pister and E. Polak - 1978 (PB 294 735)A06

UCB/EERC-78/23 "MASH - A Computer Program for the Non-Linear Analysis of Vertically Propagating Shear Waves in Horizontally Layered Deposits," by P.P. Martin and H.B. Seed - 1978 (PB 293 101)A05

UCB/EERC-78/24 "Investigation of the Elastic Characteristics of a Three Story Steel Frame Using System Identification," by I. Kaya and H.D. McNiven - 1978 (PB 296 225)A06

UCB/EERC-78/25 "Investigation of the Nonlinear Characteristics of a Three-Story Steel Frame Using System Identification," by I. Kaya and H.D. McNiven - 1978 (PB 301 363)A05

UCB/EERC-78/26 "Studies of Strong Ground Motion in Taiwan," by Y.M. Hsiung, B.A. Bolt and J. Penzien - 1978 (PB 298 436)A06

UCB/EERC-78/27 "Cyclic Loading Tests of Masonry Single Piers: Volume 1 - Height to Width Ratio of 2," by P.A. Hidalgo, R.L. Mayes, H.D. McNiven and R.W. Clough - 1978 (PB 296 211)A07

UCB/EERC-78/28 "Cyclic Loading Tests of Masonry Single Piers: Volume 2 - Height to Width Ratio of 1," by S.-W.J. Chen, P.A. Hidalgo, R.L. Mayes, R.W. Clough and H.D. McNiven - 1978 (PB 296 212)A09

UCB/EERC-78/29 "Analytical Procedures in Soil Dynamics," by J. Lysmer - 1978 (PB 298 445)A06

UCB/EERC-79/01 "Hysteretic Behavior of Lightweight Reinforced Concrete Beam-Column Subassemblages," by B. Forzani, E.P. Popov and V.V. Bertero - April 1979(PB 298 267)A06

UCB/EERC-79/02 "The Development of a Mathematical Model to Predict the Flexural Response of Reinforced Concrete Beams to Cyclic Loads, Using System Identification," by J. Stanton & H. McNiven - Jan. 1979(PB 295 875)A10

UCB/EERC-79/03 "Linear and Nonlinear Earthquake Response of Simple Torsionally Coupled Systems," by C.L. Kan and A.K. Chopra - Feb. 1979(PB 298 262)A06

UCB/EERC-79/04 "A Mathematical Model of Masonry for Predicting its Linear Seismic Response Characteristics," by Y. Mengi and H.D. McNiven - Feb. 1979(PB 298 266)A06

UCB/EERC-79/05 "Mechanical Behavior of Lightweight Concrete Confined by Different Types of Lateral Reinforcement," by M.A. Manrique, V.V. Bertero and E.P. Popov - May 1979(PB 301 114)A06

UCB/EERC-79/06 "Static Tilt Tests of a Tall Cylindrical Liquid Storage Tank," by R.W. Clough and A. Niwa - Feb. 1979 (PB 301 167)A06

UCB/EERC-79/07 "The Design of Steel Energy Absorbing Restrainers and Their Incorporation into Nuclear Power Plants for Enhanced Safety: Volume 1 - Summary Report," by P.N. Spencer, V.F. Zackay, and E.R. Parker - Feb. 1979(UCB/EERC-79/07)A09

UCB/EERC-79/08 "The Design of Steel Energy Absorbing Restrainers and Their Incorporation into Nuclear Power Plants for Enhanced Safety: Volume 2 - The Development of Analyses for Reactor System Piping,""Simple Systems" by M.C. Lee, J. Penzien, A.K. Chopra and K, Suzuki "Complex Systems" by G.H. Powell, E.L. Wilson, R.W. Clough and D.G. Row - Feb. 1979(UCB/EERC-79/08)A10

UCB/EERC-79/09 "The Design of Steel Energy Absorbing Restrainers and Their Incorporation into Nuclear Power Plants for Enhanced Safety: Volume 3 - Evaluation of Commercial Steels," by W.S. Owen, R.M.N. Pelloux, R.O. Ritchie, M. Faral, T. Ohhashi, J. Toplosky, S.J. Hartman, V.F. Zackay and E.R. Parker - Feb. 1979(UCB/EERC-79/09)A04

UCB/EERC-79/10 "The Design of Steel Energy Absorbing Restrainers and Their Incorporation into Nuclear Power Plants for Enhanced Safety: Volume 4 - A Review of Energy-Absorbing Devices," by J.M. Kelly and M.S. Skinner - Feb. 1979(UCB/EERC-79/10)A04

UCB/EERC-79/11 "Conservatism In Summation Rules for Closely Spaced Modes," by J.M. Kelly and J.L. Sackman - May 1979(PB 301 328)A03

UCB/EERC-79/12 "Cyclic Loading Tests of Masonry Single Piers; Volume 3 - Height to Width Ratio of 0.5," by P.A. Hidalgo, R.L. Mayes, H.D. McNiven and R.W. Clough - May 1979(PB 301 321)A08

UCB/EERC-79/13 "Cyclic Behavior of Dense Course-Grained Materials in Relation to the Seismic Stability of Dams," by N.G. Banerjee, H.B. Seed and C.K. Chan - June 1979(PB 301 373)A13

UCB/EERC-79/14 "Seismic Behavior of Reinforced Concrete Interior Beam-Column Subassemblages," by S. Viwathanatepa, E.P. Popov and V.V. Bertero - June 1979(PB 301 326)A10

UCB/EERC-79/15 "Optimal Design of Localized Nonlinear Systems with Dual Performance Criteria Under Earthquake Excitations," by M.A. Bhatti - July 1979(PB 80 167 109)A06

UCB/EERC-79/16 "OPTDYN - A General Purpose Optimization Program for Problems with or without Dynamic Constraints," by M.A. Bhatti, E. Polak and K.S. Pister - July 1979(PB 80 167 091)A05

UCB/EERC-79/17 "ANSR-II, Analysis of Nonlinear Structural Response, Users Manual," by D.P. Mondkar and G.H. Powell July 1979(PB 80 113 301)A05

UCB/EERC-79/18 "Soil Structure Interaction in Different Seismic Environments," A. Gomez-Masso, J. Lysmer, J.-C. Chen and H.B. Seed - August 1979(PB 80 101 520)A04

UCB/EERC-79/19 "ARMA Models for Earthquake Ground Motions," by M.K. Chang, J.W. Kwiatkowski, R.F. Nau, R.M. Oliver and K.S. Pister - July 1979(PB 301 166)A05

UCB/EERC-79/20 "Hysteretic Behavior of Reinforced Concrete Structural Walls," by J.M. Vallenas, V.V. Bertero and E.P. Popov - August 1979(PB 80 165 905)A12

UCB/EERC-79/21 "Studies on High-Frequency Vibrations of Buildings - 1: The Column Effect," by J. Lubliner - August 1979 (PB 80 158 553)A03

UCB/EERC-79/22 "Effects of Generalized Loadings on Bond Reinforcing Bars Embedded in Confined Concrete Blocks," by S. Viwathanatepa, E.P. Popov and V.V. Bertero - August 1979(PB 81 124 018)A14

UCB/EERC-79/23 "Shaking Table Study of Single-Story Masonry Houses, Volume 1: Test Structures 1 and 2," by P. Gülkan, R.L. Mayes and R.W. Clough - Sept. 1979 (HUD-000 1763)A12

UCB/EERC-79/24 "Shaking Table Study of Single-Story Masonry Houses, Volume 2: Test Structures 3 and 4," by P. Gülkan, R.L. Mayes and R.W. Clough - Sept. 1979 (HUD-000 1836)A12

UCB/EERC-79/25 "Shaking Table Study of Single-Story Masonry Houses, Volume 3: Summary, Conclusions and Recommendations," by R.W. Clough, R.L. Mayes and P. Gülkan - Sept. 1979 (HUD-000 1837)A06

UCB/EERC-79/26 "Recommendations for a U.S.-Japan Cooperative Research Program Utilizing Large-Scale Testing Facilities," by U.S.-Japan Planning Group - Sept. 1979(PB 301 407)A06

UCB/EERC-79/27 "Earthquake-Induced Liquefaction Near Lake Amatitlan, Guatemala," by H.B. Seed, I. Arango, C.K. Chan, A. Gomez-Masso and R. Grant de Ascoli - Sept. 1979(NUREG-CR1341)A03

UCB/EERC-79/28 "Infill Panels: Their Influence on Seismic Response of Buildings," by J.W. Axley and V.V. Bertero Sept. 1979(PB 80 163 371)A10

UCB/EERC-79/29 "3D Truss Bar Element (Type 1) for the ANSR-II Program," by D.P. Mondkar and G.H. Powell - Nov. 1979 (PB 80 169 709)A02

UCB/EERC-79/30 "2D Beam-Column Element (Type 5 - Parallel Element Theory) for the ANSR-II Program," by D.G. Row, G.H. Powell and D.P. Mondkar - Dec. 1979(PB 80 167 224)A03

UCB/EERC-79/31 "3D Beam-Column Element (Type 2 - Parallel Element Theory) for the ANSR-II Program," by A. Riahi, G.H. Powell and D.P. Mondkar - Dec. 1979(PB 80 167 216)A03

UCB/EERC-79/32 "On Response of Structures to Stationary Excitation," by A. Der Kiureghian - Dec. 1979(PB 80166 929)A03

UCB/EERC-79/33 "Undisturbed Sampling and Cyclic Load Testing of Sands," by S. Singh, H.B. Seed and C.K. Chan Dec. 1979(ADA 087 298)A07

UCB/EERC-79/34 "Interaction Effects of Simultaneous Torsional and Compressional Cyclic Loading of Sand," by P.M. Griffin and W.N. Houston - Dec. 1979(ADA 092 352)A15

UCB/EERC-80/01 "Earthquake Response of Concrete Gravity Dams Including Hydrodynamic and Foundation Interaction Effects," by A.K. Chopra, P. Chakrabarti and S. Gupta - Jan. 1980(AD-A087297)A10

UCB/EERC-80/02 "Rocking Response of Rigid Blocks to Earthquakes," by C.S. Yim, A.K. Chopra and J. Penzien - Jan. 1980 (PB80 166 002)A04

UCB/EERC-80/03 "Optimum Inelastic Design of Seismic-Resistant Reinforced Concrete Frame Structures," by S.W. Zagajeski and V.V. Bertero - Jan. 1980(PB80 164 635)A06

UCB/EERC-80/04 "Effects of Amount and Arrangement of Wall-Panel Reinforcement on Hysteretic Behavior of Reinforced Concrete Walls," by R. Iliya and V.V. Bertero - Feb. 1980(PB81 122 525)A09

UCB/EERC-80/05 "Shaking Table Research on Concrete Dam Models," by A. Niwa and R.W. Clough - Sept. 1980(PB81 122 368)A06

UCB/EERC-80/06 "The Design of Steel Energy-Absorbing Restrainers and their Incorporation into Nuclear Power Plants for Enhanced Safety (Vol 1A): Piping with Energy Absorbing Restrainers: Parameter Study on Small Systems," by G.H. Powell, C. Oughourlian and J. Simons - June 1980

UCB/EERC-80/07 "Inelastic Torsional Response of Structures Subjected to Earthquake Ground Motions," by Y. Yamazaki April 1980(PB81 122 327)A08

UCB/EERC-80/08 "Study of X-Braced Steel Frame Structures Under Earthquake Simulation," by Y. Ghanaat - April 1980 (PB81 122 335)A11

UCB/EERC-80/09 "Hybrid Modelling of Soil-Structure Interaction," by S. Gupta, T.W. Lin, J. Penzien and C.S. Yeh May 1980(PB81 122 319)A07

UCB/EERC-80/10 "General Applicability of a Nonlinear Model of a One Story Steel Frame," by B.I. Sveinsson and H.D. McNiven - May 1980(PB81 124 877)A06

UCB/EERC-80/11 "A Green-Function Method for Wave Interaction with a Submerged Body," by W. Kioka - April 1980 (PB81 122 269)A07

UCB/EERC-80/12 "Hydrodynamic Pressure and Added Mass for Axisymmetric Bodies," by F. Nilrat - May 1980(PB81 122 343)A08

UCB/EERC-80/13 "Treatment of Non-Linear Drag Forces Acting on Offshore Platforms," by B.V. Dao and J. Penzien May 1980(PB81 153 413)A07

UCB/EERC-80/14 "2D Plane/Axisymmetric Solid Element (Type 3 - Elastic or Elastic-Perfectly Plastic) for the ANSR-II Program," by D.P. Mondkar and G.H. Powell - July 1980(PB81 122 350)A03

UCB/EERC-80/15 "A Response Spectrum Method for Random Vibrations," by A. Der Kiureghian - June 1980(PB81 122 301)A03

UCB/EERC-80/16 "Cyclic Inelastic Buckling of Tubular Steel Braces," by V.A. Zayas, E.P. Popov and S.A. Mahin June 1980(PB81 124 885)A10

UCB/EERC-80/17 "Dynamic Response of Simple Arch Dams Including Hydrodynamic Interaction," by C.S. Porter and A.K. Chopra - July 1980(PB81 124 000)A13

UCB/EERC-80/18 "Experimental Testing of a Friction Damped Aseismic Base Isolation System with Fail-Safe Characteristics," by J.M. Kelly, K.E. Beucke and M.S. Skinner - July 1980(PB81 148 595)A04

UCB/EERC-80/19 "The Design of Steel Energy-Absorbing Restrainers and their Incorporation into Nuclear Power Plants for Enhanced Safety (Vol 1B): Stochastic Seismic Analyses of Nuclear Power Plant Structures and Piping Systems Subjected to Multiple Support Excitations," by M.C. Lee and J. Penzien - June 1980

UCB/EERC-80/20 "The Design of Steel Energy-Absorbing Restrainers and their Incorporation into Nuclear Power Plants for Enhanced Safety (Vol 1C): Numerical Method for Dynamic Substructure Analysis," by J.M. Dickens and E.L. Wilson - June 1980

UCB/EERC-80/21 "The Design of Steel Energy-Absorbing Restrainers and their Incorporation into Nuclear Power Plants for Enhanced Safety (Vol 2): Development and Testing of Restraints for Nuclear Piping Systems," by J.M. Kelly and M.S. Skinner - June 1980

UCB/EERC-80/22 "3D Solid Element (Type 4-Elastic or Elastic-Perfectly-Plastic) for the ANSR-II Program," by D.P. Mondkar and G.H. Powell - July 1980(PB81 123 242)A03

UCB/EERC-80/23 "Gap-Friction Element (Type 5) for the ANSR-II Program," by D.P. Mondkar and G.H. Powell - July 1980 (PB81 122 285)A03

UCB/EERC-80/24 "U-Bar Restraint Element (Type 11) for the ANSR-II Program," by C. Oughourlian and G.H. Powell July 1980(PB81 122 293)A03

UCB/EERC-80/25 "Testing of a Natural Rubber Base Isolation System by an Explosively Simulated Earthquake," by J.M. Kelly - August 1980(PB81 201 360)A04

UCB/EERC-80/26 "Input Identification from Structural Vibrational Response," by Y. Hu - August 1980(PB81 152 308)A05

UCB/EERC-80/27 "Cyclic Inelastic Behavior of Steel Offshore Structures," by V.A. Zayas, S.A. Mahin and E.P. Popov August 1980(PB81 196 180)A15

UCB/EERC-80/28 "Shaking Table Testing of a Reinforced Concrete Frame with Biaxial Response," by M.G. Oliva October 1980(PB81 154 304)A10

UCB/EERC-80/29 "Dynamic Properties of a Twelve-Story Prefabricated Panel Building," by J.G. Bouwkamp, J.P. Kollegger and R.M. Stephen - October 1980(PB82 117 128)A06

UCB/EERC-80/30 "Dynamic Properties of an Eight-Story Prefabricated Panel Building," by J.G. Bouwkamp, J.P. Kollegger and R.M. Stephen - October 1980(PB81 200 313)A05

UCB/EERC-80/31 "Predictive Dynamic Response of Panel Type Structures Under Earthquakes," by J.P. Kollegger and J.G. Bouwkamp - October 1980(PB81 152 316)A04

UCB/EERC-80/32 "The Design of Steel Energy-Absorbing Restrainers and their Incorporation into Nuclear Power Plants for Enhanced Safety (Vol 3): Testing of Commercial Steels in Low-Cycle Torsional Fatigue," by P. Spencer, E.R. Parker, E. Jongewaard and M. Drory

UCB/EERC-80/33 "The Design of Steel Energy-Absorbing Restrainers and their Incorporation into Nuclear Power Plants for Enhanced Safety (Vol 4): Shaking Table Tests of Piping Systems with Energy-Absorbing Restrainers," by S.F. Stiemer and W.G. Godden - Sept. 1980

UCB/EERC-80/34 "The Design of Steel Energy-Absorbing Restrainers and their Incorporation into Nuclear Power Plants for Enhanced Safety (Vol 5): Summary Report," by P. Spencer

UCB/EERC-80/35 "Experimental Testing of an Energy-Absorbing Base Isolation System," by J.M. Kelly, M.S. Skinner and K.E. Beucke - October 1980(PB81 154 072)A04

UCB/EERC-80/36 "Simulating and Analyzing Artificial Non-Stationary Earthquake Ground Motions," by R.F. Nau, R.M. Oliver and K.S. Pister - October 1980(PB81 153 397)A04

UCB/EERC-80/37 "Earthquake Engineering at Berkeley - 1980," - Sept. 1980(PB81 205 874)A09

UCB/EERC-80/38 "Inelastic Seismic Analysis of Large Panel Buildings," by V. Schricker and G.H. Powell - Sept. 1980 (PB81 154 338)A13

UCB/EERC-80/39 "Dynamic Response of Embankment, Concrete-Gravity and Arch Dams Including Hydrodynamic Interaction," by J.F. Hall and A.K. Chopra - October 1980(PB81 152 324)A11

UCB/EERC-80/40 "Inelastic Buckling of Steel Struts Under Cyclic Load Reversal," by R.G. Black, W.A. Wenger and E.P. Popov - October 1980(PB81 154 312)A08

UCB/EERC-80/41 "Influence of Site Characteristics on Building Damage During the October 3, 1974 Lima Earthquake," by P. Repetto, I. Arango and H.B. Seed - Sept. 1980(PB81 161 739)A05

UCB/EERC-80/42 "Evaluation of a Shaking Table Test Program on Response Behavior of a Two Story Reinforced Concrete Frame," by J.M. Blondet, R.W. Clough and S.A. Mahin

UCB/EERC-80/43 "Modelling of Soil-Structure Interaction by Finite and Infinite Elements," by F. Medina - December 1980(PB81 229 270)A04

UCB/EERC-81/01 "Control of Seismic Response of Piping Systems and Other Structures by Base Isolation," edited by J.M. Kelly - January 1981 (PB81 200 735)A05

UCB/EERC-81/02 "OPTNSR - An Interactive Software System for Optimal Design of Statically and Dynamically Loaded Structures with Nonlinear Response," by M.A. Bhatti, V. Ciampi and K.S. Pister - January 1981 (PB81 218 851)A09

UCB/EERC-81/03 "Analysis of Local Variations in Free Field Seismic Ground Motions," by J.-C. Chen, J. Lysmer and H.B. Seed - January 1981 (AD-A099508)A13

UCB/EERC-81/04 "Inelastic Structural Modeling of Braced Offshore Platforms for Seismic Loading," by V.A. Zayas, P.-S.B. Shing, S.A. Mahin and E.P. Popov - January 1981(PB82 138 777)A07

UCB/EERC-81/05 "Dynamic Response of Light Equipment in Structures," by A. Der Kiureghian, J.L. Sackman and B. Nour-Omid - April 1981 (PB81 218 497)A04

UCB/EERC-81/06 "Preliminary Experimental Investigation of a Broad Base Liquid Storage Tank," by J.G. Bouwkamp, J.P. Kollegger and R.M. Stephen - May 1981(PB82 140 385)A03

UCB/EERC-81/07 "The Seismic Resistant Design of Reinforced Concrete Coupled Structural Walls," by A.E. Aktan and V.V. Bertero - June 1981(PB82 113 358)A11

UCB/EERC-81/08 "The Undrained Shearing Resistance of Cohesive Soils at Large Deformations," by M.R. Pyles and H.B. Seed - August 1981

UCB/EERC-81/09 "Experimental Behavior of a Spatial Piping System with Steel Energy Absorbers Subjected to a Simulated Differential Seismic Input," by S.F. Stiemer, W.G. Godden and J.M. Kelly - July 1981

UCB/EERC-81/10 "Evaluation of Seismic Design Provisions for Masonry in the United States," by B.I. Sveinsson, R.L. Mayes and H.D. McNiven - August 1981

UCB/EERC-81/11 "Two-Dimensional Hybrid Modelling of Soil-Structure Interaction," by T.-J. Tzong, S. Gupta and J. Penzien - August 1981(PB82 142 118)A04

UCB/EERC-81/12 "Studies on Effects of Infills in Seismic Resistant R/C Construction," by S. Brokken and V.V. Bertero - September 1981

UCB/EERC-81/13 "Linear Models to Predict the Nonlinear Seismic Behavior of a One-Story Steel Frame," by H. Valdimarsson, A.H. Shah and H.D. McNiven - September 1981(PB82 138 793)A07

UCB/EERC-81/14 "TLUSH: A Computer Program for the Three-Dimensional Dynamic Analysis of Earth Dams," by T. Kagawa, L.H. Mejia, H.B. Seed and J. Lysmer - September 1981(PB82 139 940)A06

UCB/EERC-81/15 "Three Dimensional Dynamic Response Analysis of Earth Dams," by L.H. Mejia and H.B. Seed - September 1981 (PB82 137 274)A12

UCB/EERC-81/16 "Experimental Study of Lead and Elastomeric Dampers for Base Isolation Systems," by J.M. Kelly and S.B. Hodder - October 1981

UCB/EERC-81/17 "The Influence of Base Isolation on the Seismic Response of Light Secondary Equipment," by J.M. Kelly - April 1981

UCB/EERC-81/18 "Studies on Evaluation of Shaking Table Response Analysis Procedures," by J. Marcial Blondet - November 1981

UCB/EERC-81/19 "DELIGHT.STRUCT: A Computer-Aided Design Environment for Structural Engineering," by R.J. Balling, K.S. Pister and E. Polak - December 1981

UCB/EERC-81/20 "Optimal Design of Seismic-Resistant Planar Steel Frames," by R.J. Balling, V. Ciampi, K.S. Pister and E. Polak - December 1981

UCB/EERC-82/01 "Dynamic Behavior of Ground for Seismic Analysis of Lifeline Systems," by T. Sato and A. Der Kiureghian - January 1982 (PB82 218 926)A05

UCB/EERC-82/02 "Shaking Table Tests of a Tubular Steel Frame Model," by Y. Ghanaat and R. W. Clough - January 1982 (PB82 220 161)A07

UCB/EERC-82/03 "Experimental Behavior of a Spatial Piping System with Shock Arrestors and Energy Absorbers under Seismic Excitation," by S. Schneider, H.-M. Lee and G. W. Godden - May 1982

UCB/EERC-82/04 "New Approaches for the Dynamic Analysis of Large Structural Systems," by E. L. Wilson - June 1982

UCB/EERC-82/05 "Model Study of Effects of Damage on the Vibration Properties of Steel Offshore Platforms," by F. Shahrivar and J. G. Bouwkamp - June 1982

UCB/EERC-82/06 "States of the Art and Practice in the Optimum Seismic Design and Analytical Response Prediction of R/C Frame-Wall Structures," by A. E. Aktan and V. V. Bertero - July 1982

UCB/EERC-82/07 "Further Study of the Earthquake Response of a Broad Cylindrical Liquid-Storage Tank Model," by G. C. Manos and R. W. Clough - July 1982

UCB/EERC-82/08 "An Evaluation of the Design and Analytical Seismic Response of a Seven Story Reinforced Concrete Frame - Wall Structure," by A. C. Finley and V. V. Bertero - July 1982

UCB/EERC-82/09 "Fluid-Structure Interactions: Added Mass Computations for Incompressible Fluid," by J. S.-H. Kuo - August 1982

UCB/EERC-82/10 "Joint-Opening Nonlinear Mechanism: Interface Smeared Crack Model," by J. S.-H. Kuo - August 1982

UCB/EERC-82/11 "Dynamic Response Analysis of Techi Dam," by R. W. Clough, R. M. Stephen and J. S.-H. Kuo - August 1982

UCB/EERC-82/12 "Prediction of the Seismic Responses of R/C Frame-Coupled Wall Structures," by A. E. Aktan, V. V. Bertero and M. Piazza - August 1982

UCB/EERC-82/13 "Preliminary Report on the SMART 1 Strong Motion Array in Taiwan," by B. A. Bolt, C. H. Loh, J. Penzien, Y. B. Tsai and Y. T. Yeh - August 1982

UCB/EERC-82/14 "Shaking-Table Studies of an Eccentrically X-Braced Steel Structure," by M. S. Yang - September 1982

UCB/EERC-82/15 "The Performance of Stairways in Earthquakes," by C. Roha, J. W. Axley and V. V. Bertero - September 1982

UCB/EERC-82/16 "The Behavior of Submerged Multiple Bodies in Earthquakes," by W.-J. Liao - September 1982

UCB/EERC-82/17 "Effects of Concrete Types and Loading Conditions on Local Bond-Slip Relationships," by A. D. Cowell, E. P. Popov and V. V. Bertero - September 1982

UCB/EERC-82/18 "Mechanical Behavior of Shear Wall Vertical Boundary Members: An Experimental Investigation," by M. T. Wagner and V. V. Bertero - October 1982

UCB/EERC-82/19 "Experimental Studies of Multi-support Seismic Loading on Piping Systems," by J. M. Kelly and A. D. Cowell - November 1982

UCB/EERC-82/20 "Generalized Plastic Hinge Concepts for 3D Beam-Column Elements," by P. F.-S. Chen and G. H. Powell - November 1982

UCB/EERC-82/21 "ANSR-III: General Purpose Computer Program for Nonlinear Structural Analysis," by C. V. Oughourlian and G. H. Powell - November 1982

UCB/EERC-82/22 "Solution Strategies for Statically Loaded Nonlinear Structures," by J. W. Simons and G. H. Powell - November 1982

UCB/EERC-82/23 "Analytical Model of Deformed Bar Anchorages under Generalized Excitations," By V. Ciampi, R. Eligehausen, V. V. Bertero and E. P. Popov - November 1982

UCB/EERC-82/24 "A Mathematical Model for the Response of Masonry Walls to Dynamic Excitations," by H. Sucuoğlu, Y. Mengi and H. D. McNiven - November 1982